SHAPE OPTIMIZATION OF REVOLUTE-JOINTED FLEXIBLE MANIPULATORS

A Thesis Submitted in Partial Fulfillment of the Requirements

for the Degree of

DOCTOR OF PHILOSOPHY

by

Sachindra Mahto

(Roll No. 08610308)

Department of Mechanical Engineering

Indian Institute of Technology Guwahati

Guwahati–781039

INDIA

September 2015

Department of Mechanical Engineering,
Indian Institute of Technology Guwahati,
Guwahati-781039
INDIA

CERTIFICATE

It is certified that the work contained in the Thesis entitled "**Shape Optimization of Revolute-Jointed Flexible Manipulators**" submitted by **Mr. Sachindra Mahto** to the Indian Institute of Technology Guwahati for the award of the degree of Doctor of Philosophy has been carried out under our supervision in the Department of Mechanical Engineering, Indian Institute of Technology Guwahati. This work has not been submitted elsewhere for the award of any other degree or diploma.

September 5, 2015

Dr. U. S. Dixit
Professor
Department of Mechanical Engineering,
Indian Institute of Technology Guwahati,
Guwahati-781039, INDIA

Dr. A. K. Gogoi
Professor
Department of Electronics and Electrical Engineering,
Indian Institute of Technology Guwahati,
Guwahati-781039, INDIA

Dedicated to my wife

Smt. Santana Mahato

Acknowledgment

I would like to express my deep appreciation to my supervisors Prof. U.S. Dixit and Prof. A.K. Gogoi for their invaluable constant support, guidance and enthusiasm for my thesis research work. I am also grateful to my doctoral committee members Prof. U.K. Saha, Prof. S. Majhi, and Prof. G. Barua for their time devoted to reviewing my research progress work and their willingness to serve on this committee. Also, I would like to extend my sincere thanks to Prof. U.S. Dixit, Prof. R. Tiwari, Prof. D. Chakraborty and Prof. S.K. Dwivedy for their valuable lectures that delivered during my course work. I extend my great respect to Prof. A.K. Dass (Head of Mechanical Engineering) and Prof. A.K. Singh for their moral support during my research work.

I would like to extend my heartiest thanks to all my friends and batch mates especially Mr. H. Sarangi, Mr. R. Das, Mr. D. Biswal, Mr. B. Nayak, Mr. M. Chandrasekaran and Mr. J. Ramalu for providing ideas and supports. I tremendously acknowledge Mr. Vinod Yadav and Mr. Seikh M. Kamal for their direct and indirect supports and help.

I gratefully acknowledge for the financial assistance provided by All India Council for Technical Education (AICTE), New Delhi and my parent institution North Eastern Regional Institute of Science and Technology (NERIST), Itanagar. Also, I am very much thankful to Mechanical Engineering Department of IIT Guwahati and staff members for extending infrastructure facilities and their cordial support during my research work in the department.

My utmost thanks to my wife and family members for their never ending support and encouragement and also highly inspired by my children Shubhanshu, Shubhani and Pranshu throughout my academic years. Last but not least, special thanks to all individuals who have directly or indirectly offered help, suggestions and support in bringing towards the completion of this project.

Finally, I wish Almighty God with deepest gratitude and seek blessings.

September 5, 2015

Sachindra Mahto
IIT Guwahati

Abstract

Flexible robotic manipulator systems exhibit many advantages over the conventional robotic systems. However, they have not been favoured in production industries due to their vibration-control issues. This thesis presents theoretical investigation into the dynamic modelling and optimal design through shape optimization of the links. Optimized dynamic behaviour of revolute-jointed single link flexible manipulator, double link rigid-flexible manipulator, and double link flexible manipulator is studied. A constrained flexible robotic manipulator is considered that moves in horizontal plane only.

Mathematical models of the systems are developed using finite element method. Distributed systems are converted into discrete systems and equations of motions are derived using Lagrangian approach. Due to their slenderness, robotic links are considered as Euler-Bernoulli beams. Different optimization problems are considered for shape optimization of the robotic links. Each optimization problem explicitly optimizes a particular objective function. An objective function is designed to cater to a range of payloads of the robotic systems. A classical technique of optimization, sequential quadratic programming (SQP), is used for optimization of the nonlinear objective function under the nonlinear constraints. SQP based MATLAB® solver "FMINCON" is used in this work.

The main findings of the thesis are as follows-

Four optimization problems are considered *viz.*, maximization of fundamental beam/system frequency, minimization of static tip deflection, and minimization of dynamic tip deflection for single link flexible manipulator to obtain the optimized shapes. Optimized shapes for a particular objective function are also obtained for various payloads. Effects of system parameters on the dynamics are also studied. Shape optimization is done for a range of payloads, and the results highlight the advantage of shape optimization.

Two optimization schemes are proposed to obtain the single optimized shape to cater to the range of payloads and the best optimization approach is identified. Shape optimization is also considered for the maximization of higher natural frequencies with payloads. Optimized shapes provided better performance. In a similar way, shape optimization of the flexible link of the rigid-flexible manipulator is carried out for four optimization problems. It is observed that one optimized shape is not suitable for all the optimization problems. For different optimization problems, different optimized shapes are obtained. In real practice, the appropriate shape is chosen depending on the actual requirement.

Dynamics of double link flexible manipulator is more complex than single link manipulator. Effects of system parameters on its dynamics are studied. Three optimization problems are considered *viz.*, minimization of static tip deflection, maximization of fundamental beam frequency of individual links and maximization of fundamental system frequency of individual links. Improved dynamics of whole system is studied and compared. Dynamics of shape optimized double link flexible manipulator is also investigated under the excitation of energy based robust (EBR) controlled torque and a significant advantage is observed over the non-optimized shape.

Contents

List of Figures

List of Tables

Nomenclature

a, b	Hub radius at joint 1 and joint 2 (m)
d_1, d_2	Diameters of link 1 and link 2 (m)
D_{μ_i}	Static tip deflection of the shape optimized beam at payload μ_i (m)
E_1, E_2	Objective function (used in Chapter 3)
E_1, E_2	Young's modulus (used in Chapter 5) (N/m^2)
f_{n_k}	Fundamental frequency of k^{th} link (Hz)
f_{μ_m}	Frequency of the shape optimized beam at average payload μ_m (Hz)
F_{μ_i}	Frequency of the shape optimized beam at payload μ_i (Hz)
h_1, h_2	elements lengths (m)
I	Area moment of inertia of link 1 and link 2 (m^4)
I_1, I_2	mass moments of inertia (kg.m^2)
J_{h_1}, J_{h_2}	Hub inertias (kg.m^2)
J_1, J_2	Hub inertia of joint 1 and joint 2 (kg.m^2)
K_{f_k}	Gain constant of robust control for k^{th} link
K^i	Kinetic energy of the i^{th} element (N.m)
K_{P_k}, K_{V_k}	Feedback constant (used in Chapter 3)
$[K]$	global stiffness matrix
$[K_b]$	Stiffness matrix as a cantilever beam
$[K_1^i], [K_2^j]$	elemental stiffness matrices of i^{th} and j^{th} elements, respectively
L	Differential operator (used in Chapter 2)
L_k	Length of the k^{th} link (m)
L, L_1, L_2	Length of the links (m)

m_k	Mass per unit length of k^{th} link (kg/m)
m_{t_k}	Tip mass of k^{th} link (kg)
m_1 , m_2	Mass per unit lengths of link 1 and link 2 (kg/m)
M	Mass of the link (kg)
M_{m}	The motor mass at joint 2 (kg)
M_{p}	Tip mass (payload) (kg)
M^*	Mass of the optimized links (kg)
M_1 , M_2	Mass of link 1 and link 2 (kg)
M_m, M_p	Motor mass and payload (kg)
$[M]$	global mass matrix
$[M_b]$	Mass matrix as a cantilever beam
M_1, M_2	mass of links (kg)
n_1, n_2	Number of finite elements
N_i	Shape functions
q	global nodal variables or generalized co-ordinates
r_1, r_1'	position vectors of point P_1' in link 1 with respect to XOY and X_1OY_1
r_2, r_2'	position vectors of point P_2' in link 2 with respect to XOY and X_1OY_1
ROS	Non-inertial frame (used in Chapter 3)
t	Time (s)
$\backslash u$	Flexural deflection of first link (m)
u_{2i-1}, u_{2i+1}	slopes at node of i^{th} element of 1st link (rad)
u_{2i}, u_{2i+2}	deflections at node of i^{th} element of 1st link (m)
V^i	Potential energy of the i^{th} element (Nm)
w	Flexural deflection of 2nd link (m)
w_{2j-1}, w_{2j+1}	slopes at node of j^{th} element of 2nd link (rad)
w_{2j}, w_{2j+2}	deflections at node of j^{th} element of 2nd link (m)
X^{LB}, X^{UB}	Lower and upper bound of diameter of the beam elements (m)
XOY	Inertial coordinate frame

XO_1Y	Inertial coordinate frame (used in Chapter 3)
$X_1O_1Y_1$	Non-inertial coordinate frames
$X_nO_nY_n$	Inertial coordinate frames

Greeks

α	A constant depending on the damping ratios
β	Ratio of hub mass to beam mass
δ	Constant used in Newmark method
δ_{μ_m}	Static tip deflection of the shape optimized beam at average payload μ_m
δ_{tip}	Static tip deflection of the uniform link (m)
δ^*_{tip}	Static tip deflection of the optimized link (m)
η	Constant used in Newmark method
λ	A constant depending on the damping ratios
μ	Used to express payload ($\mu=M_p/M_2$)
μ_1, μ_2	Payload at the link 1 and link 2, respectively
ρ	Density of the link (kg/m^3)
ρ_1, ρ_2	Density of the link 1 and link 2, respectively (kg/m^3)
σ	Dummy variable (used in Chapter 3)
θ_f	Final angular hub rotation (rad)
θ_k	Angular displacement of the k^{th} link (rad)
θ_1, θ_2	Rigid body rotation of link 1 and link 2 (rad)
τ	Applied torque (Nm)
τ_{EBR_k}	Torque under energy based robust control at k^{th} joint (Nm)
τ_{PD_k}	Torque under position and derivative control at k^{th} joint (Nm)
τ_1, τ_2	Applied torques at joint 1 and joint 2 (Nm)
$\omega_{\max}$	Highest frequency of the beam (Hz)
Δt_{cr}	Maximum time step for numerical stability (s)

Chapter 1

Introduction

1.1 Flexible Manipulators

Manipulators are the basic part of the robots. These are composed of a series of links and joints. Links are inter–connected through revolute or prismatic joints to form open kinematic chain mechanism. Joints are defined as the connections between the two links. The device attached to the manipulator which interacts with its environment to perform tasks is called the end-effector (tool holder/gripper). The need of robot manipulator is increasing to raise the productivity and improve the quality of products in manufacturing industry. However, most industrial robots are composed of heavy and stiff links to satisfy the required repeatability and accuracy. Therefore, high power is required in the actuator to overcome the inertia and holding the system against the gravity. Also, it takes longer time to complete the motion. In order to improve industrial productivity, researchers pay more attention for the design and control of large length robotic manipulators. However, there is significant elastic deformation due to loads and hence these manipulators are termed flexible. In true sense, all the robotic systems are flexible in nature.

Flexible manipulators have the potential advantages of lower cost, larger work volume, higher operational speed, greater payload-to-weight ratio, smaller actuators, lower energy consumptions, better transportability, better manoeuvrability and safer operations due to lower inertia compared to the conventional robotic systems. They have several advantages and wide range of applications, *e.g.* space explorations, medical, transportations, *etc.* Though the compliance inherently exists in transmission and robotic structure, faster motion performance in light weight manipulators will cause considerable vibration of the robot end-points at the end of a

move. This residual vibration is primarily a result of additional kinetic energy imparted to the robotic system. As the overall structure is lightly damped, any vibration occurring after the final position is reached will require additional settling time before the new task can begin. For that reason, an effective technique is required to reduce this residual vibration.

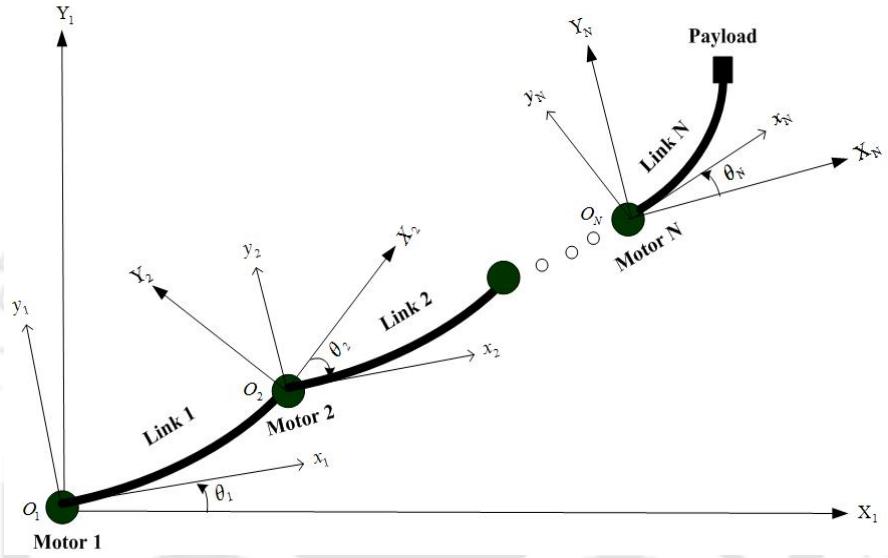

Figure 1.1 A schematic of the multi-link revolute-jointed flexible robot

Workspace of a single link revolute-jointed robotic manipulator consists of the points on the circumference of the circle. There are limited applications of single link rigid/flexible manipulators with respect to multi-link flexible manipulators. Some of the applications of single link flexible manipulator are cleaning waste tanks, operating microsurgical applications, deburring, surface polishing, grinding, *etc.*, [Hakki, *et al.*, 2012]. A planar multi-link revolute jointed flexible manipulator is shown in Figure 1.1. There are different configurations of robotic systems *viz.*, Cartesian (PPP), Cylindrical (RPP), Spherical (RRP), Articulated (RRR), Selective Compliance Assembly Robot Arm (SCARA, RRP), *etc.*, where 'P' and 'R' represent the prismatic and revolute joints respectively. In general, dynamic modeling and control of multi-link flexible robots are much more difficult and complex than the dynamic modeling and control of conventional robots. Truncated model of finite dimension is used for its dynamic analysis and control design. The complexity and order of the controller increases dramatically, as the order of model increases.

1.2 Motivation

Research on flexible manipulators has increased a lot for last some decades motivated by the need for higher speed, lower weight, and better energy consumption. Flexible manipulators possess all these characteristics. Though there are several advantages of flexible robotic systems over the bulky and heavy conventional robotic systems, vibration is the challenging task due to its low stiffness. These issues are relevant in the system design and therefore new generation industrial robotic manipulators and flexible robots for space applications need to be optimally designed.

Many techniques have been applied to overcome tip vibrations caused by manipulator's low stiffness. Traditionally, by increasing the rigidity of the robotic arm, residual vibrations can be reduced but at a higher cost of materials and energy consumption to accelerate the mechanism. This conflicts with the demand for increased productivity. Therefore, designing lightweight robotic manipulators capable of moving larger payloads without increasing the mass of the linkage is of considerable interest. Here, the shape optimization ideas are addressed from a design perspective. The goal is to build high performance flexible manipulator such that the effect of its oscillations reduces along with the improvement of the other dynamic responses.

The behaviour of the flexible robotic manipulators is highly non-linear and complex in nature and hence there are difficulties in its control. Without proper control, the vibrations caused by the structural elasticity of the links would not only reduce the operation speed but also reduce the accuracy of the control or even sometime cause instability. It is necessary to control the structural vibration in the flexible links for quick and precise tracking of the trajectories. These requirement make it necessary to take into consideration the dynamic effects of the distributed robotic link's flexibility. However, high speed operations lead to high inertial forces causing vibrations and diminishing control accuracy. Therefore, optimal design of robotic flexible system with proper control strategy is the prime goal of a design engineer.

1.3 Problem Statement

As per the recent development, manipulators can be designed either rigid manipulator or flexible manipulator. Theoretically, a rigid manipulator has an infinitely large fundamental frequency of vibration and thus it can move at any desired speed without significant tip deflection. However, rigid manipulators are of large link mass with corresponding low energy efficiency. On the other hand, a flexible manipulator has a much lower mass but experiences significant tip deflection under normal operating conditions and the oscillation become severe when the manipulator speed approaches its natural frequencies. The tip deflection during the motion depends upon the following factors:

- rotational speeds of the links,
- lengths of the links,
- material properties of the links,
- shape of the links,
- hub inertias, and payloads.

In general, shape of link is not specified as a design requirement out of these factors. Once the mass and link lengths are decided in the design stage, shape of the links can be designed for different objectives. Two essential objectives for shape optimization are:

(i) maximization of natural frequencies (particularly fundamental), and
(ii) minimization of static/dynamic tip deflections

for a given fixed mass/length of the links. The design variables that relate directly to the consistent mass and stiffness matrices of the manipulator should be the function of its shapes. The maximization of fundamental frequency is desired as it increases frequency bandwidth for flexible manipulators, and this allows for faster motion and stable end-point control. Minimized static and dynamic tip deflections help in getting desirable positional accuracy and vibration suppression respectively.

1.4 Organization

The thesis work is documented as per Table 1.1. In Chapter 2, previous work in the dynamic modelings, experimental contributions, and optimal design of the flexible

manipulators is examined. In Chapter 3, derivation of equation of motion in finite element form based on Lagrangian method is derived treating links as Euler-Bernoulli beams. Different optimization problems are addressed for exclusive objective functions under link mass and static tip deflection as constraints. Single optimized shape to cater to a range of payloads is also examined. Effects of different torque profiles and controlled torque are also presented.

Dynamic modeling and shape optimization of rigid-flexible manipulator and double link flexible manipulator unlike single link manipulator is presented in Chapter 4 and Chapter 5 respectively. Comparative dynamic study is done for both the cases. In all the cases, dynamic response is presented in time-domain. Time is discretized using Newmark's technique based on finite difference approach. Shape optimization is done in all the cases of flexible manipulators using classical optimization technique— sequential quadratic programming (SQP). Chapter 6 concludes with a discussion of results, merit of research, and directions for future research.

Table 1.1 Chapters 2–6 of thesis

Chapter 2	Review of literature
Chapter 3	Dynamic modeling and optimization of single link revolute-jointed flexible manipulator
Chapter 4	Dynamic modeling and optimization of double link rigid-flexible manipulator
Chapter 5	Dynamic modeling and optimization of double link flexible manipulator
Chapter 6	Conclusions and Scope of future

1.5 Conclusion

Six optimization design models of single-link flexible manipulator presented by Dixit *et al.* [2006] based on fundamental frequency of vibration and static tip deflection are extended further in this thesis for different payloads as well as for higher natural frequencies. Finite element model is solved by Newmark's time integration technique. An extensive analysis of optimization results and related

dynamics is provided for each optimization model for solid links with circular cross-section. Comparative dynamic response of single link flexible manipulator is carried out for different excited torque profiles. Optimized shapes to cater to a range of payloads are also presented along with its comparative dynamics. Different optimization problems for rigid-flexible links manipulator and double link flexible manipulator are also presented for the optimal shapes for flexible links. Comparative optimal dynamics of both the cases are presented. Dynamics of double link flexible manipulator highly depends upon various system parameters. Therefore, its parametric analysis is also presented.

It is observed that mass of the optimized links are the active constraints. Sensitivity analysis is presented, along with numerical results for single/double link flexible manipulator. Vibration suppression of single/double link flexible manipulator is also plotted under the excitation of energy-based robust (EBR) controlled torques.

Chapter 2

Review of Literature

2.1 Introduction

The main requirement of the flexible manipulator is to control motion to enable the manipulator end-point to follow the prescribed path with reasonable accuracy and with acceptably small vibrational amplitudes. This problem can be solved by several ways. There have been a number of studies on dynamic modeling, control, optimal system design and experimental observation. In this chapter, a brief survey of literature related to modeling and shape optimization of flexible manipulators is presented.

2.2 Dynamic Modeling

Researches in the past developed various ways of modeling the systems to predict their dynamic behavior theoretically. Out of these, finite element method and assumed mode method are preferably used by the researchers. Both these methods convert the distributed flexible manipulator system to discrete system and thereafter equations of motion are derived through different basic techniques.

2.2.1 Finite Element Based Modeling

The finite element method (FEM) originated in early 1940s [Courant, R., 1943] from the matrix methods in structural mechanics. Using variational principle initially, its applications were focussed on stress analysis problems. However, variational principles are not available for all class of continuum problems. Hence,

later research focussed on generalization of finite element formulation based on weighted residual approach. This latter approach has become extremely popular because of its suitability to a wide range of problems across different disciplines in physical science and engineering.

Finite element method requires transformation of the governing differential equation into an appropriate integral equation. This process is accomplished either through (a) variational transformation or (b) weighted residual formulation. As weighted residual formulation can be applied to any problem, it is the most widely used. Let the governing equation for a physical problems is expressed as

$$L(u) = 0, \tag{2.1}$$

where L is a differential operator with associated boundary (and initial) conditions. We seek an approximate solution $\bar{u}$ of Eq. (2.1) expressed in the form

$$u(x) \approx \bar{u}(x) = \sum_i N_i(x) u_i(x), \tag{2.2}$$

where N_i are prescribed functions, called interpolation (shape or trial) functions and u_i is still unknown value of variable u at a discrete spatial point x. Substituting the preceding approximation in Eq. (2.1) would lead to the residual (error) function R given by

$$R = L(\bar{u}). \tag{2.3}$$

To determine the nodal values u_i , the integral containing the product of the residual R with a prescribed weight function w_i is set to zero, *i.e.*,

$$\int_\Omega R w_i d\Omega = \int_\Omega L(\bar{u}) w_i d\Omega = 0. \tag{2.4}$$

Weight function w_i is also referred as the test function.

2.2.1.1 FEM Modelling of Single Link Flexible Manipulator

During the period 80s and 90s, conventional linear and non-linear finite element modeling was carried out for dynamic modeling of flexible manipulator. Lee and Wang [1988] studied a single link flexible manipulator in a 3D work space using FEM. Dynamical equations are derived rigorously by considering the robotic arm with two-degree freedom in rotation and one degree of freedom in translation. Nagarajan and Turcic [1990] derived elemental and system equations using Lagrange's equation for elastic mechanism systems. Bricout *et al.* [1990] used the

FEM to study the elastic structural behaviour of the links. Elastic constraints at the joints are incorporated with the help of Lagrange's multipliers to take into account the motion of manipulator. Maulin and Bayo [1991] used finite element discretization of the system to discuss the end-point trajectory tracking for flexible arms. Theoretical difficulties pertaining to the inverse problem for the flexible structure are exposed. It is observed that a non-casual solution for the active torque enables tracking of an arbitrary tip displacement with any desired accuracy in frequency domain. However, the inverse transfer function obtained using discrete models do not converge to that of continuous system when the model is refined.

Chang and Gannon [1990] developed an enhanced equivalent rigid link system (ERLS) model using natural mode shape functions for flexible manipulators and an experimental validation of the model was performed for a single link manipulator. Joint variables and modal displacements are taken as generalized coordinates. The model describes the dynamic behavior of manipulator and allows for application to design motion control. Alberts *et al.* [1992] used FEM analysis to study the effectiveness of viscoelastic passive damping augmentation to active control of a large flexible space manipulator. They have shown very low frequency modes due to joint flexibility and high frequency modes due to bending in the booms, which results in significant end-point motion.

Theodore and Ghosal [1995] presented comparison between the assume mode method (AMM) and finite element method (FEM) used for flexible manipulators. They represented the link flexibility of the robot manipulator efficiently and employed systematic modeling procedure based on homogeneous transformation matrices for spatial multi-link flexible manipulator for both revolute and prismatic joint. They illustrated the complexity owing to the time-dependent frequency equation of the assumed mode model arising in a prismatic jointed flexible link with payload. Ge *et al.* [1997, 1998] derived a non-linear dynamic model using finite element method associated with Lagrange approach for single link revolute-jointed manipulator and flexible prismatic jointed manipulator. State space model is obtained considering displacements and rotations of the nodes as the generalized co-ordinates of the system. Based on this method, an effective nonlinear states feedback controller was constructed for the flexible robotic system.

Furthermore, an efficient algorithm was developed to calculate the inverse of the system's inertia matrix for real-time implementation.

Since last two decades, accurate dynamic modeling of flexible manipulator is developed by some researchers considering the second order coupling in axial and transverse direction deformation of the link. Tokhi *et al.* [2000, 2001] developed a dynamic model for single link flexible manipulator using finite element approach and compared it with the experimental investigation. The modal frequencies were obtained experimentally to validate the model in time and frequency domain. The researchers used bang-bang type of torque to study the dynamic response considering structural damping. Chung and Yoo [2002] carried out dynamic analysis of rotating cantilever beam using FEM. They used stretch deformation instead of the conventional axial deformation. In the governing equations, the stretch and chord-wise deformation are coupled with other, however flap-wise deformation is not coupled with other deformations.

Yang *et al.* [2003] developed finite-element method for a flexible hub-beam system with a tip mass considering both viscous damping and air drag force. Second order displacement field approximation is proposed and dynamic stiffening is accounted. Effects of tip mass and damping on dynamic behavior of the hub-beam system is studied numerically. Mohamed and Tokhi [2004] derived the dynamic model of a single-link flexible manipulator using FEM and then studied the feed-forwarded control strategies for controlling the vibrations using command shaping technique based on input shaping, low-pass and band-stop filtering.

For a dynamic system of a rigid hub and flexible cantilever beam, axial and transverse deflection at any point of the beam are assumed to be uncoupled and such model is called zeroth–order approximation coupling model (ZOAC). Cai *et al.* [2005] studied the characteristic of a flexible hub–beam system with tip mass based on Hamilton's principle and FEM model. They considered the second–order coupling quantity of axial displacement caused by the transverse deflection of the beam referred as first–order approximation coupling (FOAC) model. At higher speed, the ZOAC may result in divergence to the dynamic response whereas FOAC model can still accurately describe the dynamics of hub–beam system.

You *et al.* [2006] presented the FOAC dynamic modeling of hub–beam system based on Hamilton's principle and finite element method considering links as a Timoshenko beam. A dynamic coupling model considering shear deformation is established. It is observed that dynamic characteristics of the hub–beam system using Timoshenko beam hypothesis and the Euler–Bernoulli beam hypothesis are almost identical for slender beam as it has little effect of the shear deformation. However, there is considerable effect when beam is short.

Teng *et al.* [2007] investigated the frequency characteristics of a flexible hub-beam system with an arbitrary position of attached mass using first-order approximation coupling model (FOAC). As the attached mass is at the tip position, vibration amplitude increases with decrease of the frequency response of the beam. Damping affects both the final position of the system and the vibration amplitude of the beam, but has little effect on frequency response of the beam. Response frequency of the beam is sensitive to the change of hub radius when radius is small but it become very small when the radius is above a certain value.

2.2.1.2 FEM Modeling of Multi Link Flexible Manipulator

Sunada and Dubowsky [1983] developed a lumped parameter FEM model for analyzing the complete behavior of industrial robotic manipulator with complex-shape flexible links. Fakuda [1985] and Fakuda and Arakawa [1987] studied the modeling and dynamic characteristics of two-link flexible robotic arms and controlled the vibration by taking into account the gravity, payload, and the coupled vibration between the first and second arm. Usoro *et al.* [1986] developed finite element models to describe the deflection of a planar multi-link model, which indicates that the system is complete non-linear in the generalized inertia matrix. Simulated results indicate that dynamic behavior of the double link flexible manipulator is highly non-linear and complex in nature. This is the base research contribution for further research work in multi-link flexible manipulator.

A decoupling method is proposed by the feedback control method to compensate for the coupling effects between the flexible robotic arms. Finite element models developed by Naganathan and Soni [1987, 1988] incorporate a fully three-dimensional element to simulate manipulator motions with effects of gravity

and strain energies from torsional, axial and lateral deformation. Fakuda *et al.* [1988] considered the modeling and control method of bending-torsion coupled vibration in the system. Ower and Vegte [1987] used a Lagrangian approach to model the planar motion of a manipulator consisting of two flexible links and two rotary joints. Lee and Wang [1988] derived the equation of motion of a two-link manipulator moving in a vertical plane. They explicitly obtained the nonlinear governing equations of the system and measurement. Low and Vidyasagar [1988] considered a two link manipulator with last link as a flexible member and used the Lagrangian method to study its dynamics. The approach is a natural extension of the well known Lagrangian method for rigid manipulator. Benati and Morro [1988] developed a Lagrangian approach for the dynamics of chain with flexible links. Each link is modeled as a system with a finite numbers of degree of freedom, one of them describing the rotation, the others the flexibility.

Bayo [1989] used FEM to deal with multi-link flexible manipulator considering Timoshenko beam theory and including nonlinear Coriolis and centrifugal effects for the elastic behavior. An iterative solution scheme is proposed for finding out the desired joint torques where the solution of each linearization is carried out in frequency domain. Jonker [1989] presented the geometrical nonlinear finite element based method for dynamic analysis of spatial mechanism with flexible links. The equations of motion are formulated in terms of generalized coordinates of the mechanism with rigid links and deformation mode coordinates that characterize deformation of the elements.

Jonker [1990] again presented a nonlinear finite element based formulation for analyzing the dynamic behavior of flexible manipulators, in which both links and joints are considered as specific finite element. The method also permits generation of locally linearized models about a nominal trajectory. This nonlinear finite element formulation is used to analyze a flexible three degree of freedom manipulator. Kalra and Sharan [1990, 1991] extended the work of Sunada and Dubowsky [1981] and Nagnathan and Soni [1987] to model flexible manipulator using the Galerkin's finite element method. The forces on the deformed link have been resolved along the link coordinate axes which results C^1 continuity in both axial as well as in transverse direction of the manipulator. The finite element derivation is carried out for multi

link manipulator and the numerical example is presented for a two-link planar manipulator with revolute joints.

Kovecses [1998] developed a distributed parameter model for modeling robotic links, considering distributed mass and flexibility without discretization. It is assumed that a robot link can contain both flexible and rigid parts, but uniform beam models can be used to describe flexibility. The concept of fictitious rigid link has been introduced. Yang and Sadler [1990] derived finite element based dynamic equations of motion for flexible planar linkage, treating the total mechanism displacements as the primary unknowns. Nonlinear equations are solved under condition of either specified input motion of the mechanism or specified input forcing function. Bares and Sasiadek [1990] and Beres *et al.* [1990] used an Lagrangian finite element approach to formulate the dynamic model of a flexible manipulator system in three-dimensional space. Beam type finite element with third degree interpolating polynomials and six generalized co-ordinate per finite element nodal point were used for description of small displacement field of the link.

Dogan and Iftar [1998] carried out the modeling and control of two-link robot manipulator, whose first link is rigid and second link is flexible. They applied the extended Hamilton's principle to obtain the equation of motion and the corresponding boundary conditions. A composite controller is designed in this work based on the singular perturbation method. Rosado and Yuhara [1999] and Rosado [2000] developed dynamic modeling of planar flexible robotic manipulator with two flexible links and two revolute joints using a Euler–Newton formulation and the finite element method based on elementary beam theory, which is used to discretize displacements under small motion.

Farid and Lukaiewicz [2000] developed an efficient finite element/ Lagrangian approach for dynamic modeling of lightweight multi-link spatial manipulators with flexible links and joints. There are constraint equations representing kinematical relations among different coordinates due to the connectivity of the links. These equations are added to the equations of motion. Proposed model takes into account the coupling effects among the rigid body motion of the system, the bending and torsion deflection of the links, and the flexibility of the links.

Zhang and Yu [2004] carried out dynamic modeling and simulation of two cooperating structurally multi-link flexible robotic manipulator in absolute coordinates.. The input joint angles and torque obtained by the proposed method can drive the cooperative flexible manipulators holding an object passing through a given trajectory accurately. The optimum load distribution and high load capacity can be obtained.

2.2.2 Assumed Mode Method Based Modeling

In the assumed modes of model formulation, the link flexibility is usually represented by truncated finite modal series, in terms of spatial mode eigenfunctions and time varying mode amplitudes. This method is widely used and link boundary conditions and mode eign-functions are chosen in several ways. Let the governing equation for a physical problems be expressed as

$$L(u) = 0, \tag{2.5}$$

where L is a differential operator, with associated boundary (and initial) conditions. We seek approximation solution $\bar{u}$ of Eq. (2.5) expressed in form

$$u(x,t) = \sum_{i=1}^{\infty} \phi_i(x) u_i(t) \quad \text{(for exact solution)}, \tag{2.6}$$

$$u(x,t) \approx \bar{u}(x,t) = \sum_{i=1}^{\infty} \psi_i(x) u_i(t) \quad \text{(for approximate solution)}, \tag{2.7}$$

where $\psi_i(x,t)$ are shape function (assumed mode), and $u_i(t)$ are generalized displacements. The assumed mode method approximate a solution by applying the principle of virtual work or Lagrangian equations which produce a generalized parameter model as given below.

Virtual Work Method:

$$\sum_{j=1}^{n} \left(P_i - K_{ij} u_j - m_{ij} \ddot{u}_j \right) \delta u_i(t) = 0, \; i = 1, 2, ..., n \tag{2.8}$$

where P_i, K_{ij}, m_{ij} denote the generalized forces, stiffness matrix and mass matrix, respectively and u_j, δu_i denote the generalized displacements and virtual displacements respectively.

Lagrangian Method:

$$\frac{\mathrm{d}}{\mathrm{dt}}\left(\frac{\partial T}{\partial \dot{q}_i}\right)-\frac{\partial T}{\partial q_i}+\frac{\partial V}{\partial q_i}=Q_i,\quad i=1,2,.....,n, \tag{2.9}$$

where T, V denote the kinetic energy and potential energies of the system respectively and Q_i, q_i denote the generalized force and generalized co-ordinates respectively. The method transfers a continuous system to a discrete system.

2.2.2.1 Modeling of Single Link Flexible Manipulator

Rakhsha and Goldenberg [1985] used a Euler–Newton formulation and assumed mode method to model single link manipulator. Hastings and Book [1986] generated the Lagrangian linear model for controlling flexible manipulator using assumed mode method. The model agreed favorably with the measured response for a selection of clamped-mass assumed modes. Wang and Wei [1987] modeled the vibration of moving slender prismatic beam using Lagrangian method and assumed mode method. They observed that the extending and contracting motions have destabilizing and stabilizing effects on the vibratory motion, respectively.

Due to distributed nature of the link flexibility, the exact model is represented by non-linear partial differential equation. Tomei and Tomambe [1988] presented a method to derive approximate dynamic models. Such models are obtained by Lagrangian approach by expanding in a limited number of terms for exact shape of the beam. Barbieri and Ozguner [1988] used an extended Hamilton's principle to derive the equation of motion and studied the unconstrained and constrained mode of vibration. Krishnamurthy [1989] presented dynamic model for a flexible cylindrical manipulator using extended Hamilton's principle considering manipulator arm as a distributed mass. The model includes the dynamics of the tail section of the manipulator.

Modeling of a slewing flexible link is carried out by Bellezza *et al.* [1990] with assumed mode technique using classical pinned eignfunctions. Exact eigen-functions are determined considering also the rotating inertia at the base and a payload at the tip. Wang and Vidyasagar [1991] observed that if the output is defined to be the net tip deflection then the relative degree of the transfer function for the single flexible link is not well defined, as the number of modes approach

infinity. However, if the output is defined to be the rigid body deflection minus the elastic deflection, then a transfer function with relative degree of two does exist, irrespective of number of modes. Singh [1991] also used the same principle to derive the equation of motion and further studied the non-linear phenomena using a perturbation technique.

2.2.2.2 Modeling of Multi Link Flexible Manipulator

Cannon and Schmitz [1984] recognized that unlike for single link manipulators, multi-link manipulators can not be considered by linearized model. The difficulties are involved in dealing with the non-linearities and the mode shapes of a linearized model vary with the configuration of the non-linear system. Dado and Soni [1987] investigated the dynamic response of a planar 2-R robot with flexible joints. Servo stiffness and damping are modeled along with stiffness and material damping of the drive system. It is observed that servo damping plays an important role in the dynamic behaviour of the system.

Tomei and Tornambe [1988] also used a Lagrangian approach and expanded the generalized coordinates describing the exact shape of the beams constituting the robot in a limited number of terms. Baruah and Tadikonda [1989] described various issues in the dynamics and control of flexible robot manipulator. An approach similar to sub-structure synthesis is used to model the system, where each link is first modeled independently of others. The joint displacements are then used as constraints to synthesize the equation of motion.

The asymptotic perturbation method is an effective tool for the analysis of the distributed parameter model of flexible manipulator. Khorrami [1989] employed the asymptotic perturbation method to two-link flexible manipulator. It holds good for multi-link open kinematic flexible manipulator. It was observed that a parameter (ε) corresponding to the stiffness of the links is naturally embedded in the dynamic equation. As this parameter vanishes, the rigid body dynamics are recovered. Asada *et al.* [1990] proposed a technique based on assumed mode model for general *n*-link case that solves the problem by using special moving co-ordinates, so called virtual rigid link coordinates.

De Luca and Siciliano [1990] developed dynamic model of a planar two-link flexible arm with rotary joints subject to bending deformation in the plane of motion considering payload and hub inertia. A finite-dimensional model of link flexibility is obtained with two assumed modes for each links. The standard Lagrangian approach is followed for the dynamic study of the system. De Luca and Siciliano [1991] presented closed-form equations of motion for planar flexible multi-link robot arm. The kinematic model is based on standard frame transformation matrices describing both rigid body rotation and flexible small deflection. Lagrangian based assumed mode model is used to derive the dynamic model. Explicit equations of motion are detailed for two link case assuming two mode of vibration for each link.

Choi and Krishnamurthy [1994] studied unconstrained and constrained motion control of a planar two-link flexible manipulator. Dynamic model is obtained by using external Hamilton's principle, Galerkin criterion and assumed mode method. The researchers approached to solve the control problem by using feedforward and feedback control torques. Morris and Madani [1995] studied the accurate modeling based on Lagrange-Euler formulation of a two link flexible manipulators. Necessary torques are generated by the corresponding actuators to provoke the desired rotations. It has been shown that the reach is shortened due to its flexibility. The researchers developed a state-space representation of the two-link flexible system, considering it to have two sub-systems— a rigid sub-system and flexible sub-system. Model is used for time response of the deflection at the end-tip of links.

Boyer and Coifflet [1996] developed dynamic equations of motion for multi-link manipulator using the Euler–Newton method. Such models are mainly used for rigid manipulators. Book [1984] and Artega [1998] used a Lagrangian based approach to model the flexible robot arms. Everett *et al.* [1999] showed that it is possible to design a two-link flexible manipulator that has nearly position invariant first natural frequency with wide separation between the first two natural frequencies, to have its behaviour similar to that of rigid manipulator to avoid vibration. Li and Wang [2000] used their analysis to simulate a vertical planar elbow arm. Payload is simulated by attaching additional masses to the arm at any specific locations.

Chen [2001] developed a linearized dynamic model for multi-link planar flexible manipulator, which can include an arbitrary number of flexible links. Flexible links are treated as Euler-Bernoulli beams. The rigid-body motion and elastic deformations are decoupled by linearizing the equations of motion around the rigid-body reference trajectory. Yang *et al.* [2001] studied the tip trajectory tracking control for flexible multi-link manipulator. Lagrangian assumed mode method incorporating the measured linear displacements and angular deflection of flexible links is used to derive the dynamic model of the flexible manipulator. An integrated optical laser sensor system is utilized to measure the tip deformation of the flexible links; an error compensation approach is also proposed.

Green and Sasiadek [2004] demonstrated the relative effectiveness in tracking control of a two-link robot manipulator. They used a rigid dynamics model and PD gains computed on dominant cantilever and pinned-pinned assumed mode frequencies by three different techniques *viz*., inverse dynamics, LQR and fuzzy logic. Lee [2005] showed that the conventional Lagrangian modeling of flexible link robot does not fully incorporate the bending mechanism of flexible link as it allows free link elongation in addition to link deflection. This elongation causes modeling inaccuracy for links with rotation. To correct this, he proposed a new dynamic model.

Zhang *et al.* [2005] derived a partial differential equation model for a flexible two-link manipulator using Hamilton's principle and then transformed this to a form suitable for design of a stable regulation scheme using Lapunov and passivity techniques. This research effectively extended the strain feedback control concept to the nonlinear two-link flexible robot case.

2.3 Experimental Observation

In this section, studies on experimental investigation for the different flexible manipulator done by researchers are derived. Due to complex behaviour of the flexible manipulator, researchers were much interested for its dynamic behaviour observation and to develop control strategies for its control. Roberts and Cannon [1984] demonstrated control strategies for a single-link, very flexible manipulator through a set of experiments, where the position of one end was to be sensed and

precisely positioned by applying torque at the other end. This initial experiments was further used by Rover and Cannon Jr. [1987] to control the vibration through adaptive control algorithm based on the self-tuning regular concept.

Naganathan and Soni [1987] developed a finite element scheme to determine the non-linear coupling effects of link flexibilities, when a manipulator undergoes gross motions at the joints. Experimental investigation has been carried out for observing the peak strains. Bellezza *et al.* [1990] presented exact eigenfunctions for a flexible slewing beam for pseudo-clamped and pseudo-pinned end conditioned. Their experimental measures made on a laboratory prototype validate the theoretical results.

Khorrami and Jain [1992] presented the experimental results for end-point positioning of multi-link manipulator, in which, two stage control design is proposed. First stage is an inner loop non-linear based controller corresponding to the rigid body motion of the manipulator and the second stage is an outer control loop based on linear output LQR design. Magee and Book [1993] compared a modified command filtering technique that eliminates the first two modes of vibration in a large flexible manipulator to track circular trajectory with that of pre-shaped command input. It is effective in eliminating residual vibration. Yoshikawa *et al.* [1994] proposed macro-micro manipulator system that consists of a single PD feedback law for the macro flexible manipulator and a dynamic trajectory tracking control law for the micro rigid manipulator. Effectiveness of the proposed scheme is verified experimentally.

Oakley and Cannon [1988], Khorammi *et al.* [1994], Nagaraj *et al.* [1997] carried out experiments on double-link fixed manipulator for different control aspects. Yang and Sadler [1996] presented a model data based and experimentally oriented method to predict the dynamic response of a time varying and non-linear robotic manipulator with elastic members. Case studies were conducted for robot trajectory planning of a prismatic and revolute manipulator with primary consideration of elasto-dynamically induced positioning inaccuracy. Kress *et al.* [1997] carried out experiments for two-degrees of freedom single link flexible manipulator with hydraulic actuator. Experimental results support the simulation

results. It was also observed that that oscillation-damped controller's performance degrades for condition for which it was not tuned.

Queriroz *et al.* [1998] presented experimental evaluation of two-link direct drive planar robot manipulator. Experimental results seem to indicate that reduced order, model-based controllers with an actuator feedback loop provide relatively good link position tracking. Milford and Asokanthan [1999] derived exact partial differential governing equations for system modes of two-link flexible manipulator. The governing equations are solved numerically to yield the exact eigen-frequencies corresponding to arbitrary angles. The eignefrequencies are strong function of manipulator configuration. The results are compared with an experimental two-link manipulator.

Kumar *et al.* [2000] studied the interaction between human and robot in micro-surgery experimentally. The experimental performance with both linear and non-linear environment is consistent with simple theoretical models. Tokhi *et al.* [2001] presented analytically the dynamic modelling of single link flexible manipulator using finite element method. Proposed model is verified experimentally.

2.4 Shape Optimization

The first application of shape optimization was in the field of structures. Hence, first a section on structural optimization is presented. Afterwards, the shape optimization of flexible manipulators is reviewed.

2.4.1 Structural Optimization

The engineers working in the field of structural optimization attempted first to optimize a flexible beams using fundamental frequency. Niordson [1965] first showed that fundamental frequency of vibration of optimized beam is significantly larger than that of the corresponding uniform beam. He presented a simple successive iteration scheme to solve the optimality equations. Brach [1968] introduced the second area moment (I) and cross-sectional area (A) relation, $I = \gamma_p A^P$, and inves- tigated the particular cantilever optimization problem for $p = 1$.

Here, γ_p is a constant implicitly dependent upon p. Prager and Taylor [1968] presented a uniform method of treating a variety of problems of optimal design of sandwitch structure. Sheu [1968] considered segment-wise constant stiffness for the optimal design of a vibrating cantilever beam.

Karihaloo and Niordson [1973] extended the work of Niordson [1965] to compute the optimal shape functions using successive iteration scheme. They showed that an increase of up to 678% in the fundamental frequency of vibration was possible for vibrating cantilevers with tip mass. Olhoff and Parbery [1982] demonstrated the maximization of the difference between adjacent higher natural frequencies of given order for transversely vibrating beams and rotating shafts. In comparison to a uniform beam or shaft, the frequency difference is substantially increased, particularly for small minimum cross-sectional area constraint values.

Balchut [1982] determined the optimal cross-sectional area of a column with a tip mass minimizing the volume under the given external load, fixed frequency and geometrical constraints. Elwary and Barr [1983] presented the maximization of a given fundamental frequency for a given cantilever beam weight. The beams considered are of rectangular section subjected to a variety of constraints (lower and upper bounds) for maximizing transverse fundamental frequency. Similar way, Berger and Porat [1989] presented the optimal shape of Euler beam subject to space constraints (lower-upper bounds) for maximizing transverse fundamental frequency.

Lio [1993] developed a generalized method for the design of a cantilever cross-section in flexural vibration. The dynamic rigidity of the overhang bar can be increased if the root of a portion of the bar is made of high elastic modulus material while the free end portion is composed of two density material. Wang [1995] simplified and improved the formulation and solution technique presented by Karihaloo and Niordson [1973]. New asymptotic expressions for the optimum design solution have been obtained and verified by numerical results.

All of the above discussed researched in the field of structural optimization were devoted to the beams that are rigidly attached to an inertial frame. But, flexible robotic links must rotate about an axis at the link's base. Also, the base of the flexible link must be rigidly attached to the rotating hub for mechanical support. Thus, the structural optimization results can not be directly carried over into the field

of robotics. On the other hand, optimum design models developed for robotic applications can easily be utilized in structural problems.

2.4.2 Optimum Shape Design of Flexible Manipulators

Up to the early 1990s, a majority of research work was concentrated on the optimization of flexible manipulator from a control perspective. Some researchers included shape design as an integral part of an overall control scheme. Wang and Guan [1992] discussed different models of flexible manipulators and examined the effect of tip loads on the fundamental frequency of vibration modes. They showed that fundamental frequency of vibration is very less affected by both rotary inertia and shear deformation. Wang and Russell [1992] concentrated on the Euler-Bernoulli model of flexible manipulator with tip loads and numerous examples for various tip load design vectors. They also investigated the minimum weight design of a flexible manipulator with no tip load.

Wang [1993] applied previous work in the optimum design of flexible robot arms under close loop control formulation, *i.e.*, mechatronics approach. Wang and Russell [1995] extended their previous work to include constrained designs by expanding the displacement function in a base set of modal shape function derived for uniform links. In the same year, they also presented an innovative new segmentized model of a flexible manipulator for its optimum design through programming techniques.

Xu and Ananthasuresh [2003] employed sequential quadratic programming (SQP) method available in MATLAB for shape optimization of the segment of compliant mechanism. Yoo *et al.* [2005] used the assumed mode method for dynamic modeling of rotating flexible manipulator for modal analysis and then shape optimization is carried out to increase the fundamental frequency of the beam. Dixit *et al.* [2006] presented a finite element model of single link robotic manipulator for revolute as well as prismatic joint. They used SQP for optimizing beam shapes under different optimization conditions and compared its dynamic responses and fundamental frequencies. They presented six optimization problems for explicit optimization of particular dynamic parameter and studied the comparative results.

Gunjal and Dixit [2007] addressed the shape optimization of a rotating beam at different speeds with constraints on its mass and static tip deflection. They studied natural frequencies and dynamic response of the optimized beam. Hegde *et al.* [2009] formulated optimal dynamic design (ODD) of the flexible link robotic manipulator and solved the problem optimally using a finite element method and Interface Theory methodology. In the interface theory methodology, the linear redundant equation in general form with '*n*' number of terms is given by

$$\sum_{i=1}^{n} a_i X_i = b, \tag{2.10}$$

where X_i is the interface variable, 'a_i' is the coefficient and 'b' is the output.

In the same year, Lou *et al.* [2009] presented general framework of the integrated design method for point-to-point control of planar two-link flexible manipulator. Finite element dynamic model is developed and PD control strategy is applied in close loop system. The structural parameters and control parameters are optimized simultaneously. Simulation results show that the integrated design method gives improved system performance.

Finite element method and assumed mode method have been employed widely for dynamic analysis of flexible robotic manipulator. However, finite element method is preferable due to its versatility, high accuracy and convergence. Dynamic behaviour of robotic manipulator can be improved through proper control strategy, but, there is a addition of sub-system which requires further analysis of its stability. Optimum system design is always requisite for overall improvement. Improvement in dynamic response through structural shape optimization has high importance in design step. However, there is no much research carried out on shape optimization of flexible robotic manipulator.

2.5 Challenging Issues

In the field of flexible robotic manipulator, shape optimization is an upcoming research area. There is some research contribution in shape optimization of different structure from 1960s onwards. However, there are only a few publications that try to present in depth information of shape optimization of flexible robotic manipulators. Some challenging issues are as follows:

- The dynamic responses *viz*. natural frequencies, static tip deflection, dynamic tip deflection, hub rotation angle of flexible robotic manipulator are the parameters required to be extremized. Some of the parameters conflict with each other. Under these circumstances, defining objective function to improve explicitly a particular parameter through shape optimization is a challenging issue. The problem is even more difficult in the presence of payloads.
- Robot design is meant for carrying a range of payloads. Thus, it is required to design the objective functions to improve particular dynamic response through shape optimization to cater to a range of payloads.
- Maximization of higher natural frequencies through shape optimization provides higher frequency band-width for operation of the flexible robotic system. Due to node(s) in higher natural frequencies, shape optimization is a challenging issue.
- Multi-link flexible robotic manipulators are more useful in engineering applications. Improved dynamics of multi-link flexible robots through shape optimization is worth exploring.
- Shape optimization of flexible robotic manipulator to improve its dynamics with link's mass constraint is meaningful. To retain the advantages of flexible robot system, active constraints are required to be analysed for their sensitivities.
- Dynamics of optimized flexible robotic manipulator under designed controlled torque excitation needs to be explored.

2.6 Scope and Detailed Objectives of the Present Work

Based on the literature survey and major challenges identified, it is decided to investigate the shape optimization of the robotic flexible manipulators in this thesis with emphasis on the following aspects:

1. **Different objective functions:** Shape optimization of flexible manipulator is the simplest and easiest way to improve its dynamic response. Hence, the first objective is to formulate different objective functions for improving the particular dynamic

response explicitly. Classical technique— sequential quadratic programming is used for optimization nonlinear function under nonlinear constraints. The cross-section of the manipulator is taken as circular, considering aesthetics and ease of manufacturing.

2. **Objective function to cater to a range of payloads:** Robots are generally used for a range of payloads. The shape optimization of the links for a particular payload may not improve the dynamic response at higher payloads. To obtain the overall dynamic response improvement of the robotic system for a range of payloads is a challenging issue and it is the second objective of the thesis.
3. **Maximization of higher natural frequencies:** The third objective is the shape optimization for the higher natural frequency to increase the frequency band-width for smooth operation.
4. **Optimized dynamics of multi-link flexible manipulator:** Dynamics of multi-link flexible robot manipulator is more complex than single link manipulator but there find various applications in engineering. Shape optimization of link(s) to improve the dynamics of multi-link flexible manipulators is fourth objective of this thesis.
5. **Active constraint analysis:** The mass of the manipulator comes out to be an active constraint. A study of the sensitivity of this constraint is the fifth objective of the thesis.
6. **Dynamics under controlled torque**: Dynamics of the optimized flexible robotic manipulator through proper control strategy torque is very important task for a designer. As a last objective of this thesis work, a preliminary study on this aspect is carried out.

Chapter 3

Dynamic Modeling and Optimization of Single Link Revolute-Jointed Flexible Manipulator

3.1 Introduction

Single link revolute-jointed flexible robotic manipulator is a rotating hub-beam system, in which the link may undergo severe deflection during operation. Though it has single link, there are its several engineering applications e.g. cleaning waste tanks, operating microsurgical applications, deburring, surface polishing, grinding, *etc* [Hakki, *et al.*, 2012]. Flexible robotic system has several advantages over the conventional rigid and bulky system. However, due to flexibility, vibration is the serious concern for the researchers. Dynamics of the robotic system can be improved through optimal design and proper control strategy.

It is necessary to describe the modeling of the system accurately. There have been various modeling techniques used by the researchers to describe the behaviors of the flexible system. A common way of modeling flexible robot manipulator is combined Lagrange-assumed mode approach [Book, 1984, De Luca and Siciliano 1991, Yuan *et al.,* 1993, Arteaga, 1998]. This modeling technique is more appropriate for control strategy implementation in real application than finite element method (FEM). However, finite element method is good for dynamic modeling to predict the dynamic behavior of the flexible systems. Particularly, complex boundary conditions are handled comparatively easier than other method.

Galerkin finite element formulation is very much suited for single link flexible robotic system. However, in case of multi-link flexible robotic links, it is very difficult to solve the series of coupled equations. Therefore, in this thesis, basics of mechanics are used with fundamentals of finite element technique to

convert this continuous system to discrete system. Afterwards, Lagrange method is used to obtain the equations of motion of the flexible systems in the finite element matrix form.

3.2 Mathematical Modeling

High speed rotating flexible beams have significant transverse deflections. They behave like a nonlinear elastic beams and exhibit vibratory motions in both chord-wise and flap-wise directions. Robotic manipulators usually work at moderate speed. Induced transverse force in the chord-wise direction due to the applied excitation torque is much higher compared to the gravity force in flap-wise direction. Due to it, vibrations are predominant in chord-wise directions.

The finite element method (FEM) formulation has been developed with the help of basic mechanics described by Usoro *et al.* [1986]. Figure 3.1(a) shows single link flexible manipulator in which ROS and XO_1Y represents the stationary and moving co-ordinate frames respectively. Applied torque is represented by τ and E, I, L, ρ, A, J_h and M_p represent the Young's modulus, area moment of inertia, length, mass density, cross-sectional area, hub-inertia and payload of the manipulator, respectively. Motion of the manipulator is represented by fixed ROS co-ordinate frame and the link of manipulator is considered slender in this work. The transverse shear and rotary inertia effects are neglected and the link is treated as an Euler-Bernoulli beam. The beam is assumed to vibrate predominantly in horizontal plane (ROS), neglecting gravity effects (acting in flap-wise direction).

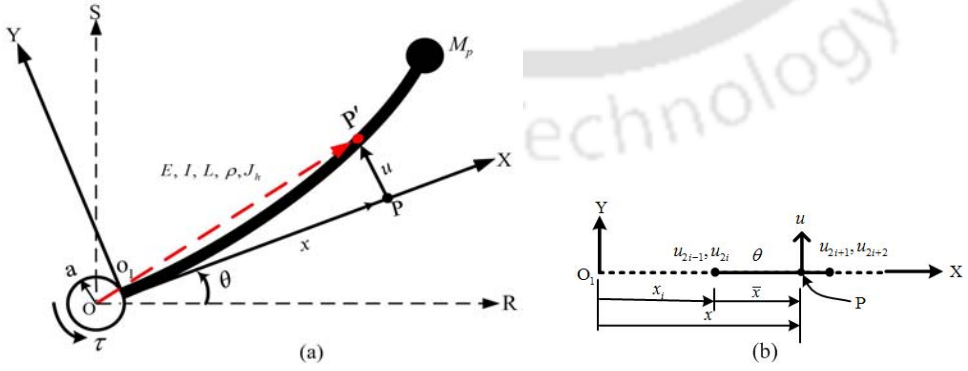

Figure 3.1 (a) Configuration of flexible manipulator, (b) Typical i^{th} element with 5 dof

Consider a point P in the i^{th} element on the manipulator at a distance x from the hub. The point P attains the position P′ with respect to non-inertial frame of reference (ROS) after having rigid body motion $\theta(t)$ and flexural deflection $u(x,t)$. Flexural deflection $u(x,t)$ of point P is approximated in finite element technique as

$$u(x,t) = N_1 u_{2i-1} + N_2 u_{2i} + N_3 u_{2i+1} + N_4 u_{2i+2} = \lfloor N \rfloor \{U\}, \tag{3.1}$$

where $\lfloor N \rfloor = \lfloor N_1 \; N_2 \; N_3 \; N_4 \rfloor$ and $\{U\}^T = \lfloor u_{2i-1} \quad u_{2i} \quad u_{2i+1} \quad u_{2i-2} \rfloor$.

Hermitian shape functions here are

$$\left.\begin{aligned} N_1 &= 1 - 3\left(\frac{\bar{x}}{h}\right)^2 + 2\left(\frac{\bar{x}}{h}\right)^3, \; N_2 = \bar{x}\left(1 - \frac{\bar{x}}{h}\right)^2, \\ N_3 &= 3\left(\frac{\bar{x}}{h}\right)^2 - 2\left(\frac{\bar{x}}{h}\right)^3, \; N_4 = \bar{x}\left\{\left(\frac{\bar{x}}{h}\right)^2 - \frac{\bar{x}}{h}\right\} \end{aligned}\right], \tag{3.2}$$

where h is the element length and $\bar{x}$ is the local variable inside the element.

In FEM formulation, the manipulator is divided into finite number of elements with each element having 5 degrees of freedom. Detail of i^{th} element of the link is shown in Figure 3.1(b), where θ is the hub rotation, u_{2i-1}, u_{2i} and u_{2i+1}, u_{2i+2} are the transverse deflection and slope at the first and second node of the element respectively. The position vector of P′ with respect to non-inertial system ROS is given by

$$\boldsymbol{r} = T_R^0 T_T^0 \boldsymbol{r}', \tag{3.3}$$

where

$$\boldsymbol{r}' = \boldsymbol{o_1 p}' = \begin{bmatrix} x \\ u(x,t) \\ 1 \end{bmatrix} = \begin{bmatrix} (i-1)h + \bar{x} \\ \lfloor N \rfloor \{U\} \\ 1 \end{bmatrix}, \tag{3.4}$$

is the homogeneous position vector of P′ with respect to XO_1Y and T_R^0, T_T^0 are the rotational and translation matrices defined as

$$T_R^0 = \begin{bmatrix} \cos\theta & -\sin\theta & 0 \\ \sin\theta & \cos\theta & 0 \\ 0 & 0 & 1 \end{bmatrix}, \tag{3.5}$$

$$T_T^0 = \begin{bmatrix} 1 & 0 & a \\ 0 & 1 & 0 \\ 0 & 0 & 1 \end{bmatrix}. \tag{3.6}$$

Global position vector of the point P′ is given as

$$\boldsymbol{r} = \boldsymbol{op'} = \begin{bmatrix} X \\ Y \\ 1 \end{bmatrix} = T_R^0 \begin{bmatrix} a + (i-1)h + \bar{x} \\ \lfloor N \rfloor \{U\} \\ 1 \end{bmatrix} = f\left(\theta, u_{2i-1}, u_{2i}, u_{2i+1}, u_{2i+2}\right). \quad (3.7)$$

In finite element method, variables are converted into nodal variables.

Let $Z = \lfloor \theta \quad u_{2i-1} \quad u_{2i} \quad u_{2i+1} \quad u_{2i+2} \rfloor$, then

$$\frac{\partial \boldsymbol{r}}{\partial t} = \left[\frac{\partial \boldsymbol{r}}{\partial Z}\right] \dot{Z}^T. \quad (3.8)$$

3.2.1 Computation of Kinetic Energy of the Link Element

The Kinetic energy of the i^{th} element of the link is given by

$$K_i^e = \frac{1}{2}\int_0^h m \left[\frac{\partial \boldsymbol{r}^T}{\partial t} \cdot \frac{\partial \boldsymbol{r}}{\partial t}\right] d\bar{x}. \quad (3.9)$$

Using chain rule,

$$\frac{\partial \boldsymbol{r}^T}{\partial t} \cdot \frac{\partial \boldsymbol{r}}{\partial t} = \dot{Z}^T \left[\frac{\partial \boldsymbol{r}}{\partial Z}\right]^T \left[\frac{\partial \boldsymbol{r}}{\partial Z}\right] \dot{Z}, \quad (3.10)$$

Substituting Eq. (3.10) in Eq. (3.9),

$$K_i^e = \frac{1}{2} \dot{Z}^T \left[\int_0^h m \left[\frac{\partial \boldsymbol{r}}{\partial Z}\right]^T \cdot \left[\frac{\partial \boldsymbol{r}}{\partial Z}\right] d\bar{x}\right] \dot{Z}. \quad (3.11)$$

Thus, the elemental mass matrix is given by

$$\left[M_i^e\right] = \int_0^h m \left[\frac{\partial \boldsymbol{r}}{\partial Z}\right]^T \cdot \left[\frac{\partial \boldsymbol{r}}{\partial Z}\right] d\bar{x} = \begin{bmatrix} M_{11} + M_{nl} & M_{12} & M_{13} & M_{14} & M_{15} \\ M_{21} & & & & \\ M_{31} & & P_i & & \\ M_{41} & & & & \\ M_{51} & & & & \end{bmatrix}. \quad (3.12)$$

All the constants of the above matrix in Eq. (3.12) are given in Appendix-I.

3.2.2 Computation of Elastic Potential Energy of the Link Element

The potential energy of the i^{th} element of link due to elastic deformation is given by

$$V_i^e = \frac{1}{2}\int_0^h EI \left[\frac{\partial^2 u}{\partial x^2}\right]^2 d\bar{x} = \{U\}^T \frac{1}{2}\int_0^h EI \lfloor N'' \rfloor^T \lfloor N'' \rfloor d\bar{x} \{U\}. \quad (3.13)$$

Thus, elemental stiffness matrix is given by

$$\left[K_i^e\right] = EI\int_0^h \left\lfloor N'' \right\rfloor^T \left\lfloor N'' \right\rfloor d\bar{x} = \frac{EI}{h^3}\begin{bmatrix} 0 & 0 & 0 & 0 & 0 \\ 0 & 12 & 6h & -12 & 6h \\ 0 & 6h & 4h^2 & -6h & 2h^2 \\ 0 & -12 & -6h & 12 & -6h \\ 0 & 6h & 2h^2 & -6h & 4h^2 \end{bmatrix}. \tag{3.14}$$

3.3 Lagrange's Equation of Motion in Discretized Form

The kinetic energy and the potential energy of the system are obtained by computing the energy of each element of the system and then summing over all the elements. The global mass matrix and global stiffness matrix can be obtained as

$$[M] = \sum_{i=1}^{n}\left[M_i^e\right]_g \tag{3.15}$$

and

$$[K] = \sum_{i=1}^{n}\left[K_i^e\right]_g, \tag{3.16}$$

where $\left[M_i^e\right]_g$ and $\left[K_i^e\right]_g$ denote the mass and stiffness matrix of the i^{th} element of the link respectively expressed in global form. Total kinetic energy and potential energy can be expressed as

$$T = \frac{1}{2}[\dot{q}]^T[M][\dot{q}] \text{ and } V = \frac{1}{2}[q]^T[K][q] \tag{3.17}$$

respectively. Here $[q] = [\theta \quad u_1 \quad u_2 \quad . \quad . \quad u_{2n+1} \quad u_{2n+2}]$ is the global nodal vector. The Lagrangian of the system is given by $L = T - V$ and then Lagrange's equations of motion of this dynamic system may be written as

$$\frac{\partial}{\partial t}\left[\frac{\partial L}{\partial \dot{\boldsymbol{q}}}\right] - \frac{\partial L}{\partial \boldsymbol{q}} = \boldsymbol{F}_q, \tag{3.18}$$

where $\boldsymbol{F}_q$ is the generalized force vector. Equation of motion of flexible robotic system is non-linear in nature. However, modelling may be linearized for small vibration amplitude. The global mass and stiffness matrices become constants and equation of motion is expressed as

$$[M]\{\ddot{\boldsymbol{q}}\} + [K]\{\boldsymbol{q}\} = \{\boldsymbol{F}\}. \tag{3.19}$$

Global load vector $\{\boldsymbol{F}\}$ for 'n' number of finite elements are given by $\{\boldsymbol{F}\}=[\tau\ 0\ 0.....0\ 0]^{\mathrm{T}}$. The effects of hub inertia and payload mass are incorporated in the global mass matrix and stiffness matrix using Dirac-delta function as described by Dixit *et al*. [2006].

Neglecting load vector, Eq. (3.19) becomes standard eigenvalue problem and it is solved for natural frequencies of the system. Then, numerical integration of Eq. (3.19) is carried out by using Newmark's integration scheme for obtaining transverse deflection (u), slope (u'), rigid body motion (θ) and their derivatives.

Hub mass and tip mass/payload is defined in terms of β (ratio of hub mass to beam mass) and μ (ratio of tip mass to beam mass). Element system damping is employed using Rayleigh damping giving element damping matrix

$$[C]=\alpha[M]+\lambda[K]. \tag{3.20}$$

The constants α and λ are determined from different modal damping ratios (ξ_1,ξ_2). After assembling element equations, the global system governing equation can be expressed as

$$[M]\{\ddot{\boldsymbol{q}}\}+[C]\{\dot{\boldsymbol{q}}\}+[K]\{\boldsymbol{q}\}=\{F\}, \tag{3.21}$$

where [*M*], [*C*] and [*K*] are the global mass, damping and stiffness matrices respectively.

Concentrated load Q acting on any element is incorporated as a distributed load in the element load vector using Direc-delta function. For example, for a concentrated load at 1st node of an element:

$$\{F^e\}=\int_0^h Q\{N^e\}\delta(x-0)\mathrm{d}x=Q\{N^e\}\big|_{x=0} \tag{3.22}$$

Numerical integration of Eq. (3.19) is carried out by using Newmark's integration scheme [Bathe, 1996] to obtain transverse deflection u, rigid body motion θ and its derivative $\dot{\theta}$. Following approximation are made for nodal variables in this method:

$$\left\{{}^{t+\Delta t}U\right\}=\left\{{}^{t}\dot{U}\right\}+\left[(1-\delta)\left\{{}^{t}\ddot{U}\right\}+\delta\left\{{}^{t+\Delta t}\ddot{U}\right\}\right]\Delta t, \tag{3.23}$$

$$\left\{{}^{t+\Delta t}U\right\}=\left\{{}^{t}U\right\}\Delta t+\left[\left(\frac{1}{2}-\eta\right)\left\{{}^{t}\ddot{U}\right\}+\eta\left\{{}^{t+\Delta t}\ddot{U}\right\}\right]\Delta t^2 \tag{3.24}$$

For integration accuracy and stability, constants δ and η should satisfy: $\delta \geq 0.5$ and $\eta \geq 0.25(0.5+\delta)^2$. In this work, $\delta = 0.5$ and $\eta = 0.25$ has been taken based on some numerical experiments. The time step is kept small (0.0002s) satisfying the condition $\Delta t \leq \left(\frac{2}{\omega_{\max}} = \Delta t_{\text{cr}} \right)$ [Bathe, 1996], where $\omega_{\max}$ is the highest frequency of the beam and Δt_{cr} denotes the maximum time step consistent with numerical stability.

3.4 Boundary Conditions

3.4.1 Natural Boundary Conditions

Natural boundary condition is applied at the free end of the link *i.e.*, bending moment and shear force are zero at the last node of the link given by

$$EI \left. \frac{\partial^2 u}{\partial x^2} \right|_{(L,t)} = 0, \tag{3.25}$$

and

$$\frac{\mathrm{d}}{\mathrm{d}x} \left(EI \frac{\partial^2 u}{\partial x^2} \right) \Bigg|_{(L,t)} = 0. \tag{3.26}$$

3.4.2 Essential Boundary Condition

Link is considered as a rotating cantilever beam. Hence, slope and deflection at the first node of the link should be zero with respect to time *'t'*, *i.e.,*

$$u(0,t) = 0, \tag{3.27}$$

and

$$\left. \frac{\partial u}{\partial x} \right|_{(0,t)} = 0. \tag{3.28}$$

For finding out the beam frequency, hub rotation is arrested.

3.5 Model Validation

The equation of motion of the system is given by Eq. (3.19). The developed model is popularly known as zeroth order approximation coupling (ZOAC) for inextensible beam. First order approximation coupling (FOAC) is more accurate model to

represent the dynamics of high speed rotating flexible link systems. However, the modeling is highly complex and nonlinear. As the robotics system operates at moderate speed, the model is linearized by neglecting the nonlinear term (M_{nl}) of the elemental mass matrix in Eq. 3.12.

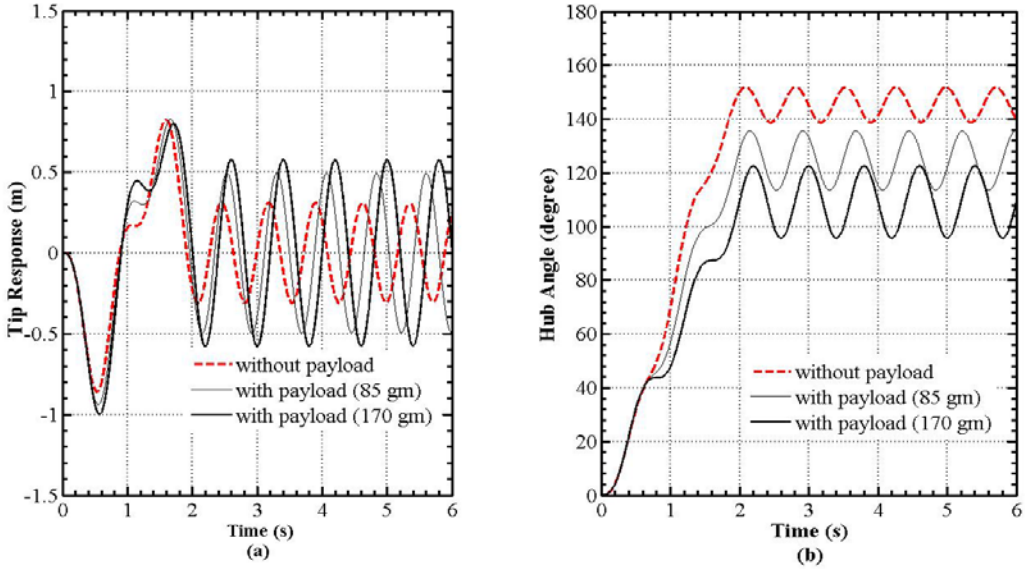

Figure 3.2 (a) Tip response of the beam, (b) Rotating angle of the hub

The structural dimension of Cai *et al.*[2005] are considered for the validation of result. Here the same sinusoidal excitation torque ($7\sin \pi t$) Nm acted for 2 sec about the axis of rotation is considered. Simulation results for dynamic tip deflections and hub angles for without payload and payloads are plotted in Figure 3.2. It is observed that the linearized model here at very high torque amplitude (7 Nm), tip responses and hub angles are very close to that of Cai *et al.* [2005]. The results of Cai *et al.* [2005] are not plotted here to maintain the clarity of the figures.The developed model may be considered for shape optimization of rotating link for four different optimization problems.

3.6 Optimization Procedure

Length of the manipulator is generally decided based on the kinematics and space constraints of the robotic system. Varying cross-section is the only option for optimization to improve its dynamic behaviour. In this work, circular cross-section

is considered because of the ease of the manufacturing as well as to have equal stiffness in all directions.

Robotic system is interdisciplinary in nature and it becomes a challenging task for a designer to meet its multi-objective characteristics *viz.* maximization of fundamental frequency, required displacement with less torque/force, minimization of manipulator mass, response/vibration time, static tip deflection, *etc*. Some of the objectives are conflicting with respect to one another [Dixit *et al.,*2006]. Maximization of fundamental frequency is considered as an objective for high speed operation of the robotic system and minimization of static deflection is considered as an objective for accurate positioning of the robotic manipulator. General form of an optimization problem is expressed as

Objective function (Maximize/Minimize)

$$f(X), \tag{3.29a}$$

subject to

$$g_j(X) \le 0, \quad j=1, 2,\ldots, m \tag{3.29b}$$

$$h_k(X) = 0, \quad k=1, 2,\ldots, n \tag{3.29c}$$

and

$$X^L \le X \le X^U, \tag{3.29d}$$

where $X = [d_1 \;\; d_2 \;\ldots\; d_{20}]^T$ is a design vector with d_i indicating diameter of the i^{th} finite element, $f(X)$ indicates the objective function (fundamental frequency or static tip deflection) and $g_j(X)$ and $h_k(X)$ indicate j^{th} constraint among m inequality constraints and k^{th} constraint among n equality constraints respectively. X^L and X^U are the vectors of lower and upper bounds of design variables respectively.

For known design variables, the optimization problem may be approximated by a quadratic program. A Quadratic program (QP) is a nonlinear programming problem having quadratic objective function and linear constraints. SQP solves a QP at each iteration till the convergence is obtained. There are several variants of SQP method. The principle of SQP is explained in Appendix-VII. The MATLAB function "*fmincon*" is used in this work which uses SQP for constrained optimization of nonlinear function.

3.7 Results and Discussion

Numerical study is carried out for the manipulator by considering uniform diameter of 0.01 m, length of 0.75 m, mass of 0.1596 kg and Young's modulus of elasticity 71 GPa. This structural model is considered with hub inertia (J_h) of 0.003 kg.m^2 and hub radius (a) of 0.015 m. Dixit *et al.* [2006] did not consider hub inertia and hub radius. Further, the cross-section of flexible link is considered circular preferably for two-dimensional effect in its shape optimization. Its modal damping ratios for the first and second mode are taken as 0.11 and 0.29 respectively which are found experimentally by Dixit *et al.* [2006] for the considered structural dimension.

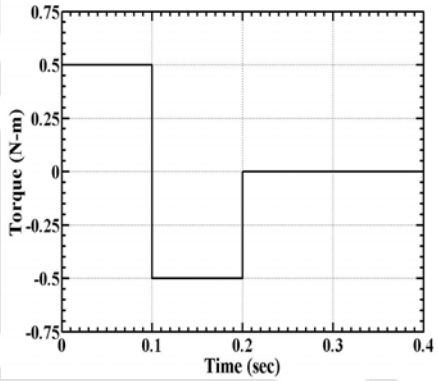

Figure 3.3 Bang-bang torque profile

Table 3.1 Different optimization problems

Optimization Problems for	Objective	Constraints
Prob-I	Maximization of fundamental beam frequency (as a cantilever beam)	$M - M^* \le 0$
Prob-II	Minimization of static tip deflection	$M - M^* \le 0$
Prob-III	Maximization of fundamental beam frequency	$M - M^* \le 0$ & $\delta_{\text{tip}} - \delta^*_{\text{tip}} \le 0$
Prob-IV	Maximization of fundamental system (hub+beam) frequency	$M - M^* \le 0$
Permissible Bound : $X^{LB} < X < X^{UB}$		

In Table 3.1, M is the mass of the optimized manipulator, M^* is the prescribed mass of the uniform beam manipulator and δ_{tip}, δ^*_{tip} are the static tip deflection of the optimized manipulator and uniform beam manipulator respectively. X^{LB}, X^{UB} are the prescribed minimum and maximum diameter of the beam elements (X) respectively. Optimized beams are subjected to a bang-bang torque of magnitude 0.5 Nm (Figure 3.3) about the axis of rotation for its dynamic analysis. For comparative static tip deflections, 1 N static load is considered at the end of the manipulator.

Optimization problems are defined in Table 3.1 for shape optimization of the manipulator. They are designated from Prob-I to Prob-IV. Mass of the manipulator is considered a constraint in all optimization problems in addition to other constraints. To assess the adequacy of the simulation results, dynamic behaviour of the flexible manipulator in the time domain is compared and found in well agreement (within ±2%) with the results of Dixit *et al.* [2006] for the case of no payload and no hub mass.

3.7.1 Shape Optimization

Different optimization problems yield different shapes. Various circular solid shapes having minimum diameter up to 2 mm are obtained by solving the optimization

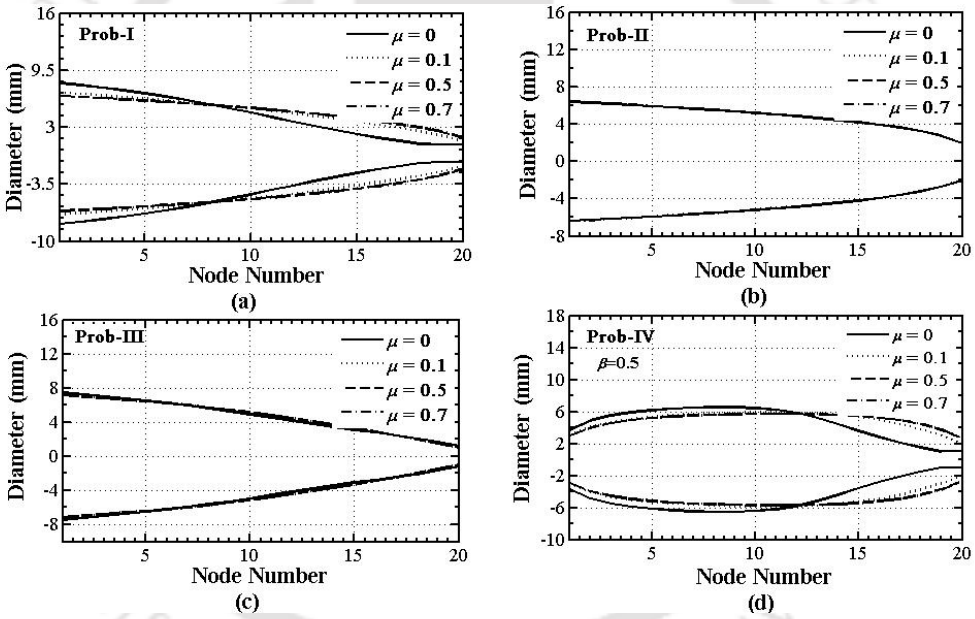

Figure 3.4 Optimized shapes obtained through optimization problems-I, II, III and IV

problem as shown in Figure 3.4. Optimized shapes show the cross-sectional diameter variation along the length of the revolute joint manipulator for the variation of tip mass (μ=0–0.7) and hub mass (β=0.1–0.9). It is observed that there is no effect of hub mass on the first three optimization problems I, II and III, since the manipulator is considered as a cantilever beam and hub is acting as a fixed support.

When the entire system (consisting of hub and beam) is considered for the optimization of fundamental frequency as in optimization problems IV, there is a

possibility for having different optimum shapes for different tip mass (μ) as well as hub mass (β).

3.7.1.1 Beam/System Frequency

First Fundamental frequency is an important parameter of a system, which completely depends upon the system parameters. For high speed operation of the manipulator, fundamental frequency needs to be maximized. Figure 3.5 shows the variation of optimum beam and system frequency with corresponding hub mass and payload. From Figure 3.5(a), it is observed that Prob-I gives higher beam frequency compared to other optimization problems, whilst Prob-II has almost same fundamental frequency as that of Prob-I. Figure 3.5(b) shows that Prob-IV gives higher system frequency compared to other beams. The hub mass does not have much significant effect on the fundamental frequency of Prob-IV, except that a combination of low hub mass and high tip mass produces convergence problem.

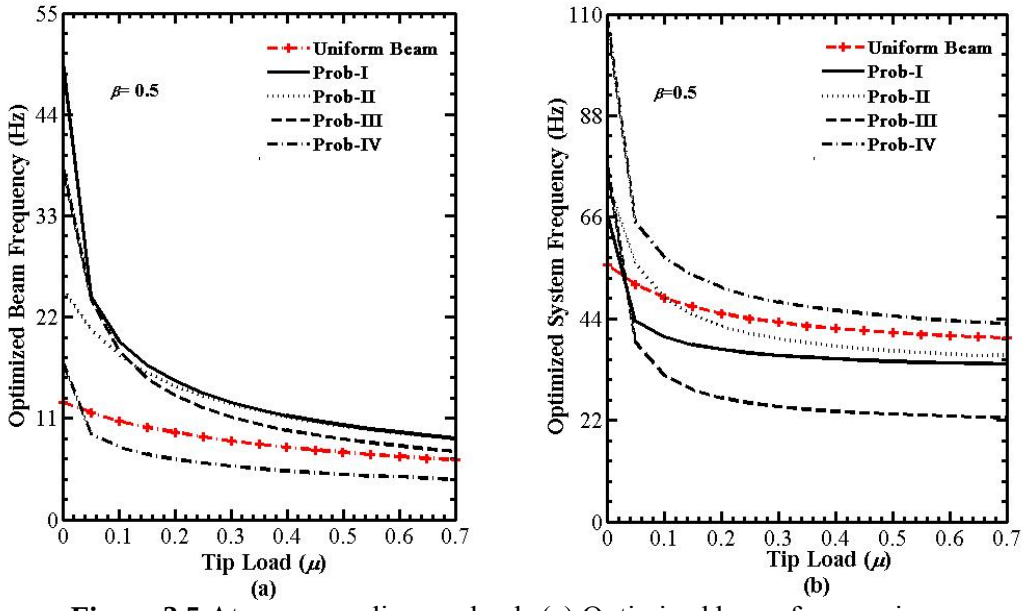

Figure 3.5 At corresponding payloads (a) Optimized beam frequencies, (b) Optimized System frequencies

It is observed that optimized shape of the manipulator treating it as a cantilever beam (Prob-I, II and III) gives higher beam frequency and lower system frequency and vice-versa holds good in case of Prob-IV, where the hub-beam system is considered together. As there is no effect of hub mass on Prob-I, II and III, there is a particular beam frequency of optimized beam corresponding to a payload. However,

in actual practice, beam optimized at certain tip mass (μ) is used for some range of payloads to minimize the robot's operation time. It is not possible to change the shape of manipulator with variation in tip mass. Hence, a strategy needs to be developed for optimizing the manipulator for a range of tip mass (section 3.6.2).

3.7.1.2 Hub Angle and Static Tip Deflection

Hub angle is an important dynamic response of the system and is required to be maximized. Hub angle of the optimized beams due to bang-bang torque are shown in Figure 3.6 for different tip loads. For beams with tip load, Prob-III attained the

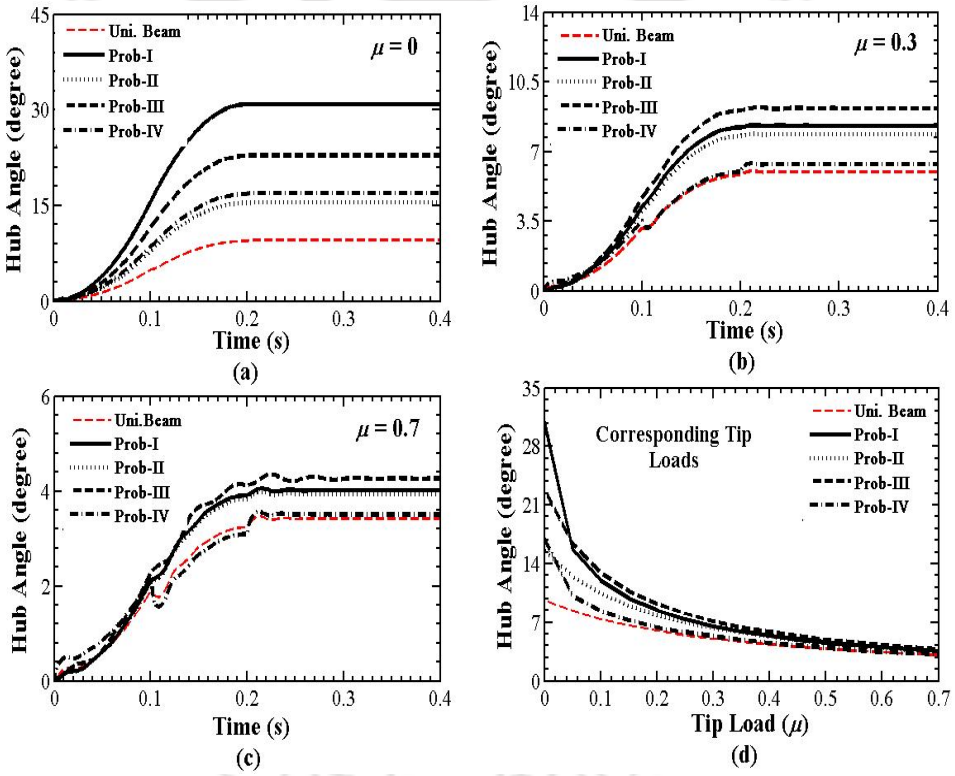

Figure 3.6 Hub angle due to bang-bang torque of optimized beams for (a) μ= 0, (b) μ= 0.3, (c) μ=0.7 and (d) corresponding payload, with β=0.5

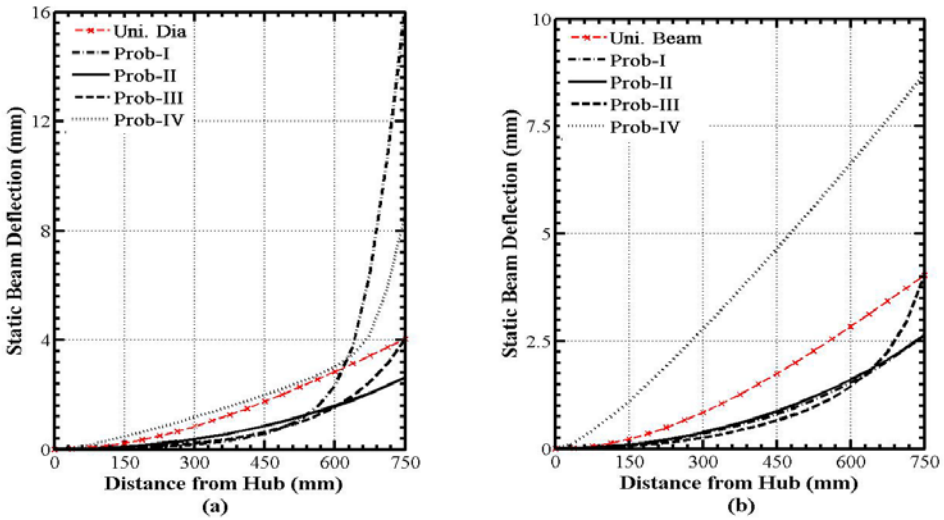

Figure 3.7 Static beam deflections due to 1 N tip load of optimized beams at (a) μ =0 & β=0.5,(b) μ =0.7 & β=0.5

highest hub rotation for a given torque and Prob-I for no payload case. However, each optimized beam attains higher hub rotation than the uniform diameter beam. Hub angle rotation for a given torque, of shape optimized link decreases with increase of payload (Figure 3.6d). Static tip deflection is also an important design parameter of the flexible manipulator. It is required to be minimized for good positional accuracy. Static deflections of the optimized beams for two payloads (μ=0, 0.7) are shown in Figure 3.7 with 1 N static load at the tip of the manipulator.

It is observed that in no payload case (Figure 3.7a) Prob-I provides the highest tip deflection, although from beam frequency maximization point of view, it is the optimal shape. But, it improves its static deflection with increase of payload consideration for shape optimization. The shape providing the minimum tip deflection may provide a very low fundamental frequency. In practice, the designer has to consider both the aspects.

3.7.1.3 Dynamic Response

Dynamic responses of the optimized beams and uniform beam due to bang-bang torque are computed by using Newmark's method. These are shown in Figure 3.8. Dynamic response comprising tip displacement, rising time and total vibration time is required to be minimized during the operation for enhancing the productivity of the system. To get the better overall dynamic response, stiffness and mass of the

system are required to be maximized and minimized respectively. Damping of the system is required to be optimal, as both under and over damped robotic systems have some drawbacks. However, optimization of damping is not considered in this work.

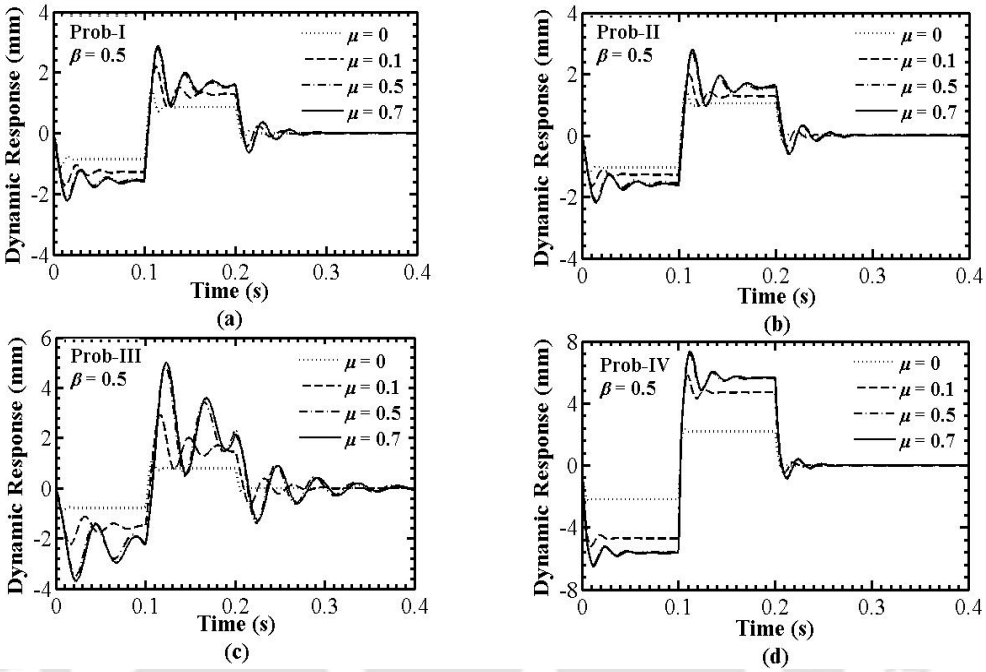

Figure 3.8 End point dynamic displacement of optimized beams due to bang-bang torque with corresponding payloads (a) beam-I, (b) beam-II, (c) beam-III and (d) beam-IV

Dynamic response of the optimized beams are plotted in Figure 3.8 for bang-bang torque. It is observed that vibration increases with increase of payloads. However, Prob-I and II have the minimum vibration. Later, a optimization problem is considered explicitly to suppress the vibration (Section 4.6.4).

3.7.1.4 Comparison of Optimization Problems and Links

Table 3.2 shows the comparative performance of various objective functions. The numerical values are shown in Tables 3.3 and 3.4. From these tables, it is very clear that the beam and system frequencies of the various optimized beams vary dramatically with the change of tip load even in case of flexible uniform beam manipulator also. Prob-III has higher beam frequency and higher hub angle than

uniform beam manipulator (Figures 3.5 and 3.6), however in all other cases, it is not superior.

Prob-IV gives higher system frequency (Figure 3.5b) than uniform beam manipulator but all other dynamic characteristics *viz*., beam frequency, static tip deflection, hub angle, maximum dynamic displacement, vibration time, *etc.,* are not superior. However, Prob-I and II give significant improvement in their dynamic characteristics with respect to uniform beam manipulator except for system frequency.

Table 3.2 Comparative performance of different optimized beams

Criterion	Rank		
	1st	2nd	3rd
Beam Frequency	I	II	III
System Frequency	IV	II	I
Static Tip Deflection	II	I	III
Maximum Dynamic Tip Deflection	II	I	III
Maximum Dynamic Hub Velocity	III	I	II
Hub Rotation	III	I	II
Vibration Time	IV	II	I

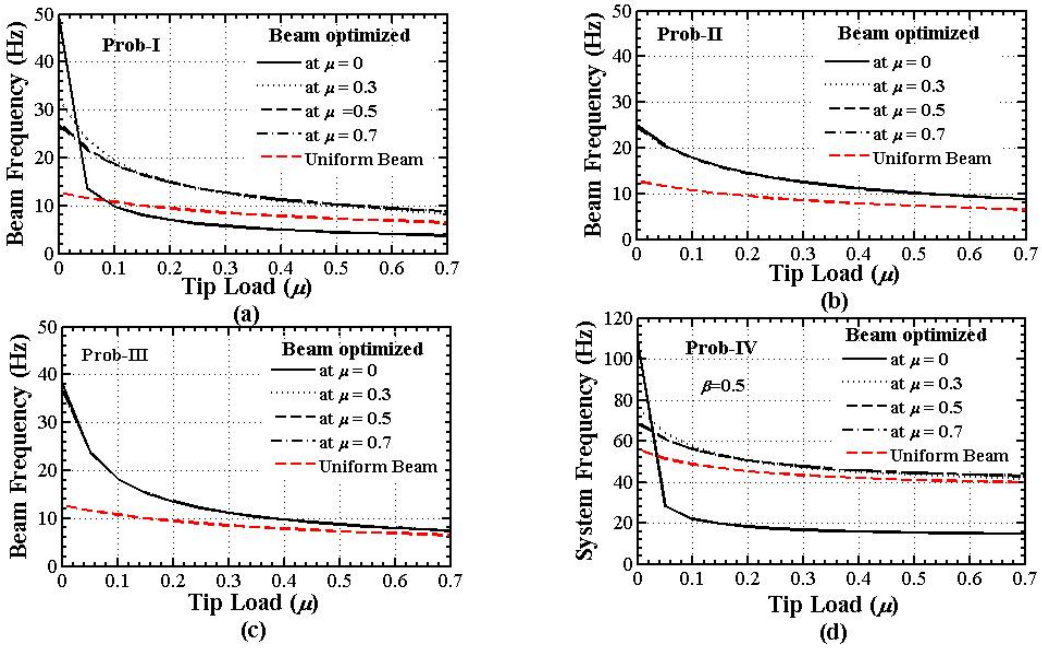

Figure 3.9 Beam/System frequencies of a optimized beam at a particular hub/tip mass for varying tip loads (0–0.7)

In optimization problems-IV, flexible manipulator is considered as a hub-beam system. The optimized beam may not be the best for all the goals. However, the optimization problems I, II and III provide superior overall performance in comparison to optimization problems IV. Figure 3.9 shows that variation of beam and system frequency with respect to payload of a beam which is optimized for particular hub and payload. In practice, the beam optimized for the particular value of tip mass may not be used for that particular tip mass only. However, the hub mass can be considered constant for a particular manipulator. In case of optimization problem–I and IV, beams optimized at no tip load (μ=0) yield drastic decrease of beam or system frequency (even lesser than uniform beam manipulator), when used for higher payloads.

Table 3.3 Comparison of fundamental frequencies and static tip deflection of various optimized beams at different payloads with β=0.5

Beam Shapes	Fundamental frequency (Hz)						Static tip deflection (mm)		
	Beam			System					
	μ=0	μ=0.1	μ=0.5	μ=0	μ=0.1	μ=0.5	μ=0	μ=0.1	μ=0.5
Uni.Beam	12.731	10.746	7.301	55.687	48.525	40.965	4.034	4.034	4.034
Prob-I	49.780	19.392	10.248	66.763	40.027	34.749	16.004	2.717	2.669
Prob-II	24.967	17.869	10.161	73.691	48.659	36.997	2.629	2.629	2.629
Prob-III	38.336	18.304	8.730	77.524	31.652	23.296	4.034	4.034	4.034
Prob-IV	17.076	7.909	4.905	109.19	57.285	44.502	8.577	8.540	8.710

Table 3.4 Comparison of hub angles, maximum tip deflection and maximum hub velocity of various optimized beams at different payloads with β=0.5

Beam Shapes	Angular displacement (deg.)			Max. tip deflection (mm)			Max. hub velocity (deg./sec)		
	μ=0	μ=0.1	μ=0.5	μ=0	μ=0.1	μ=0.5	μ=0	μ=0.1	μ=0.5
Uni.Beam	9.567	7.360	3.828	3.239	3.527	3.977	96.718	78.109	50.405
Prob-I	30.887	11.971	4.616	1.367	2.192	2.774	308.277	119.452	49.528
Prob-II	15.467	10.423	4.518	1.428	1.999	2.674	154.377	104.033	49.028
Prob-III	22.841	12.935	4.925	1.096	2.907	4.820	227.970	129.312	53.072
Prob-IV	16.961	8.367	3.954	2.350	5.768	7.221	169.283	124.600	142.125

However, as there is not much change in the shape of optimized Prob–II and III, there is no such observation. It is also observed that beams optimized at lower payload are more sensitive to the variation of tip load. From Table 3.2 and the above discussion, it is clear that a designer can opt Prob-I, II or III for robotic manipulator

depending on the requirement. Dynamic response viz., fundamental frequency, static tip deflection, angular displacement, maximum dynamic tip deflection and maximum hub velocity are presented numerically in the tabulated form (Tables 3.3 and 3.4).

3.7.2 Proposed Optimum Shape for Varying Tip Loads

In real situation, an optimized beam is used for a range of payloads. Hence, a single optimized shape has to be obtained for catering to different payloads, which minimize the overall deviation from the optimum shape in a least square sense. It has been decided to cover the entire range of payload by 15 discrete values of payloads. Two objective functions A and B are proposed with the constraints listed in Table 3.1 for the optimization problems-I, II and III for range of payloads.

The objective functions are as follows:

(1) Objective function A:

For Prob-I and III

$$E_1 = \sum_{i=1}^{15} \left(F_{\mu_i} - f_{\mu_m} \right)^2 \tag{3.30a}$$

For Prob-II

$$E_2 = \sum_{i=1}^{15} \left(D_{\mu_i} - \delta_{\mu_m} \right)^2 \tag{3.30b}$$

where f_{μ_m} & δ_{μ_m} are the frequency and static tip deflection of the shape optimized beam at mean payload respectively and F_{μ_i}, D_{μ_i} are the frequencies and static tip deflections of the different shape optimized beams at payloads μ_i respectively (i=1 to 15). The values of μ_i vary from 0 to 0.7 with increment 0.05 and f_{μ_m} and δ_{μ_m} are the frequency and static tip deflection of the shape optimized beam at average payload respectively. The objective function A is the deviation of the fundamental frequencies/static tip deflections at different payloads with that of fundamental frequency/static tip deflection at average payload respectively. Minimization of this function through shape optimization of the manipulator reduces the range of fundamental frequency/static tip deflection for varying payloads. Also, it exhibits its

vibratory frequencies (Prob-I and III) and static tip deflections (Prob-II) nearby to that of average payload during its operation for varying payloads.

(2) Objective function B:

For Prob-I and III

$$E_3 = \sum_{i=1}^{15} \left(F_{\mu_i} - f_{\mu_i} \right)^2 \tag{3.31a}$$

For Prob-II

$$E_4 = \sum_{i=1}^{15} \left(D_{\mu_i} - \delta_{\mu_i} \right)^2 \tag{3.31b}$$

where f_{μ_i}, δ_{μ_i} are the frequencies and static tip deflections of the shape optimized beam at payloads μ_i. Minimization of function B through shape optimization of

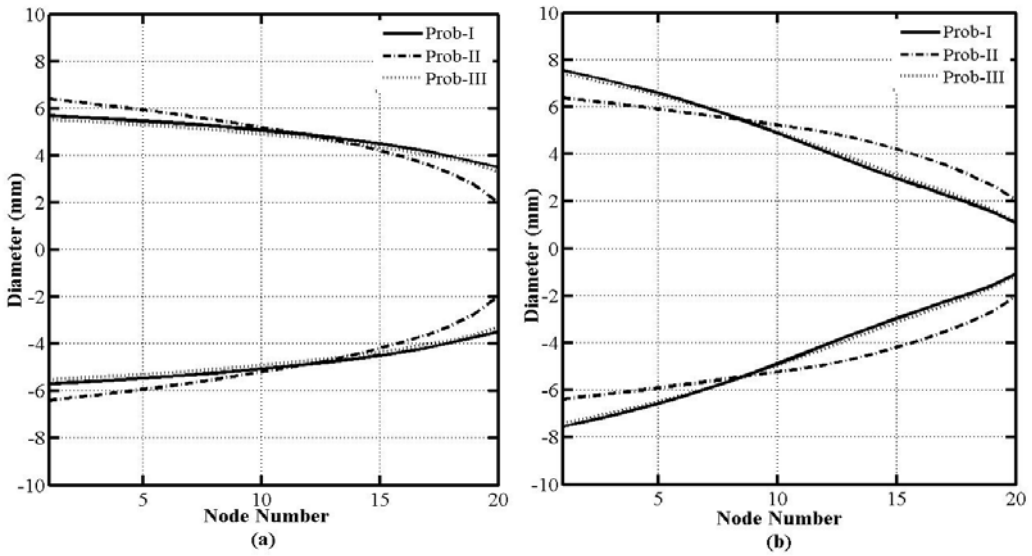

Figure 3.10 Propose optimized shapes based on (a) optimization problem-A (b) optimization problem-B

manipulator is equally important for its operation to cater to varying payloads. It allows the manipulator to have minimum variation of fundamental frequencies and static tip deflections with that of optimal values of the corresponding payloads.

3.7.2.1 Comparative Study of Proposed Designed Shapes

From Table 3.2 and the above discussion, it is clear that a designer can opt Prob-I, Prob-II or Prob-III for robotic manipulator depending on the requirement. To cater to the different payloads on these beams, shape optimized beams are obtained based on the objective functions A and B as shown in Figure 3.10. A comparative dynamic characteristic of these single optimized shapes are plotted in the Figure 3.11 for Prob-I and Figure 3.12 for Prob-II. Similar trend of dynamic response of Prob-III is observed like Prob-I (Figure 3.11). It is observed that no shape is optimal from the point of view of all criteria. For Prob-II, both the objective functions (A or B) provide the same result (Figure 3.12).

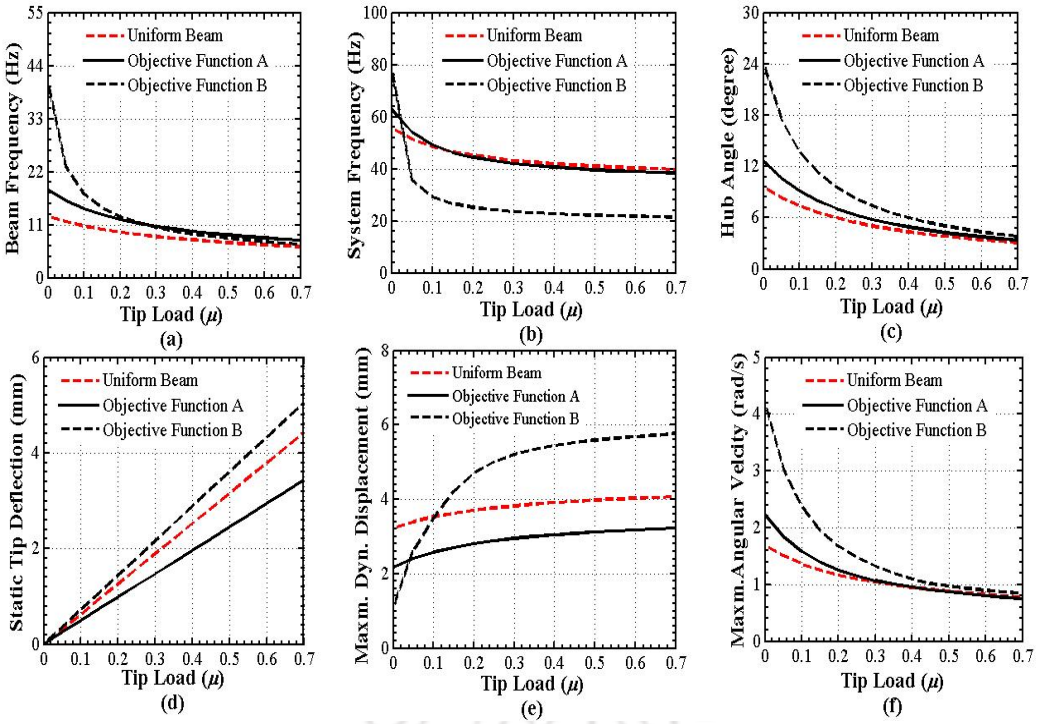

Figure 3.11 Comparative results of shape optimized Prob-I

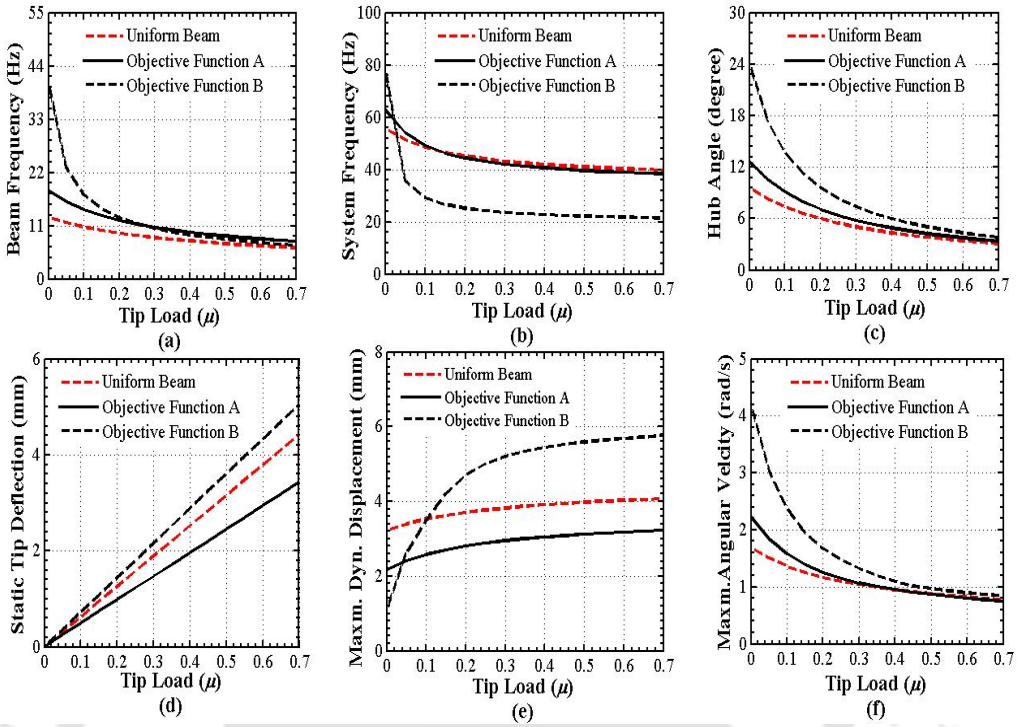

Figure 3.12 Comparative results of shape optimized Prob-II

3.7.3 Effect of Different Excitation Torque Profile

For the numerical study, manipulator is considered of length 750 mm, 159.6 gm mass and having Young's modulus of elasticity 71 GPa. This is the same data as taken in

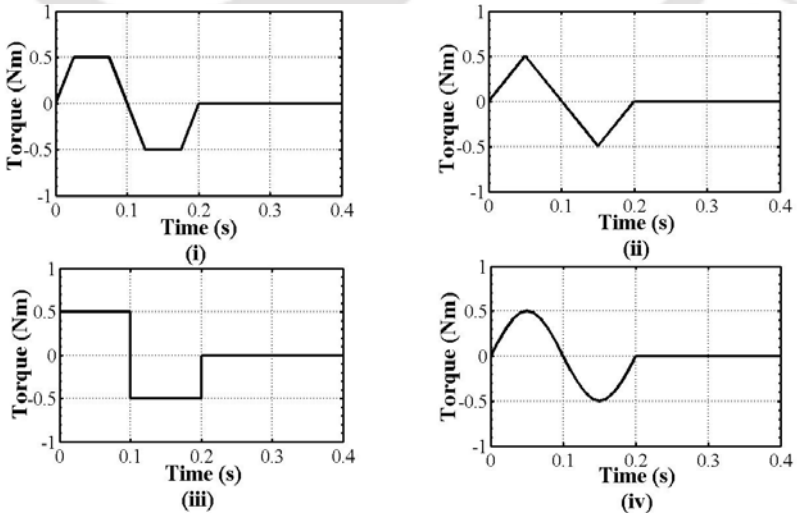

Figure 3.13 Input torque : (i) Torque-I , (ii) Torque-II , (iii)Torque-III, (iv) Torque-IV

Dixit *et al.* [2006], where modal damping ratios of first and second mode of vibration are taken as ξ_1=0.011 and ξ_2=0.029 respectively. Proportional damping of the manipulator can be expressed using modal damping coefficients. Four different type of input torque are considered as shown in Figure 3.13 to predict the dynamic behavior of the optimized beams.

3.7.3.1 Hub Angle

Angular displacement (hub angle) of a robotic system is important for a applied input torque. In Figure 3.14, Prob-II optimized under optimization problem-A (Prob-IIA) gives the maximum hub angle for all type of torque profiles. However, beam optimized under optimization problem-B (Prob-IB) gives the highest hub rotation (Figure 3.15). There is not much difference in hub angle between Prob-IIIB and Prob-IB.

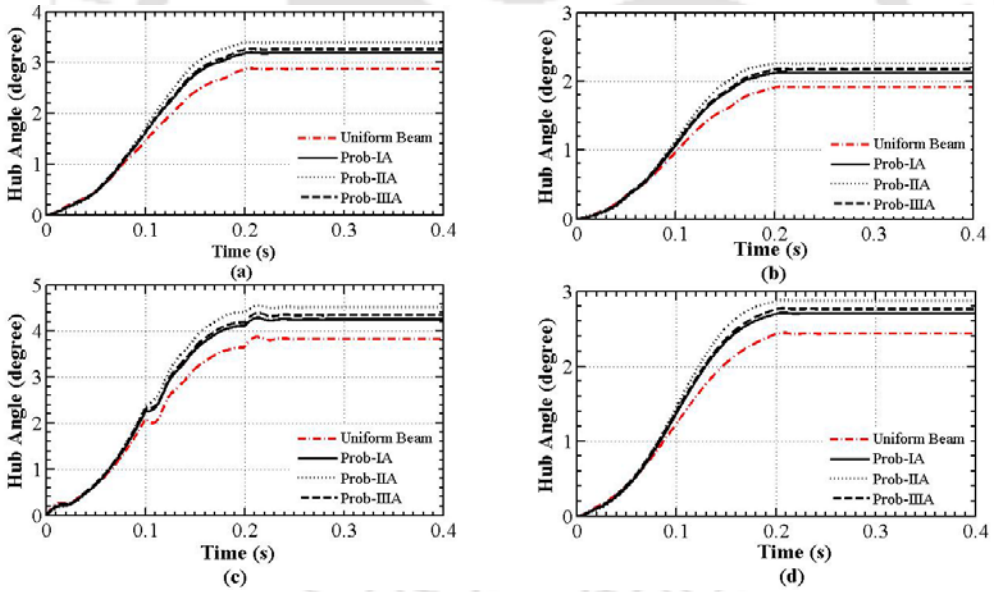

Figure 3.14 Variation of hub angles due to : (i) Torque-I, (ii) Torque-II, (iii) Torque-III , (iv) Torque-IV

Importantly, all the optimized beams give higher hub angle than uniform beam in both the optimization problems. Beams optimized in both the optimization problems A & B give maximum hub rotation under Torque-III (bang-bang) torque.

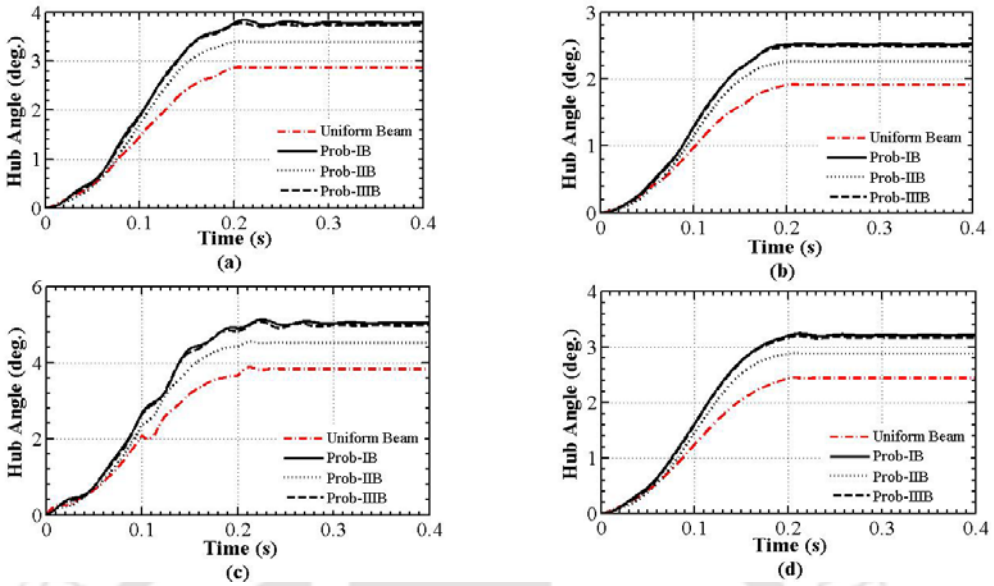

Figure 3.15 Variation of hub angles due to (i) Torque-I, (ii) Torque-II , (iii) Torque-III , (iv) Torque-IV

3.7.3.2 Dynamic Tip Deflection

Excessive tip displacement is undesirable for any robotic system. Tip displacements of the optimized beams are shown in Figure 3.16 and Figure 3.17. Prob-IIA and IIB

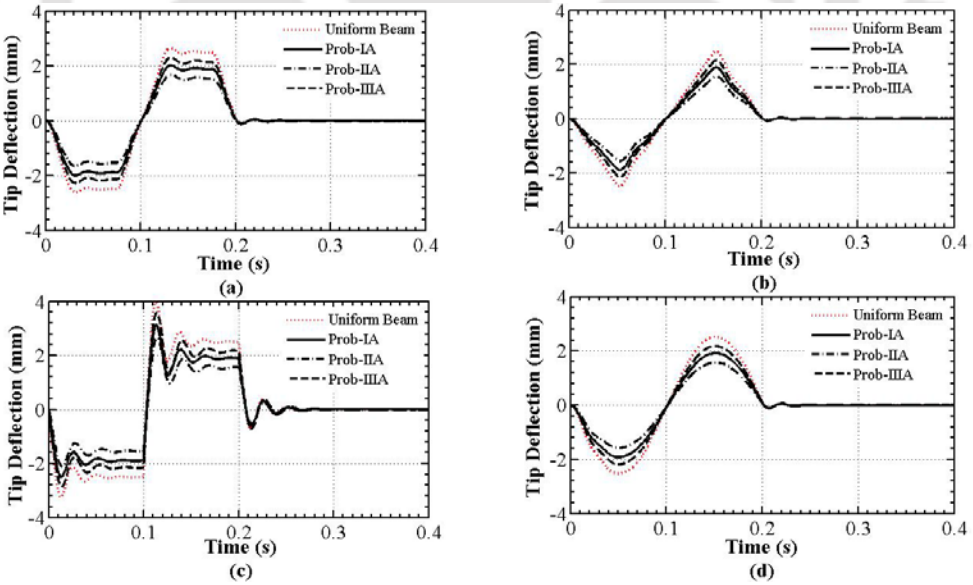

Figure 3.16 Dynamic response due to : (i) Torque-I, (ii) Torque-II , (iii) Torque-III , (iv) Torque-IV

exhibits the lowest maximum tip deflection for all type of torque inputs. All the optimized beam's the maximum tip deflection is lower than that of uniform beam.

Out of four torque profile, Torque-III (bang-bang) produces maximum tip deflection to all the optimized beams.

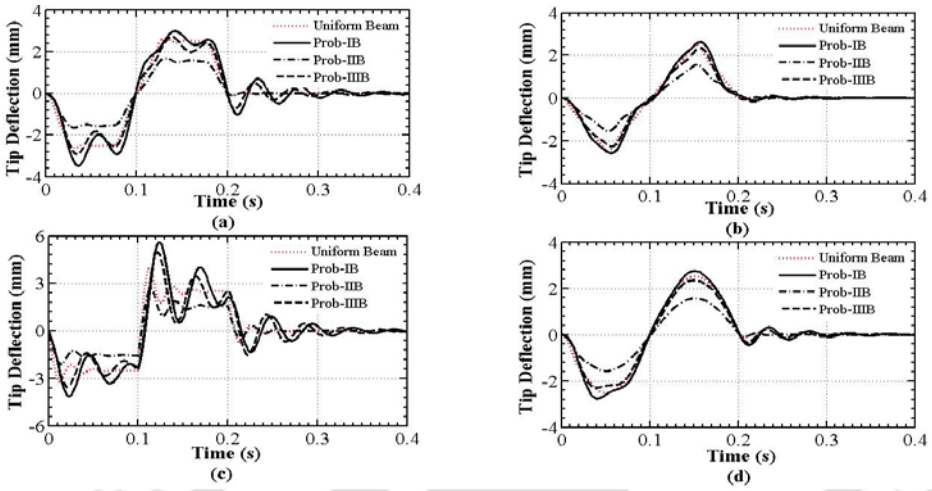

Figure 3.17 Dynamic response due to : (i) Torque-I, (ii) Torque-II , (iii) Torque-III , (iv) Torque-IV

3.7.3.3 Bending Stress

Variation of maximum bending stress at the hub and beam interface is shown in

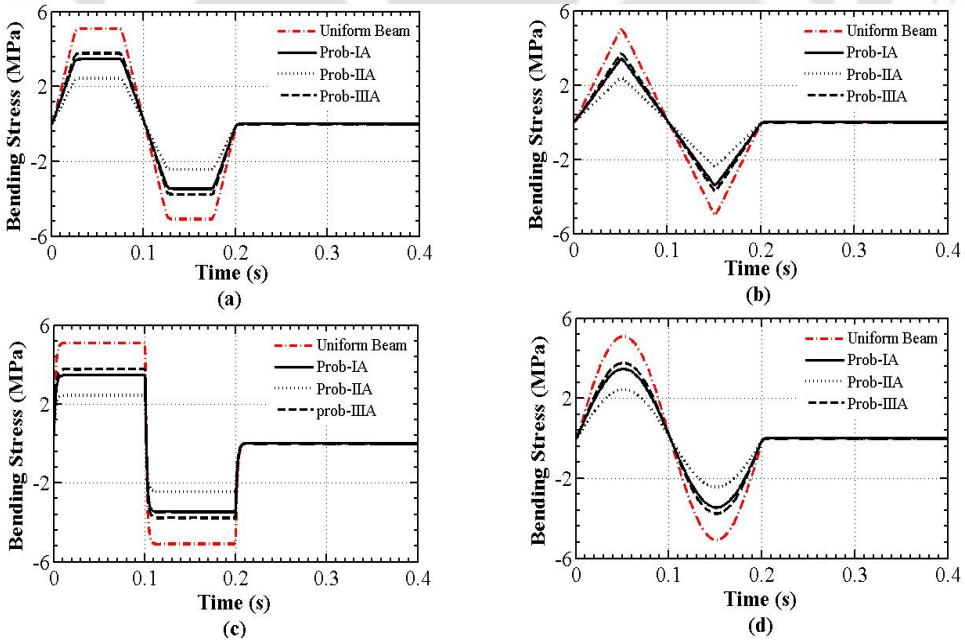

Figure 3.18 Variation of maximum bending stress at the hub-beam interface due to : (i) Torque-I, (ii) Torque-II , (iii) Torque-III , (iv) Torque-IV

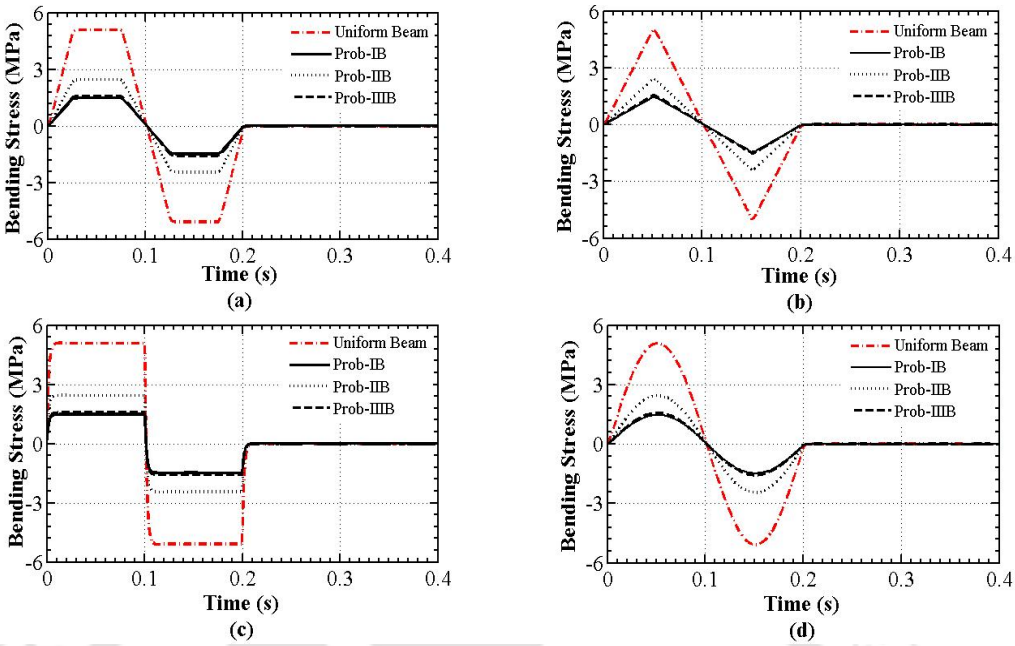

Figure 3.19 Variation of maximum bending stress at the hub-beam interface due to (i) Torque-I, (ii) Torque-II , (iii) Torque-III , (iv) Torque-IV

Figure 3.18 and Figure 3.19. For strength and load carrying capacity point of view, bending stress of the robotic system should be known during its operation. It is observed that all the optimized beams have less induced stress for all type of excitations with respect to uniform beam. Beam optimized under optimization problem-A (Beam-IIA) or optimization problem-B (Prob-IB) produces less bending stresses in all four excitations.

3.7.4 Shape Optimization for Vibration Suppression

Shape optimized beams improve the residuals. However, a new objective function (Prob-IV) is defined exclusively to minimize the maximum dynamic tip deflection to obtain the vibration suppression. Static tip deflection is important for positional accuracy, therefore in all redefined problems, static tip deflection is either taken up as a constraint or as a objective function as shown in Table 3.5. Here also, also the shape functions are derived from the finite element formulation.

Table 3.5 Different optimization problems

Optimization Problems for	Objective	Constraints
Prob-I	Minimization of static tip deflection	$M^* - M \le 0$
Prob-II	Maximization of fundamental beam frequency	$M^* - M \le 0$ & $\delta^*_{tip} - \delta_{tip} \le 0$
Prob-III	Maximization of fundamental system frequency	$M^* - M \le 0$ & $\delta^*_{tip} - \delta_{tip} \le 0$
Prob-IV	Minimization of maximum dynamic tip deflection	$M^* - M \le 0$ & $\delta^*_{tip} - \delta_{tip} \le 0$
Permissible Bound : $X^{LB} < X < X^{UB}$		

There are different optimal shapes for different payloads. These shapes extremize that particular objective function under the given constraints.

The rotating torque (Nm)

$$\tau(t) = \begin{cases} 0.5\sin(10\pi t), & 0 \le t \le 0.2 \\ 0, & t > 0.2 \end{cases} \tag{3.32}$$

is applied in hub is considered (t in sec) for all the objective problems. The same torque is considered for numerical experiments of the optimized beams for predicting the dynamic behaviour of the systems.

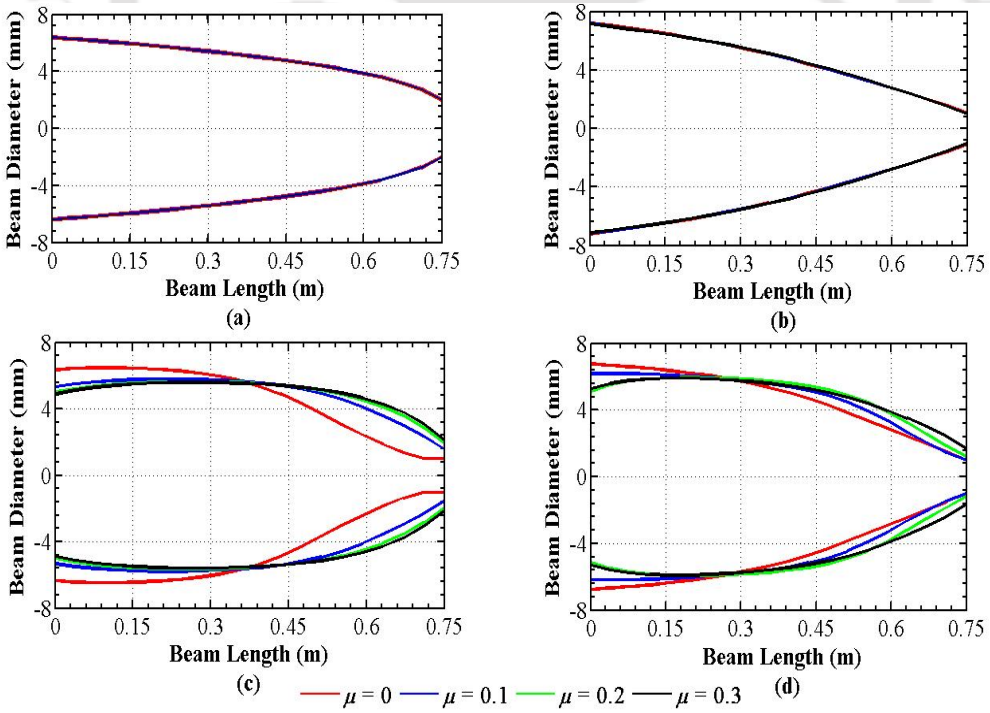

Figure 3.20 Optimized shapes for different payloads (μ) (a) Prob-I, (b) Prob-II, (c) Prob-III, (d) Prob-IV (β=0.5)

For comparative static beam deflections, 1 N static load is considered at the tip of the manipulator and the deflections are shown in Figure 3.21. Optimized beams tip deflected less than or equal to the static tip deflection of the uniform beam manipulator which satisfy the constraint imposed in the optimization problems. Beam-I gives the lowest static tip deflection.

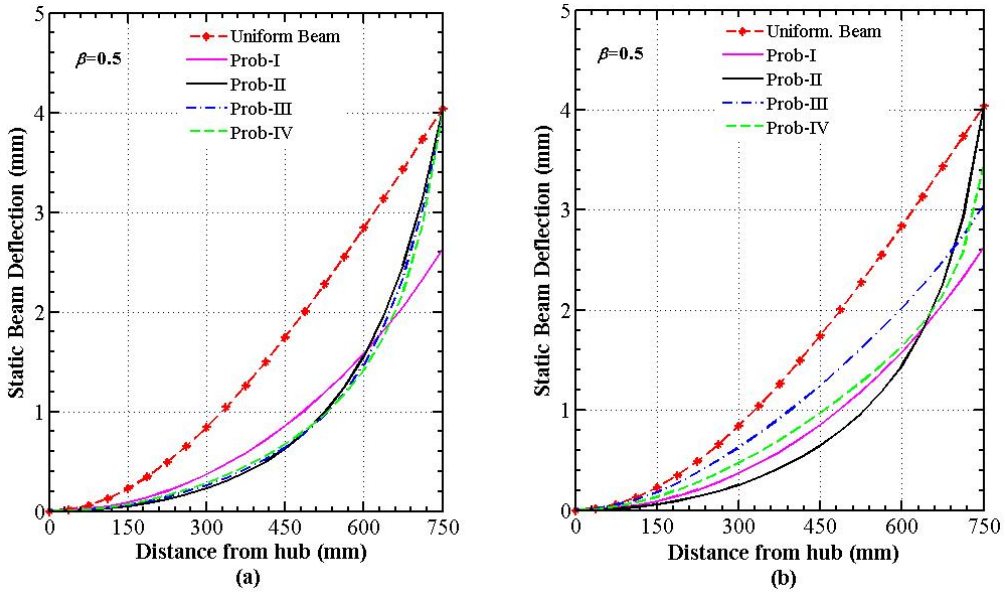

Figure 3.21 Comparison of static beam deflection due to 1 N force at the tip, beam optimized at (a) μ=0, (b) μ=0.2

3.7.4.1 Beam and System Frequencies

Beam frequency is the frequency of the flexible manipulator system when it vibrates as a cantilever beam, whereas system frequency is the frequency when whole system (hub+beam) vibrates about the axis of rotation. Beam and system resonant frequencies of the optimized beams at $\mu = 0$ and $\mu = 0.2$ for that selective payload are shown in Figure 3.22. All the optimization problems increase the fundamental beam frequencies with respect to uniform beam fundamental frequency. Prob-II attains the highest fundamental beam frequency for without payload and payload conditions.

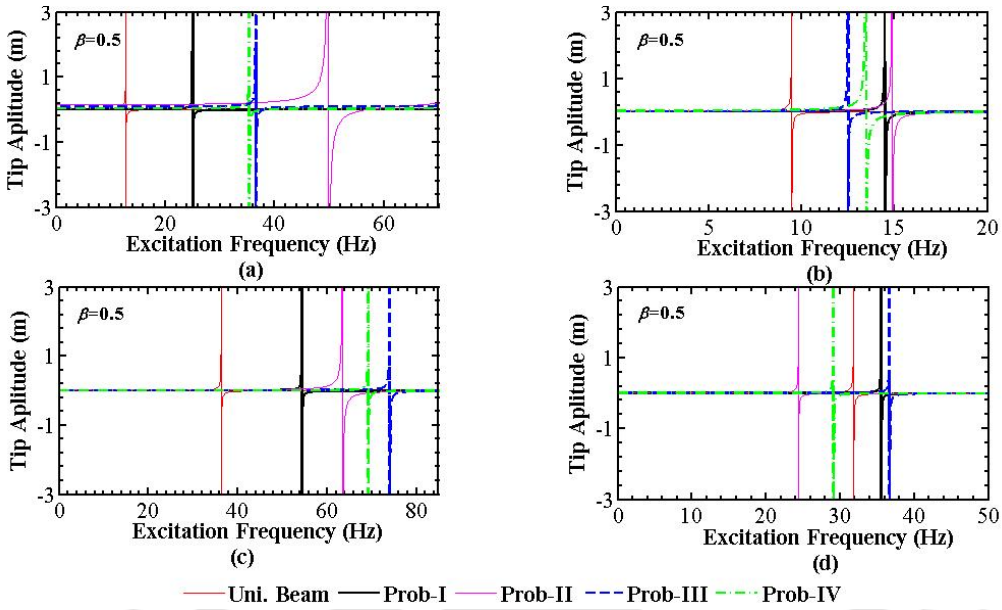

Figure 3.22 Resonant Beam Frequencies of optimized beams at (a) μ=0, (b) μ=0.2, Resonant System Frequencies of optimized beams at (c) μ=0, (d) μ=0.2

All the optimization problems increase the system frequencies for no payload cases but not necessarily for the case of payload conditions with respect to uniform beam fundamental system frequency. Optimization problem-IV gives the highest system frequency corresponding to payload and no payload conditions as expected. However, improvement of fundamental frequencies (beam/system) of optimized beams decreases with increase of payload.

3.7.4.2 Dynamic Response of the System

Dynamic tip deflection due to sinusoidal torque (Eq. 3.32) of all the beams have been plotted in Figure 3.23. Excitation frequency is 5 Hz and is away from the resonant system frequencies of all the beams. All optimized beams at no payload cases have more vibration suppression than the optimized beam at higher payload cases with respect to the uniform beam manipulator. The advantage of vibration suppression through shape optimization reduces with the increase of payload mass. It is observed that Prob-IV suppress the dynamic tip deflection the maximum under same condition.

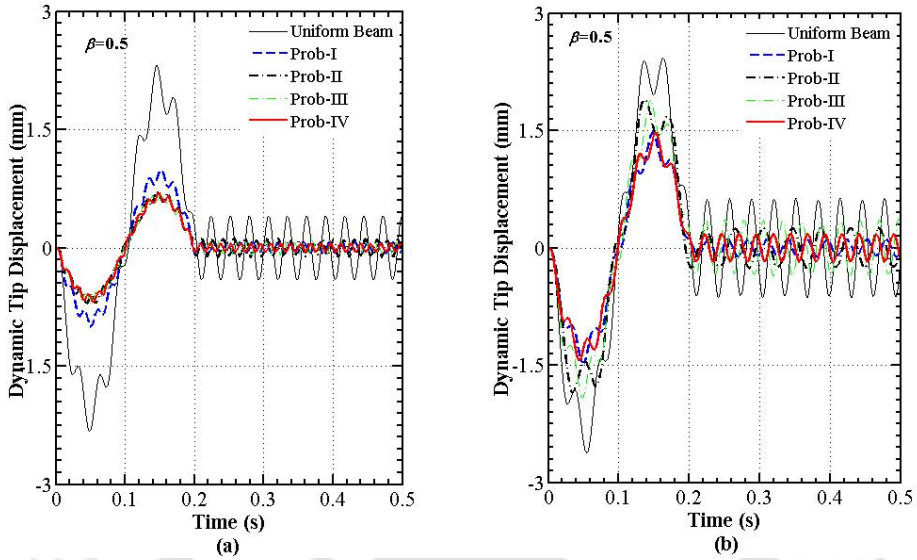

Figure 3.23 Comparison of dynamic tip deflection of beams optimized at (a) μ=0, (b) μ=0.2

Hub angle of all the optimized beams are shown in Figure 3.24 for payload $\mu = 0$ and $\mu = 0.2$. Inertia effects of optimized beams are reduced and hence attain the desirable higher hub rotation angle than the uniform beam manipulator. Prob-II and Prob-IV attain the highest hub angle for a given input torque for both the cases. Maximum dynamic tip deflection and hub rotation are the important parameters for a rotating flexible manipulator. Therefore, Prob-IV is more effective for vibration suppression as well as for improved hub rotation angle.

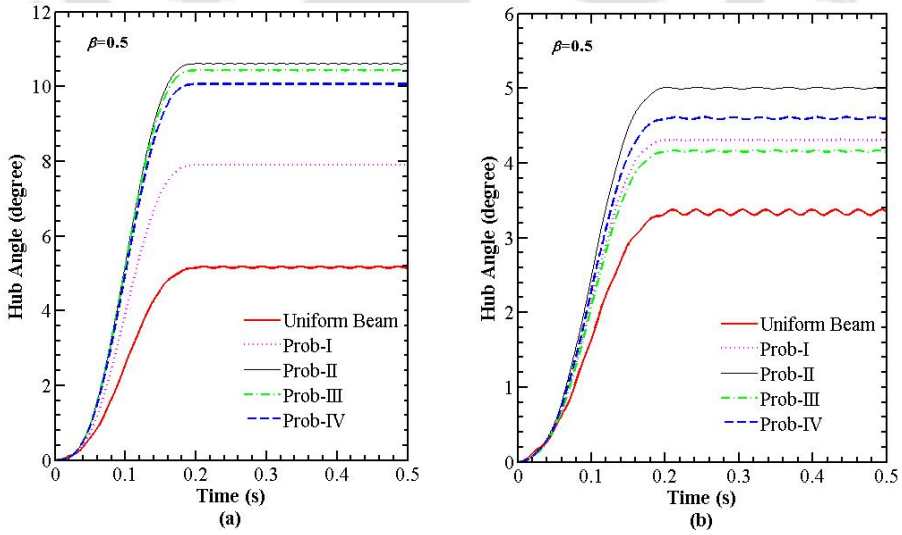

Figure 3.24 Comparisons of hub angles of optimized beams at (a) $\mu = 0$, (b) $\mu = 0.2$

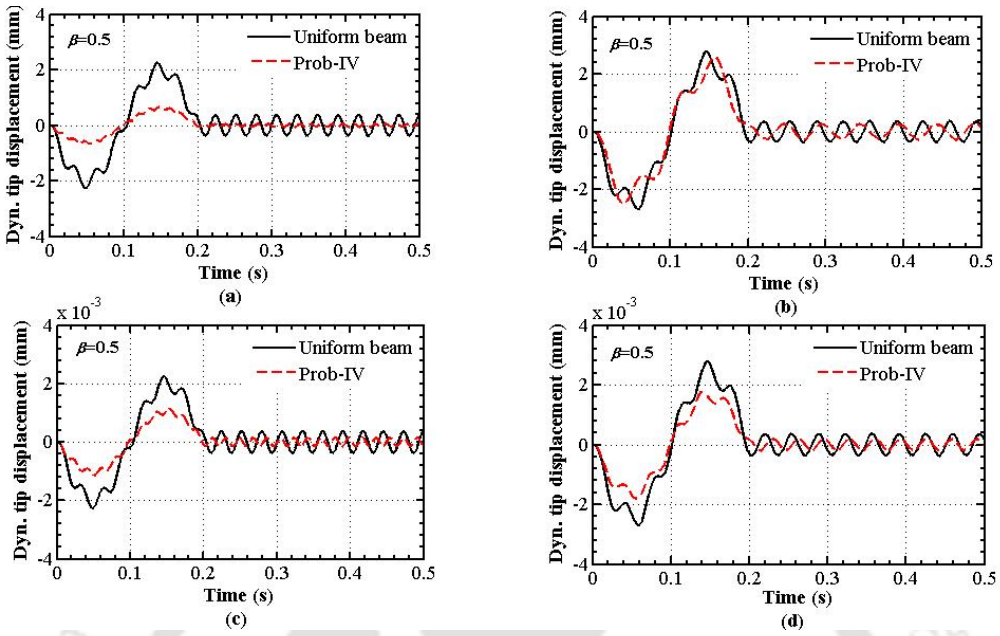

Figure 3.25 Prob-IV optimized at $\mu = 0$ for payload (a) $\mu = 0$, (b) $\mu = 0.5$, Prob-IV optimized at $\mu = 0.5$ for payload (c) $\mu = 0$, (d) $\mu = 0.5$

Shape optimized beam for a particular payload ascertain the improvement of dynamic response for that selective payload. Importantly, it is observed that optimized shapes at higher payloads always give improved dynamic response at lower payload but not the vice-versa (Figure 3.25). Designer may also opt for single optimized shape to cater to range of payloads to get average improvement of dynamic response.

3.7.4.3 Sensitivity Analysis of Active Constraint M^*

All the aforementioned dynamic responses of the optimized beams under different optimization problems are shown in tabulated form in Table 3.6. It is observed that masses of the optimized beams are equal to the mass of uniform beam (0.1596 kg). Here, masses of the optimized beams are the active constraints.

For the sensitivity analysis of the active constraint M^*, upper limit of the mass of optimized beam is taken as $M^* \le 1.3M\,(0.2075\,\text{kg})$. Similar optimized shapes are obtained through all four proposed optimization problems. Dynamic response of all the optimized beams are tabulated in Table 3.7 for no payload case

($\mu = 0$). The corresponding changes (in %) of the dynamic responses are evaluated for 30% increase of active constraint (M^*) and are shown in the same table.

Table 3.6 Comparative dynamic response of optimized beams ($M^* \leq M$)

Beam Shapes	Mass (kg)	Fundamental frequency (Hz)				Static Tip Deflection due to 1N force at tip (mm)		Maximum Dynamic Tip Deflection (mm)		Hub Angle (deg.)	
		Beam Frequency		*System Frequency*							
		μ=0	μ=0.2	μ=0	μ=0.2			μ=0	μ=0.2	μ=0	μ=0.2
Uni. Beam	0.1596	12.731	9.461	36.227	31.559	4.03		2.248	2.365	5.27	3.447
Prob-I	0.1596	24.978	14.506	54.163	35.104	2.63	2.63	0.962	1.470	7.97	4.388
Prob-II	0.1596	49.780	14.873	63.454	24.376	4.03	4.03	0.705	1.580	10.61	4.995
Prob-III	0.1596	36.546	12.495	74.029	36.676	3.96	3.05	0.704	1.510	10.44	4.131
Prob-IV	0.1596	35.366	13.461	69.103	28.824	4.0	3.46	0.649	1.460	10.09	4.461

Table 3.7 Comparative dynamic response of optimized beams ($M^* \leq 1.3M$)

Beam Shapes	Mass (kg)	Fundamental frequency (Hz)				Static Tip Deflection due to 1N force (mm)		Maximum Dynamic Tip Deflection (mm)		Hub Angle (deg.)	
		Beam Frequency		System Frequency							
		μ=0	% Change	μ=0	% Change	μ=0	% Change	μ=0	% Change	μ=0	% Change
Prob-I	0.2075	28.477	14.0	65.151	20.28	1.56	-40.8	0.564	-41.37	6.32	-20.71
Prob-II	0.2075	59.112	18.7	84.413	33.03	4.0	-0.74	0.424	-39.85	9.35	-11.89
Prob-III	0.2075	48.571	32.9	93.431	26.2	3.89	-1.84	0.503	-28.55	9.06	-13.17
Prob-IV	0.2075	46.297	30.9	90.832	31.44	3.97	-0.75	0.372	-42.68	8.85	-12.26

By increasing the optimized mass, rigidity of the system increases and hence the stiffness. Therefore, static/dynamic tip deflections are reduced. But inertia of the optimized systems increase and hence hub angles are reduced. Beam frequency, system frequency and dynamic tip deflection depend upon mass and stiffness of the system. As stiffness as well as mass of the optimized system increases, optimization problem-II, III and IV restrict the increase of optimized beam mass (active constraint M^*) by 35 to 40%. However, there is always convergence of optimization problem-I and hence system moves towards the conventional rigid system with increase of active constraint.

3.7.5 Shape Optimization for Higher Natural Frequencies

As length of the manipulator is generally decided based on the kinematics and space constraints of the robotic system, it is kept constant. Varying the cross-section is the only option for optimization to improve its dynamic behavior. Based on the past research, two optimization problems are taken into consideration by treating manipulator as a cantilever beam rather than as a system (hub+beam).

Optimization problems I and II are defined in Table 3.8. In this Table, M is the prescribed mass of the uniform beam manipulator, M^* is the mass of the optimized manipulator and $\delta_{\text{tip}}, \delta^*_{\text{tip}}$ are the static tip deflection of the optimized manipulator and uniform beam manipulator respectively. X^{LB}, X^{UB} are the lower and upper bounds of diameters of the beam elements (X) respectively.

Table 3.8 Optimization problems

Optimization Problems	Objective	Constraints
I (Prob-I)	Maximization of natural frequency of the cantilever beam (Permissible Bound : $X^{LB} < X < X^{UB}$)	$M - M^* \leq 0$
II (Prob-II)		$M - M^* \leq 0$ and $\delta_{\text{tip}} - \delta^*_{\text{tip}} \leq 0$

It may be noted that shape optimized manipulator considering optimization problem-I for payload μ=0 is designated as Prob-IA and for payload μ=0.05 is Beam-IB. Similarly, Prob-IIA and Prob-IIB are designated for optimization problem-II. Also, first, second and third mode of vibration are termed as simply mode-I, II and III respectively throughout this article. The payload (μ) is defined as the ratio of tip mass to the prescribed mass of the manipulator.

For the numerical study, same structural dimension (manipulator) is considered as mentioned in the section 3.6. Different optimized shapes are obtained under both the optimization problems-I and II. It is observed that there are different optimized shapes for different payloads to increase natural frequencies. However,

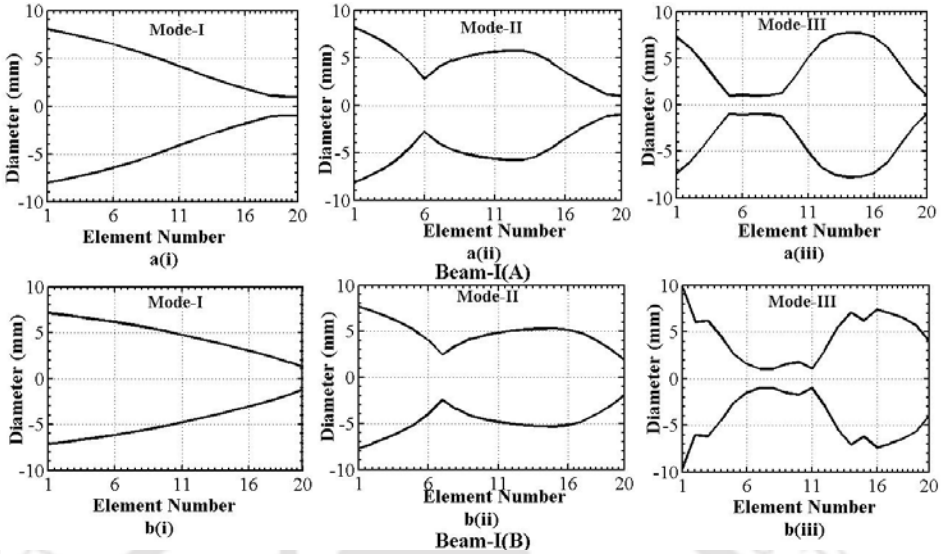

Figure 3.26 Optimized shapes obtained through optimization problem-I in mode-I, II & III for (a) payload (μ=0) & (b) payload (μ=0.05)

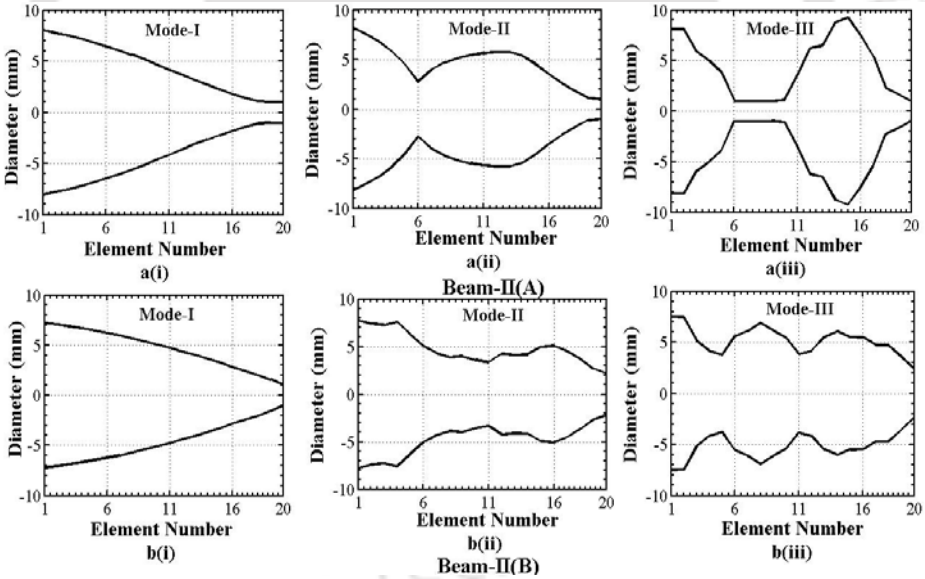

Figure 3.27. Optimized shapes obtained through optimization problem-II in mode-I, II & III for (a) payload (μ=0) & (b) payload (μ=0.05)

there is convergence problem to obtain optimized shapes at higher payloads for higher mode of vibrations. So, optimized shapes of flexible manipulator at payloads μ=0 and 0.05 for first 3 modes of vibrations are plotted in Figure 3.26 and 3.27. These shapes are analyzed for range of payloads for improved natural frequencies in

higher modes of vibration. Hub mass has no effect on the optimized shapes as manipulator is considered as a cantilever beam in the optimization problems.

3.7.5.1 Natural Frequencies

Natural frequencies are important parameters and depend upon the mass and stiffness of the system. As the shape of the manipulator changes, mass distribution changes and hence the stiffness of the system. It helps the designer to control the response of the system due to externally applied torque or force particularly at resonance.

Optimized beams at no payload as shown in Figures 3.26(a) and 3.27(a) give higher frequency at no payload case but give lower frequency at higher payloads in comparison to even uniform beam. Beams-IB & IIB are obvious to be considered for detail comparative studies. In this work, authors are interested to increase 2nd higher frequency bandwidth (difference of frequencies at 1st and 2nd mode of vibration). For its operation in this bandwidth, only fundamental frequency will be encountered as far as resonance is concerned. Variation of natural frequencies due to varying payloads of optimized Beam-IB & IIB for a particular mode are plotted in Figures 3.28 and 3.29 for all first three mode of vibration *viz.* mode-I, II and III.

From numerical solution, it is observed that shape optimized beam at particular payload gives higher/lower fundamental frequency for decrease/increase of the actually applied payload respectively. Observations from Figures 3.28 and 3.29 are summarized as below-

(i) beams optimized for mode-I gives higher natural frequencies in mode-I and lesser frequency bandwidth between higher mode of vibrations as shown in Figs 3.28(a) and Fig. 3.29(a).

(ii) beams optimized for mode-II gives adverse effect in fundamental frequency in case of Prob-IB (Fig. 3.28b) and some increase of fundamental frequency at lower payloads in case of Prob-IIB (Fig. 3.29b). However, there is significant increase of frequency bandwidth in between 1st and 2nd mode of vibration and decrease of frequency

bandwidth in between 2nd and 3rd mode of vibration in case of both the Prob-IB & IIB (Fig. 3.28b and Fig. 3.29b).

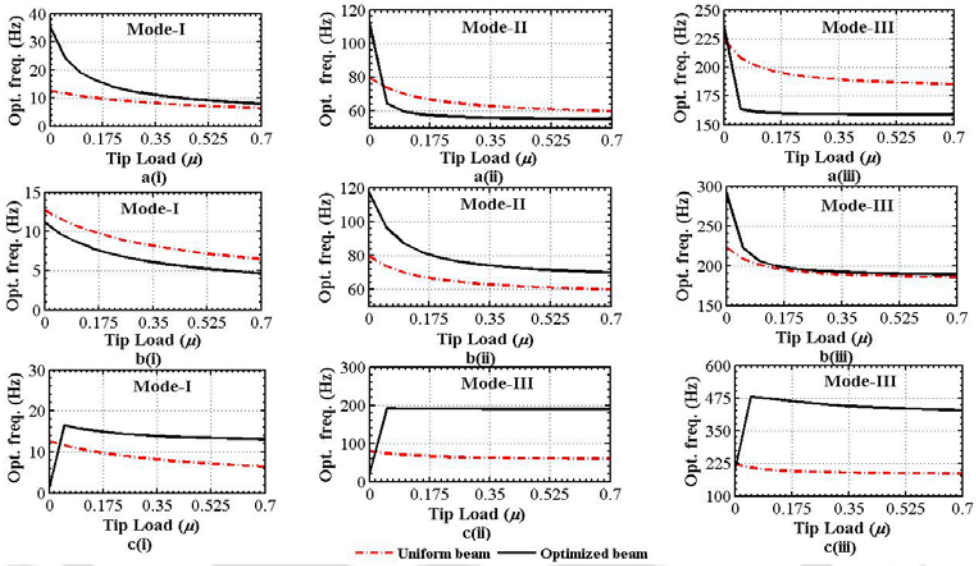

Figure 3.28 Variation of natural frequency of optimized beam under optimization problem-I for payload μ=0.05 (Prob-IB) for varying payloads, (a) shape optimized beam for fundamental frequency, (b) shape optimized beam for 2nd natural frequency, (c) shape optimized beam for 3rd natural frequency

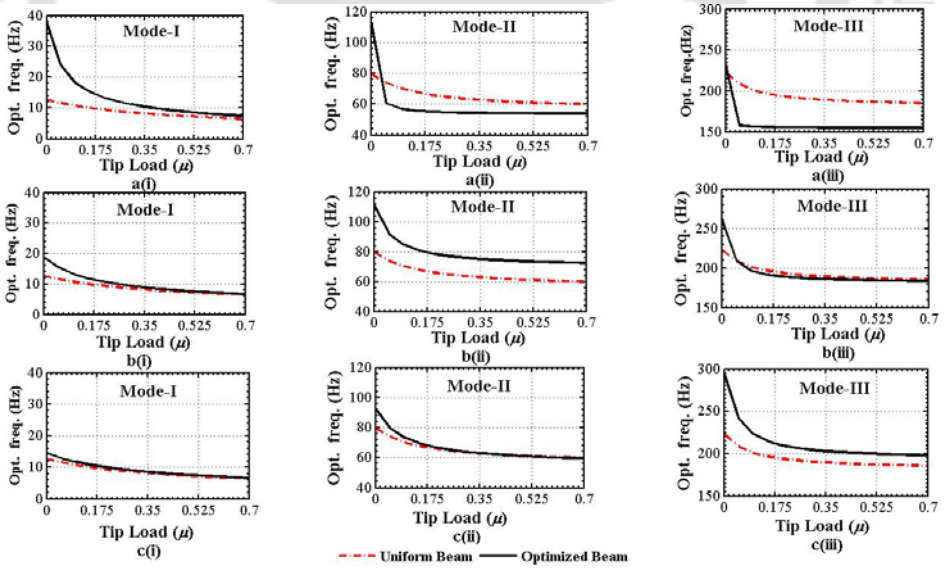

Figure 3.29 Variation of natural frequency of optimized beam under optimization problem-II for payload μ=0.05 (Beam-IIB) for varying payloads, (a) shape optimized beam for fundamental frequency, (b) shape optimized beam for 2nd natural frequency, (c) shape optimized beam for 3rd natural frequency

(iii) beams optimized for mode-III gives significant increase of all first three natural frequencies and 2nd and 3rd frequency bandwidth in case of Prob-IB in Figure 3.28c.

However, there is improvement of 3rd fundamental frequency only in case of Prob-IIB as shown in Figure 3.29c.

3.7.6 Improved Dynamics through Controlled Torque

Yigit [1994] presented the position and derivative (PD) control law for double link revolute-jointed flexible manipulator as given below

$$\tau_{PD_k} = -K_{p_k}(\theta_k - \theta_{f_k}) - K_{v_k}(\dot{\theta}_k). \tag{3.33}$$

The values of k's are 1 and 2 for first and second link respectively. The feedback gains K_{p_k} and K_{v_k} depend upon the equivalent rigid system parameters and are expressed as

$$K_{p_k} = (J_{h_k} + \frac{1}{3} m_k L_k^3 + m_{t_k} L_k^2) f_{n_k}^2, \tag{3.34}$$

and

$$K_{v_k} = 2(J_{h_k} + \frac{1}{3} m_k L_k^3 + m_{t_k} L_k^2) f_{n_k}. \tag{3.35}$$

PD controller is able to stabilize the system but vibration of the flexible beam can not be controlled. Ge *et al.* [1996] extended the work of Yagit [1994] and introduced energy-based robust (EBR) control law and added the nonlinear deflection feedback to improve the performance of the PD controller by adding the nonlinear control term as given by

$$\tau_{EBR_k} = \tau_{PD_k} - K_{f_k} y_k(L_k, t) \int_0^t \dot{\theta}_k(\sigma) y_k(L_k, \sigma) \, \mathrm{d}\sigma, \tag{3.36}$$

where, K_f is the gain constant of robust control, σ is the dummy variable, $\dot{\theta}$ is the hub angular acceleration and y is the deflection at the tips. Energy-based controller always guarantees close-loop stability. Gain of the non-linear control term plays an important role in obtaining satisfactory performance. Through numerical experiments, it is observed that when the gain (K_f) is too small, the control performance is very oscillatory. If the gain is too large, the control action may become not admissible. Unfortunately, it is not easy to find optimal gain of the robust controller term.

3.7.6.1 Optimization Procedure

As mentioned in Section 3.6 (Eq. 3.29), two optimization problems are considered to obtain the optimized shapes for comparative study of residual vibration under control torque.

Table 3.9 Different Optimization Problems

Optimization Problem /Beam referred	Objective	Constraints
I(Prob-I)	Minimization of static tip deflection	$M^* - M \le 0$
II(Prob-II)	Maximization of fundamental beam frequency	$M^* - M \le 0$
Permissible Bound : $X^{LB} < X < X^{UB}$		

Optimized beams obtained through optimization problems I, and II are referred as Beam-I, and Beam-II respectively. Minimum and maximum diameter of the beam elements (X) are denoted by X^{LB}, X^{UB} respectively.

3.7.6.2 Comparative Dynamic Study under Controlled Torque

A comparative dynamic analysis has been carried out for shape optimized single link revolute flexible manipulator. For the numerical study, a manipulator having uniform diameter (d) 15 mm, length (L) 1500 mm, mass (M) 718.3 gm, Young's modulus of elasticity (E) 71.1 GPa, hub inertia (J_h) 1.5 kg.m^2 , hub radius (a) 10 mm is considered. A flexible link is optimized as per the optimization Problem-I and II (Table 1) and plotted in Figure 3.30 and 3.31 respectively. In Problem-I, shape is optimized

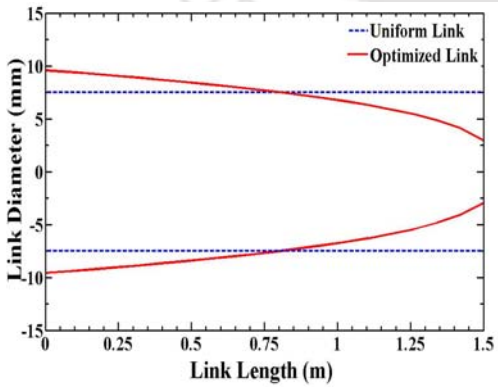

Figure 3.30 Optimized shape (Prob-I)

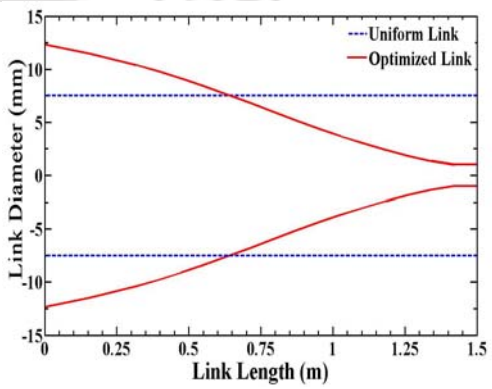

Figure 3.31 Optimized shape (Prob-II)

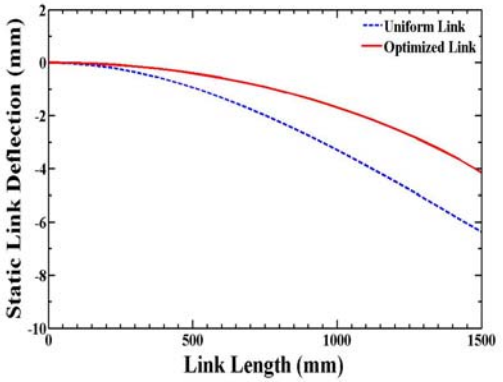

Figure 3.32 Comparative static deflection (Prob-I)

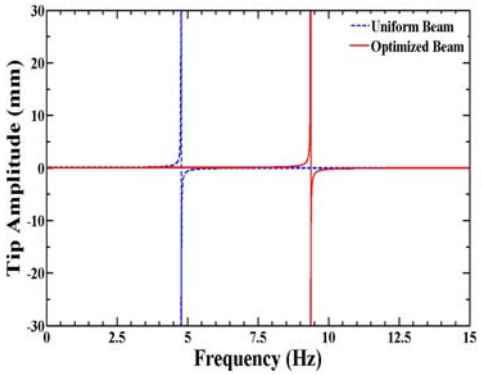

Figure 3.33 Fundamental frequencies (Prob-II)

as to get minimum tip deflection of flexible manipulator due to 1 N force acting at the tip. In both the problems, flexible link is considered as a cantilever beam and optimized mass is the redistribution of the mass of the uniform flexible link. Comparative static link deflections of optimized link (Prob-I) and uniform link due to 1N force at the tip is shown in Figure 3.32. Static link deflection is reduced. Enhanced fundamental frequency of the optimized link (Prob-II) with respect to uniform link is shown in Figure 3.33.

For the comparative dynamic response of the flexible robotic link, a sinusoidal torque applied about the axis of rotation for numerical study is as given below-

$$\tau = 10\sin(2\pi t/0.5)\,\text{Nm}\ (0 \le t \le 0.5\,\text{sec}), \qquad (3.37a)$$

$$= 0\ \ \text{Nm}\,(t > 0.5\ \text{sec}). \qquad (3.37b)$$

Structural parameters considered for which the values are $K_p = 15.239$, and $K_v = 11.148$. Hub angle rotation of the flexible robotic manipulator of the considered structural dimension due to sinusoidal applied torque is $11.2^0(\theta_f)$. An equivalent controlled torque as per the Eq. (19) is applied for the same angular hub rotation ($\theta_f = 11.2^0$) for the comparative dynamic response of the robotic flexible system. Comparative dynamic responses of uniform link and optimized links due to sinusoidal torque and controlled torque are plotted in Figures 3.34 and 3.35 for Prob-I and Prob-II respectively.

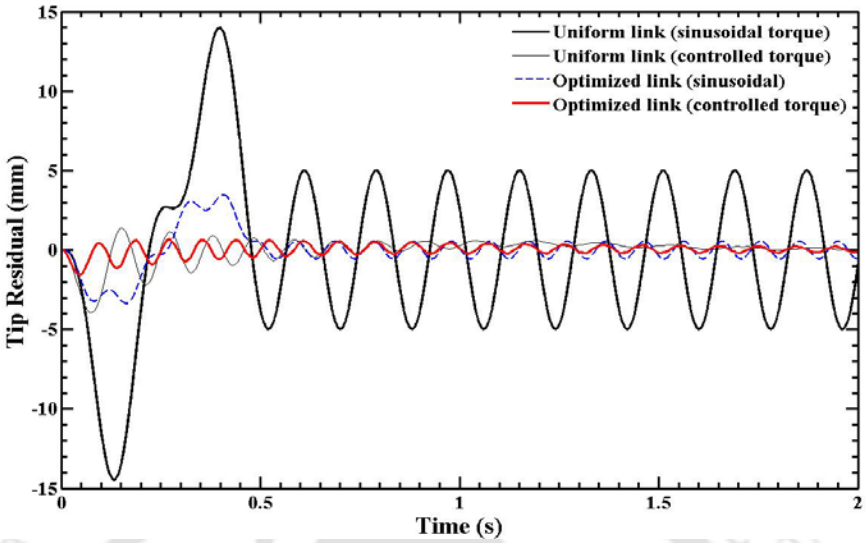

Figure 3.34 Comparative dynamic response (Prob-I)

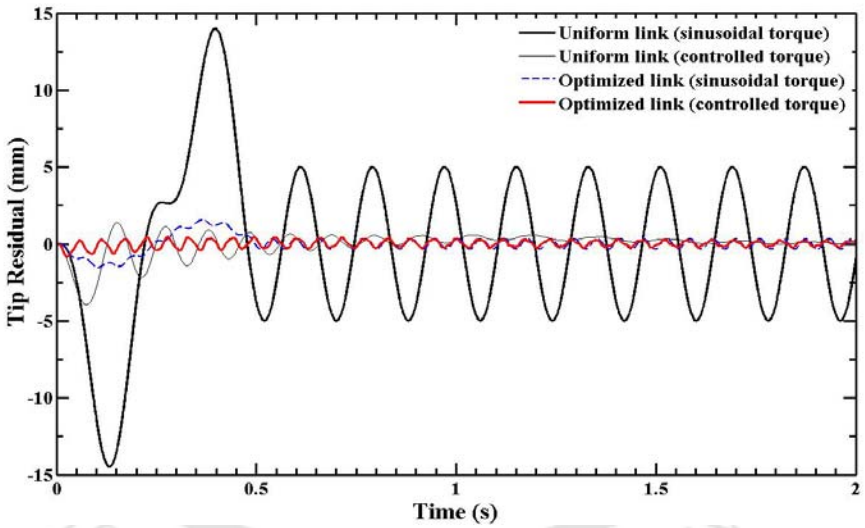

Figure 3.35 Comparative dynamic response (Prob-II)

In the simulated numerical results, it is observed that residual vibration of the tip of uniform link under controlled torque is improved. Also, the residual vibration of shape optimized link improves under the sinusoidal excitation torque. However, vibration suppression is maximum, when shape optimized robotic flexible system is excited by controlled torque under energy-based robust control strategy. There are different shapes of robotic flexible link under different objective functions. Among these two objective functions (Prob-I and Prob-II), unwanted tip residual of optimized robotic link (Prob-II) is the most suppressed. However, controlled torque

is not optimal. Through proper selection of gain constant for robust control further improvement of the tip vibration is possible.

3.8 Summary

An FEM based analysis has been conducted for single link revolute-jointed flexible manipulators and successive sequential quadratic programming (SQP) iteration scheme has been used to solve constrained optimum shape design problems. Following are the salient observations:

- There are different optimum shapes for different optimization problems. Also, optimum shapes change for different payloads.
- Optimal dynamic parameters (frequency, static/dynamic tip deflection, hub angle, etc.) are sensitive to the payload variations.
- There are more optimum improved dynamics in case of no-payload case.
- Shape optimization is a multi-objective problem. There is no optimized shape through which all dynamic responses will be improved.
- Prob-I, II and III are preferred design problem for overall static/dynamic improvement of the system.
- There are different optimum shapes to cater to a range of payloads for different exclusive objectives.
- For same amplitude/duration of excitations, sinusoidal torque profile is preferred with respect to triangular, trapezoidal, bang-bang torque profile to have better overall dynamic response of the system.
- Position accuracy is equally important for a robotic system operation. Hence, minimization of static tip deflection should also be incorporated as a objective function or as a constraint.
- All the optimization problems suppress the residual vibration, but shape optimized exclusively to minimize the dynamic tip deflection suppresses the vibration more.
- Dynamics of the beam optimized at higher payload improves the dynamics for lower payloads as well as higher payloads but not the vice-versa.

- Energy-based robust controlled torque suppresses the vibration of non-optimized robotic system. However, it suppresses vibration of optimized robotic link system more significantly.

Chapter 4

Dynamic Modeling and Optimization of Double Link Rigid-Flexible Manipulator

4.1 Introduction

Flexible multi-body systems includes nonlinear coupled dynamics. Its behaviour is highly complex in nature. However, these systems have many practical applications in engineering, such as aerospace, medical, robotics, *etc*. Light weight flexible robotic systems have several advantages over the conventional systems, but control of vibrations of flexible robotic systems have been a challenging problem. Therefore, in conventional robotic system, sometimes to take the advantages of flexibility, some of the rigid links are replaced by flexible links. A rigid-flexible link manipulator can be considered an ideal starting system for more complicated multi-link flexible manipulators.

Now-a-days robots are usually structurally flexible, reflecting the necessity for their light weight based upon minimum energy consumption and cost, as well as handling of heavy payloads. The residual vibration of those flexible robots usually delays subsequent operation because longer settling time is required for the next operation. The requirements of precise motion and short settling time compels end-point vibration control for these manipulators. Designing lightweight robot manipulators capable of moving larger payloads without increasing the mass of the linkages are of considerable interest. Control of a flexible robot manipulator is complex. Without proper control, the vibrations caused by the structural elasticity of the links would not only reduce the operation speed but also reduce the accuracy of control, or even cause instability in some cases (Balas,1978).

Therefore, it is necessary to control the structural vibration in the flexible arm for quick, precise tracking of the trajectories and accomplishment of tasks.

These requirements make it necessary to take into consideration the dynamic effects of the distributed link flexibility, since high speed operation leads to high inertial forces which in turn cause vibration and diminish. As the residual vibrations of flexible manipulators affect the tasks to be executed by robotic system, combination of rigid-flexible links are considered for its optimal design.

4.2 Modeling and Solution Technique

Rotating flexible beams have significant transverse deflections. Due to flexibility of one link, it exhibits vibratory motions in both chord-wise and flap-wise directions. But induced transverse force here in the chord-wise direction due to the applied excitation torque is much higher compared to the gravity force in flap-wise direction and hence the gravitational effects are ignored to simplify the analysis. Moreover, the gravitational force is static in nature.

The finite element (FE) formulation has been adopted here as described by Usoro *et al.* [1986]. Figure 4.1(a) shows the rigid-flexible manipulator comprising 2 links, 2 joints and tip load. Shoulder joint (joint 1) located at the origin of XOY represents the stationary co-ordinate frame and the elbow joint (joint 2) located at the origin of $X_1O_1Y_1$ and $X_2O_1Y_2$ represents the moving co-ordinate frames. The manipulator is considered slender in this work. The transverse shear and rotary inertia effects of flexible link are neglected and the manipulator is treated as an Euler-Bernoulli beam.

Consider a point P in the i^{th} element on the manipulator at a distance 'x' from the elbow hub. The point P attains the position P' with respect to inertial frame of reference (XOY) after having rigid body motion $\theta_1(t)$ and $\theta_2(t)$ of shoulder and elbow joint respectively and flexural deflection $w(x,t)$. The flexural deflection $w(x,t)$ of the point P is approximated in finite element (FE) technique as

$$\begin{aligned} w(x,t) &= N_1 w_{2i-1} + N_2 w_{2i} + N_3 w_{2i+1} + N_4 w_{2i+2} \\ &= \lfloor N \rfloor \{W\}, \end{aligned} \tag{4.1}$$

where $\lfloor N \rfloor = \lfloor N_1 \; N_2 \; N_3 \; N_4 \rfloor$ and $\{W\}^{\mathrm{T}} = \lfloor w_{2i-1} \quad w_{2i} \quad w_{2i+1} \quad w_{2i-2} \rfloor$.

Hermitian shape functions are

$$N_1 = 1-3\left(\frac{\bar{x}}{h}\right)^2 + 2\left(\frac{\bar{x}}{h}\right)^3,\ N_2 = \bar{x}\left(1-\frac{\bar{x}}{h}\right)^2,$$
$$N_3 = 3\left(\frac{\bar{x}}{h}\right)^2 - 2\left(\frac{\bar{x}}{h}\right)^3,\ N_4 = \bar{x}\left\{\left(\frac{\bar{x}}{h}\right)^2 - \frac{\bar{x}}{h}\right\} \Bigg], \tag{4.2}$$

where h is the element length and $\bar{x}$ is the local variable inside the element.

In FEM formulation, the manipulator is divided into finite number of elements with each element having six degrees of freedom. Detail of i^{th} element of the link is shown in Fig. 4.1(b), where θ_1 and θ_2 are the hub rotation of shoulder and

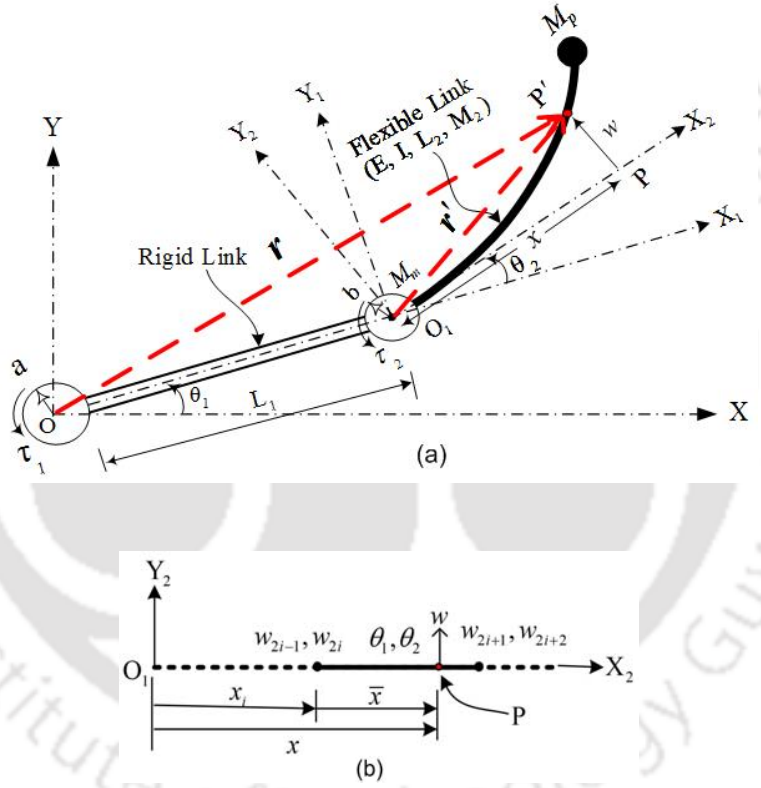

Figure 4.1 Double link rigid-flexible manipulator (a) Configuration, (b) typical i^{th} element with 6 degree of freedom

is the elbow joints respectively, w_{2i-1}, w_{2i} and w_{2i+1}, w_{2i+2} are the transverse deflection and slope at the first and second nodes of the element respectively. The position vector of P′ with respect to inertial system XOY is given by

$$\boldsymbol{r} = T_R^0\, T_T^0\, T_R^{0_l}\, \boldsymbol{r}', \tag{4.3}$$

where

$$\boldsymbol{r}' = \boldsymbol{o_1 p}' = \begin{bmatrix} x+b \\ w(x,t) \\ 1 \end{bmatrix}, \tag{4.4}$$

homogeneous position vector of P' with respect to $X_2O_1Y_2$; $T_R^0, T_R^{0_l}$ are the rotational matrices and T_T^0 the translation matrix defined as

$$T_R^0 = \begin{bmatrix} \cos\theta_1 & -\sin\theta_1 & 0 \\ \sin\theta_1 & \cos\theta_1 & 0 \\ 0 & 0 & 1 \end{bmatrix}, \tag{4.5}$$

$$T_T^o = \begin{bmatrix} 1 & 0 & a+\mathrm{L}_1 \\ 0 & 1 & 0 \\ 0 & 0 & 1 \end{bmatrix}, \tag{4.6}$$

and

$$T_R^{0_l} = \begin{bmatrix} \cos\theta_2 & -\sin\theta_2 & 0 \\ \sin\theta_2 & \cos\theta_2 & 0 \\ 0 & 0 & 1 \end{bmatrix}. \tag{4.7}$$

For the prediction of approximate dynamic behaviour of the optimized beams, smaller excitation torque is considered for linearization of the system modeling. Global position vector of the point P' under smaller angular and flexural displacement is given by

$$\boldsymbol{r} = \boldsymbol{OP}' = \begin{bmatrix} X \\ Y \\ 1 \end{bmatrix} = \begin{bmatrix} a+L_1+b+x \\ (a+L_1)\theta_1 + (x+b)(\theta_1+\theta_2) + w \\ 1 \end{bmatrix}, \tag{4.8}$$

In finite element method, variables are converted into nodal variables. Thus,

$$\boldsymbol{r} = \boldsymbol{OP}' = f(\theta_1, \theta_2, w_{2i\text{-}1}, w_{2i}, w_{2i+1}, w_{2i+2}). \tag{4.9}$$

Let $Z = \lfloor \theta_1 \quad \theta_2 \quad w_{2i\text{-}1} \quad w_{2i} \quad w_{2i+1} \quad w_{2i+2} \rfloor$, then the absolute velocity of the point P of the flexible link is obtained as

$$\frac{\partial \boldsymbol{r}}{\partial t} = \left\lfloor \frac{\partial \boldsymbol{r}}{\partial Z} \right\rfloor \dot{Z}^T. \tag{4.10}$$

4.2.1 Kinetic Energy Computation of the Link Element

The kinetic energy of the i^{th} element of the link is given by

$$T_i^e = \frac{1}{2}\int_0^h \mathrm{m}_2 \left[\frac{\partial \mathbf{r}^{\mathrm{T}}}{\partial \mathrm{t}} \cdot \frac{\partial \mathbf{r}}{\partial \mathrm{t}}\right] \mathrm{d}\bar{x}. \tag{4.11}$$

Using chain rule

$$\frac{\partial \mathbf{r}^{\mathrm{T}}}{\partial \mathrm{t}} \cdot \frac{\partial \mathbf{r}}{\partial \mathrm{t}} = \dot{z}^T \left[\frac{\partial \mathbf{r}}{\partial z}\right]^T \left[\frac{\partial \mathbf{r}}{\partial z}\right] \dot{z} \tag{4.12}$$

Substituting Eq. (4.12) in Eq. (4.11)

$$T_i^e = \frac{1}{2}\dot{Z}^{\mathrm{T}} \left[\int_0^h m_2 \left[\frac{\partial \mathbf{r}}{\partial Z}\right]^{\mathrm{T}} \cdot \left[\frac{\partial \mathbf{r}}{\partial Z}\right] \mathrm{d}\bar{x}\right] \dot{Z}, \tag{4.13}$$

The elemental mass matrix is given by

$$\left[M_{\mathrm{i}}^{\mathrm{e}}\right] = \int_0^h m_2 \left[\frac{\partial \mathbf{r}}{\partial Z}\right]^{\mathrm{T}} \cdot \left[\frac{\partial \mathbf{r}}{\partial Z}\right] \mathrm{d}\bar{x}$$

$$= \begin{bmatrix} M_{11} & M_{12} & M_{13} & M_{14} & M_{15} & M_{16} \\ M_{21} & M_{22} & M_{23} & M_{24} & M_{25} & M_{26} \\ M_{31} & M_{32} & & & & \\ M_{41} & M_{42} & & P_i(4\mathrm{X}4) & & \\ M_{51} & M_{52} & & & & \\ M_{61} & M_{62} & & & & \end{bmatrix}. \tag{4.14}$$

All the constants of the above matrix in Eq. (4.14) are provided in Appendix-II.

4.2.2 Elastic Potential Energy of the Link Element

The potential energy of the i^{th} element of link due to elastic deformation is given by

$$V_{\mathrm{i}}^{\mathrm{e}} = \frac{1}{2}\int_0^h EI \left[\frac{\partial^2 w}{\partial x^2}\right]^2 \mathrm{d}\bar{x} = \{W\}^{\mathrm{T}} \frac{1}{2}\int_0^h EI \left\lfloor N'' \right\rfloor^{\mathrm{T}} \left\lfloor N'' \right\rfloor \mathrm{d}\bar{x} \{W\}. \tag{4.15}$$

Thus, elemental stiffness matrix is given by

$$\left[K_{\mathrm{i}}^{\mathrm{e}}\right] = EI\int_0^h \left\lfloor N'' \right\rfloor^{\mathrm{T}} \left\lfloor N'' \right\rfloor \mathrm{d}\bar{x}$$

$$\left[K_{\mathrm{i}}^{\mathrm{e}}\right]=\frac{EI}{h^3}\begin{bmatrix}0&0&0&0&0&0\\0&0&0&0&0&0\\0&0&12&6h&-12&6h\\0&0&6h&4h^2&-6h&2h^2\\0&0&-12&-6h&12&-6h\\0&0&6h&2h^2&-6h&4h^2\end{bmatrix}. \tag{4.16}$$

4.3 Lagrange's Equation of Motion in Discretized Form

Here, first link is considered rigid and possesses kinetic energy only. However, the second link, being flexible possesses both kinetic and potential energy. The kinetic energy and the potential energy of the system are obtained by computing energy of rigid link; the energy of each element of the flexible link and then summing over all the elements. The global mass matrix and global stiffness matrix can be obtained as

$$[M]=\sum_{i=1}^{n}\left[M_i^e\right]_{\mathrm{g}} \tag{4.17}$$

and

$$[K]=\sum_{i=1}^{n}\left[K_i^e\right]_{\mathrm{g}}, \tag{4.18}$$

where $\left[M_i^e\right]_{\mathrm{g}}$ and $\left[K_i^e\right]_{\mathrm{g}}$ denote the mass and stiffness matrix of the i^{th} element of the link respectively expressed in global form. Total kinetic energy and potential energy can be expressed as

$$T=\frac{1}{2}[\dot{\boldsymbol{q}}]^{\mathrm{T}}[M][\dot{\boldsymbol{q}}] \text{ and } V=\frac{1}{2}[\boldsymbol{q}]^{\mathrm{T}}[K][\boldsymbol{q}] \tag{4.19}$$

respectively.

Here $[\boldsymbol{q}]=\lfloor\theta_1 \quad \theta_2 \quad w_1 \quad w_2 \quad . \quad . \quad w_{2n+1} \quad w_{2n+2}\rfloor$ is the global nodal vector. The Lagrangian of the system is given by $L=T-V$ and then Lagrange's equations of motion of this dynamic system may be written as

$$\frac{\partial}{\partial t}\left[\frac{\partial L}{\partial \dot{\boldsymbol{q}}}\right]-\frac{\partial L}{\partial \boldsymbol{q}}=\boldsymbol{F_q}, \tag{4.20}$$

where $\boldsymbol{F}_q$ is the generalized force vector. Due to modelling linearization, global mass and stiffness matrices are constant and the equation of motion of undamped system is expressed as

$$[M]\{\ddot{\boldsymbol{q}}\}+[K]\{\boldsymbol{q}\}=\{\boldsymbol{F}\}. \tag{4.21}$$

Global load vector $\{F\}$ and global nodal displacement vector $\{\boldsymbol{q}\}$ for 'n' number of finite elements are given by $\{\boldsymbol{F}\}=[T_1\ \tau_2\ 0\ 0.....0\ 0]^{\mathrm{T}}$.

4.3.1 Effects of Hub, Rigid Link, Motor Mass and Payload Inertia

The effects of payload mass (M_p) are incorporated in the elemental mass matrix using Dirac-delta function for the last element (n^{th}) in the Eq. (4.12) to obtain

$$M'_n=\int_0^h M_p\delta(\bar{x}-\mathrm{h})\left[\frac{\partial \boldsymbol{r}}{\partial z}\right]^T\cdot\left[\frac{\partial \boldsymbol{r}}{\partial z}\right]\mathrm{d}\bar{x}. \tag{4.22}$$

Kinetic energy due to hub inertias (J_1,J_2), link 1 and motor mass (M_{m}) at joint 2 is given by

$$T'=\frac{1}{2}J_1\dot{\theta}_1^2+\frac{1}{2}J_2(\dot{\theta}_1+\dot{\theta}_2)^2+\frac{1}{6}M_1\{3a(a+L_1)+L_1\}^2\dot{\theta}_1^2+\frac{1}{2}M_m(a+L_1)^2\dot{\theta}_1^2 \tag{4.23}$$

Hence, the inertia effects of hubs, link 1 and motor mass and payload are incorporated based on the Eq. (4.22) and Eq. (4.23) by adding additional mass matrix terms (M') in the global mass matrix as provided in Appendix-II.

Neglecting load vector, Eq. (4.21) becomes standard eignvalue problem and it is solved for natural frequencies of the system (beam frequency of link 2 and overall system frequency). Beam frequency is the frequency when flexible link is considered as a cantilever beam *i.e.* hub and link 1 are fixed. After incorporation of the effect of hub, rigid link, and payloads, the Eq. (4.21) becomes

$$[M_b]\{\ddot{\boldsymbol{q}}\}+[K_b]\{\boldsymbol{q}\}=\{\boldsymbol{F_b}\}, \tag{4.24}$$

where $[M_b]$, $[K_b]$ and $\{\boldsymbol{F_b}\}$ are the associated mass, stiffness and load vector. Additional constants of Eq. (4.24) are expressed in Appendix-III. Slope and deflection at the first node of the flexible link is made zero. Total shear force and bending moment due to the joint interaction is balanced. Numerical integration of Eq. (4.21) is carried out by using Newmark's integration scheme for obtaining transverse deflection (w), slope (w'), rigid body motions (θ_1,θ_2) and their derivatives. In the present work, structural and viscous damping are neglected.

4.4 Boundary Conditions

4.4.1 Natural Boundary Conditions

Natural boundary conditions are applied at the second joint of the manipulator system *i.e.*, component of the shear force at the end point of the first link $(\tilde{F}_1)$ is to be balanced by the shear force at the same node to the second link $(\tilde{F}_{2,1})$ of the manipulator given by

$$\tilde{F}_1 + \tilde{F}_{2,1}\cos(\theta_2) = 0. \tag{4.25}$$

Torque at the first joint is added by the reactive torque on first link (rigid) by the second link is given by

$$T_1 = \tau_1 - \tau_2. \tag{4.26}$$

Other forced boundary conditions, bending moment and shear force at the end of second link are zero are as given by

$$EI\frac{\partial^2 w}{\partial x^2}\bigg|_{(L_2,t)} = 0, \tag{4.27}$$

and

$$\frac{d}{dx}\left(EI\frac{\partial^2 w}{\partial x^2}\right)\bigg|_{(L_2,t)} = 0. \tag{4.28}$$

4.4.2 Essential Boundary Condition

Link 2 is considered as a rotating cantilever beam. Hence, slope and deflection at the first node of the second link should be zero with respect to time '*t*', *i.e.,*

$$w(0,t) = 0, \tag{4.29}$$

and

$$\frac{\partial w}{\partial x}\bigg|_{(0,t)} = 0. \tag{4.30}$$

In the beam frequency minimization, the hub rotation is arrested.

4.5 Optimization Procedure

Light-weight robotic systems have several advantages over the conventional robotic systems. To retain and optimize the advantage, upper limit of the optimized mass (M^*) is a constraint to the prescribed mass (M). In the rigid-flexible robotic system, flexible link is considered for the shape optimization. Four problems are considered to improve the particular dynamic parameter although some of the objectives are in conflict with each other.

The generalized form of an optimization problem can be expressed as

$$\text{Objective function} \quad f(X), \tag{4.31a}$$

subject to

$$M^* - M \le 0, \tag{4.31b}$$

and

$$X^{\mathrm{L}} \le X \le X^{\mathrm{U}}, \tag{4.31c}$$

where $f(X)$ is the objective function and $X = [d_1 \;\; d_2 \;\; \ldots\ldots \; d_n]^T$ is the design vector with d_i indicating diameter of the i^{th} finite element of the link 2. Lower and upper bound vectors of design variables are X^{L} and X^{U} respectively. The objectives of four different optimization problems are presented in Table 4.1.

Table 4.1 Different optimization problems

Optimization Problem/ Beam referred	Objective	Constraint
I (Prob-I)	Minimization of static tip deflection (δ_s)	$M^* - M \le 0$
II (Prob-II)	Maximization of fundamental beam frequency (ω_b)	$M^* - M \le 0$
III (Prob-III)	Maximization of fundamental system frequency (ω_s)	$M^* - M \le 0$
IV (Prob-IV)	Minimization of maximum dynamic tip deflection (δ_d)	$M^* - M \le 0$
Permissible Bound : $X^{LB} < X < X^{UB}$		

Static tip of the flexible link is obtained by treating it as a cantilever beam. Beam frequency, system frequency and dynamic tip deflection are obtained from the finite element equation of motion (Eq. 4.24). Optimized beams obtained through optimization problems I, II, III and IV are referred as Prob-I, Prob-II, Prob-III and

Prob-IV respectively. Minimum and maximum diameter of the beam elements (X) are denoted by X^{LB}, X^{UB} respectively. The MATLAB solver "*fmincon*" employing sequential quadratic programming (SQP) technique is used for constrained minimization of nonlinear function. The solver minimizes the function $f(X)$ and for maximization, the function is re-written as $-f(X)$.

4.6 Results and Discussion

The equation of motion of the system is given by Eq. (4.24). The developed model is popularly known as zeroth order approximation coupling (ZOAC) for inextensible beam. Generally, linearized model is preferred for control purpose as well as optimization purpose to predict its approximate dynamic behavior. Structural dimensions of this revolute-jointed rigid-flexible robotic manipulator for numerical experiments are taken as per Table 4.2.

Table 4.2 Structural dimensions

Symbol	Parameter	Value	Unit
L_1 , L_2	Lengths of link 1 and link 2	0.75, 0.75	m
d_1, d_2	diameters of link 1 and link 2	0.03, 0.01	m
ρ_1, ρ_2	Mass density of link 1 and link 2	2710, 2710	kg/m^3
a, b	Hub radius at joint 1 and joint 2	0.02, 0.01	m
J_1, J_2	Hub inertia of joint 1 and joint 2	0.03, 0.03	Kg.m^2
E	Young's Modulus of link 2	7.11x10^{10}	N/m^2
M_m	Mass of the motor	0.1	kg

4.6.1 Model Validation

A revolute-jointed planar 2 degree of freedom conventional robotic system (both rigid links) is considered for model validation. From basics of mechanics, nonlinear equation of motion of the system is derived (Eq. 4.32) as Fu *et al.* [1987]. In this derivation, hub radii 'a' and 'b' are not considered.

$$\begin{bmatrix} D_{11} & D_{12} \\ D_{21} & D_{22} \end{bmatrix} \begin{Bmatrix} \ddot{\theta}_1 \\ \ddot{\theta}_2 \end{Bmatrix} + \begin{Bmatrix} \varphi_1(\theta_2, \dot{\theta}_1, \dot{\theta}_2) \\ \varphi_2(\theta_2, \dot{\theta}_1, \dot{\theta}_2) \end{Bmatrix} = \begin{Bmatrix} \tau_1 \\ \tau_2 \end{Bmatrix}. \tag{4.32}$$

The terms $D_{11}, D_{12}, D_{21}, D_{22}$ and φ_1, φ_2 are given in Appendix-IV.

The rotating torque

$$\tau_j(t) = \begin{cases} 0.1\sin(2\pi t), & 0 \le t \le 1 \\ 0, & t > 1 \end{cases} \tag{4.33}$$

applied in both the hubs are considered for dynamics simulation for model validation as well as in all the objective problems. To predict the dynamic behaviour of the systems, same torque is considered for numerical experiments of the optimized beams. Simulation results for dynamic hub angles without payload and payloads of the rigid-flexible robotic system are plotted in Figure 4.2 and compared with the conventional robotic system considering finite difference method. Finite difference technique is a numerical method. The finite difference approximations for derivatives are one of the simplest and one of the oldest methods to solve differential equations. Finite difference based MATLAB solver ODE45 is used to solve Eq. (4.32).

It is observed that due to the applied torque (Eq. 4.33), hub angles of the linearized model are very close to that of conventional robotic system. The slight difference in the simulation result is due to energy present in free vibration of the flexible link. The developed model may be considered for shape optimization of rotating flexible link of rigid-flexible manipulator.

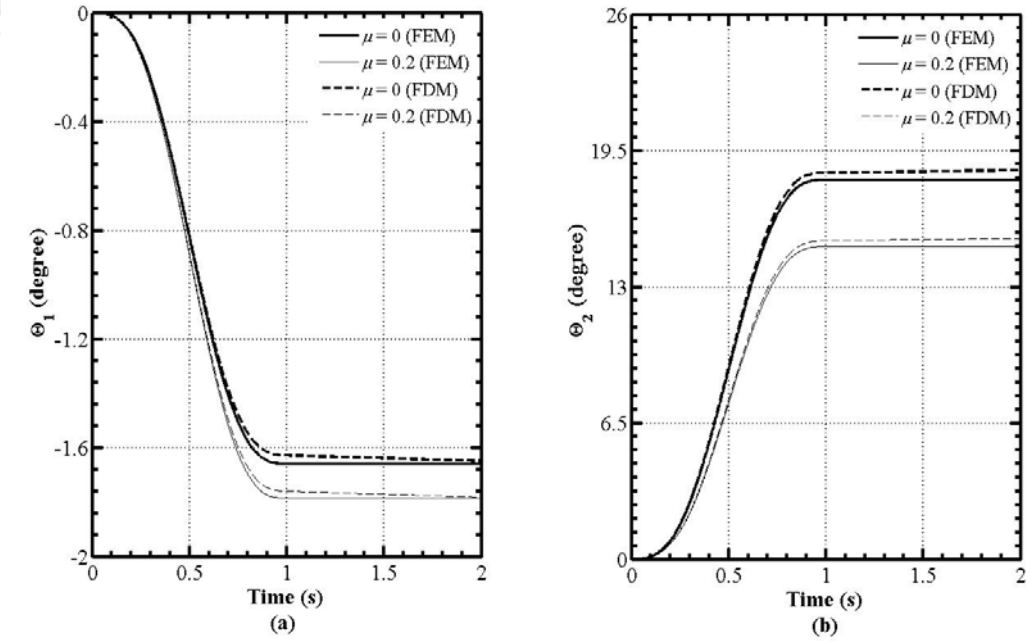

Figure 4.2 (a) Tip response of the beam, (b) Rotating angle of the hub

4.6.2 Shape Optimization and Static Tip Deflection

The cross-section of flexible link is considered circular. For kinematics design point of view, the length of the flexible link is kept constant. For different payloads, optimized shapes are different under different optimization problems. As the first link is rigid, objective functions behave similar to that of single link flexible manipulator. However, its dynamics will be different.

These shapes explicitly optimize the particular objective function under the given constraints. Optimized shapes of the manipulator for the optimization problem defined in Table 4.1 are plotted in Figure 4.3. Applied torques at both the joints (Eq. 4.33) with amplitudes 0.03 Nm is used for dynamic analysis of the system. There are different optimal shapes for different payloads. These shapes extremize the particular objective function under the given constraints.

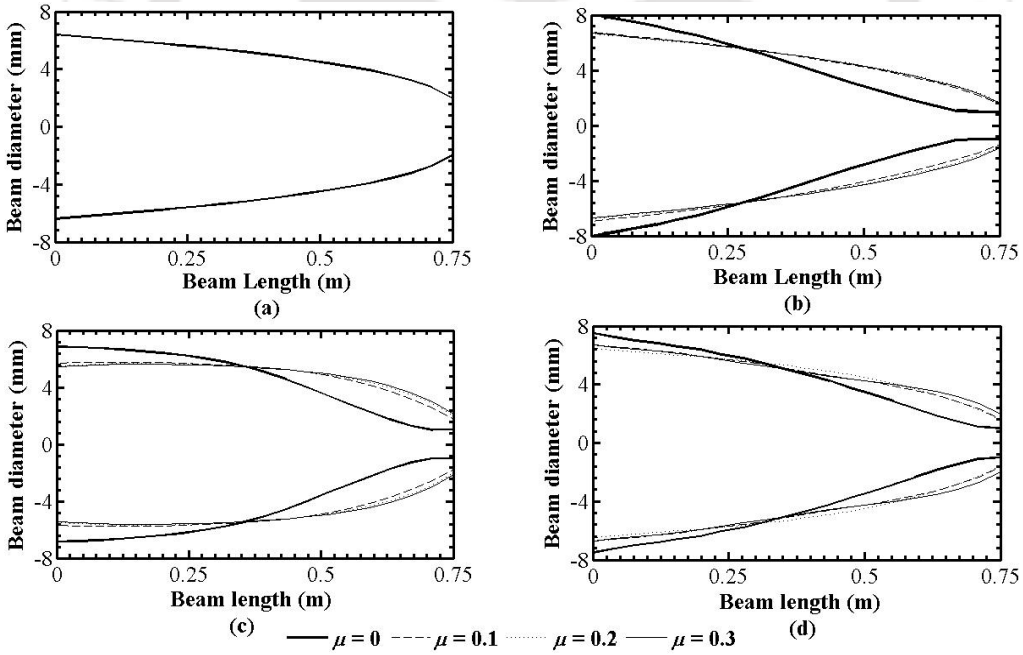

Figure 4.3 Optimized shapes for different payloads (μ) (a) Prob-I, (b) Prob-II, (c) Prob-III, (d) Prob-IV

Static load of 1 N is considered at the tip of the manipulator for comparative static beam deflections and plotted in Figure 4.4. As per the objective function, Prob-I gives the lowest static tip deflection for both the cases ($\mu = 0$ and 0.2). For no payload cases, Prob-II, III, and IV are optimized explicitly for particular objective

function under prescribed mass constraint but static tip deflection of the beams worsened. However, all optimized beams have lesser static tip deflection than that of uniform beam for payload cases.

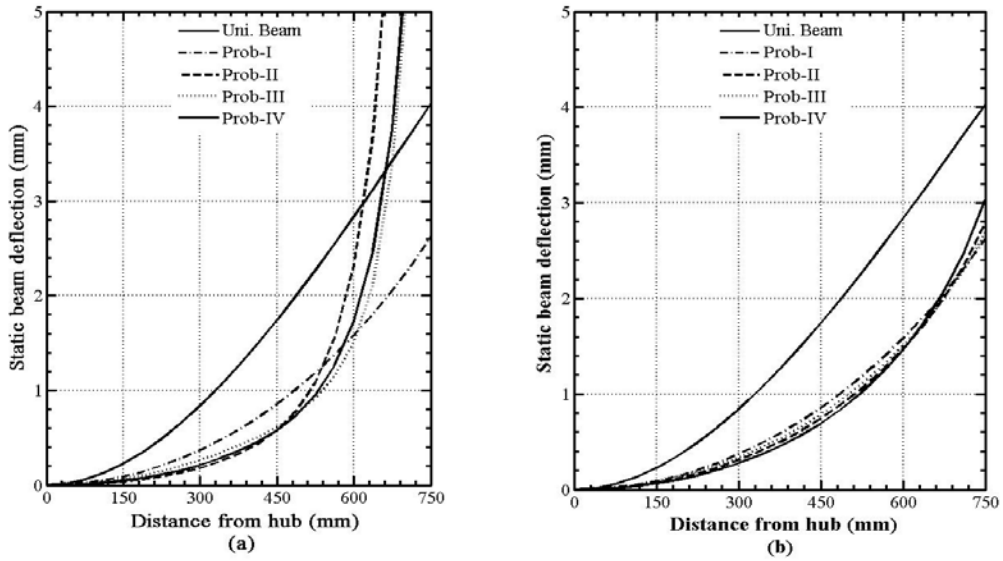

Figure 4.4 Comparison of static beam deflection due to 1 N force at the tip, flexible beam optimized at (a) μ=0, (b) μ=0.2

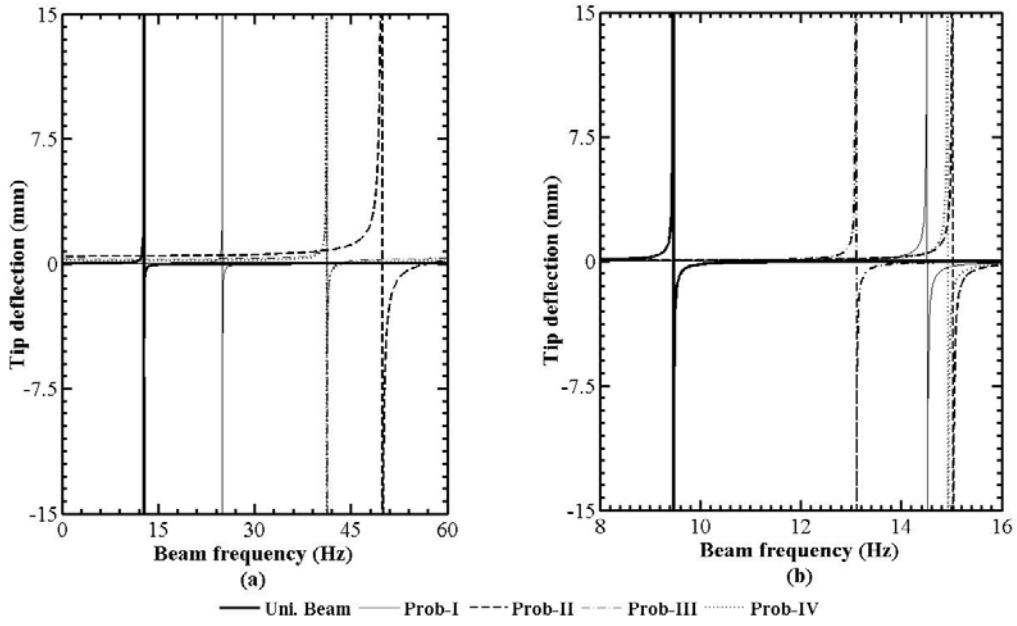

Figure 4.5 Beam Frequencies of optimized beams at (a) μ=0, (b) μ=0.2

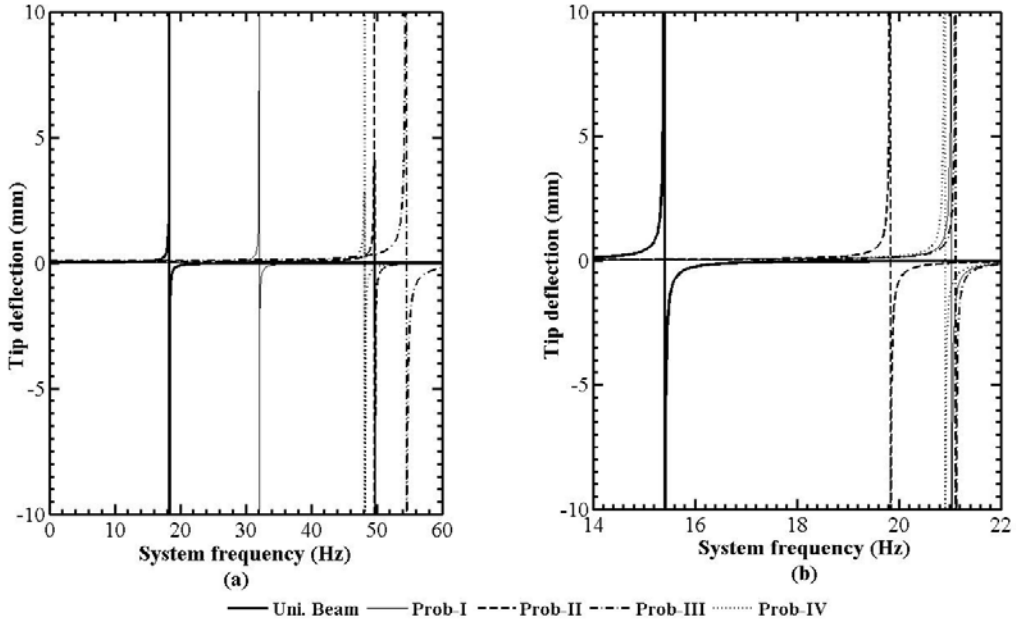

Figure 4.6 System Frequencies of optimized beams at (a) μ=0, (b) μ=0.2

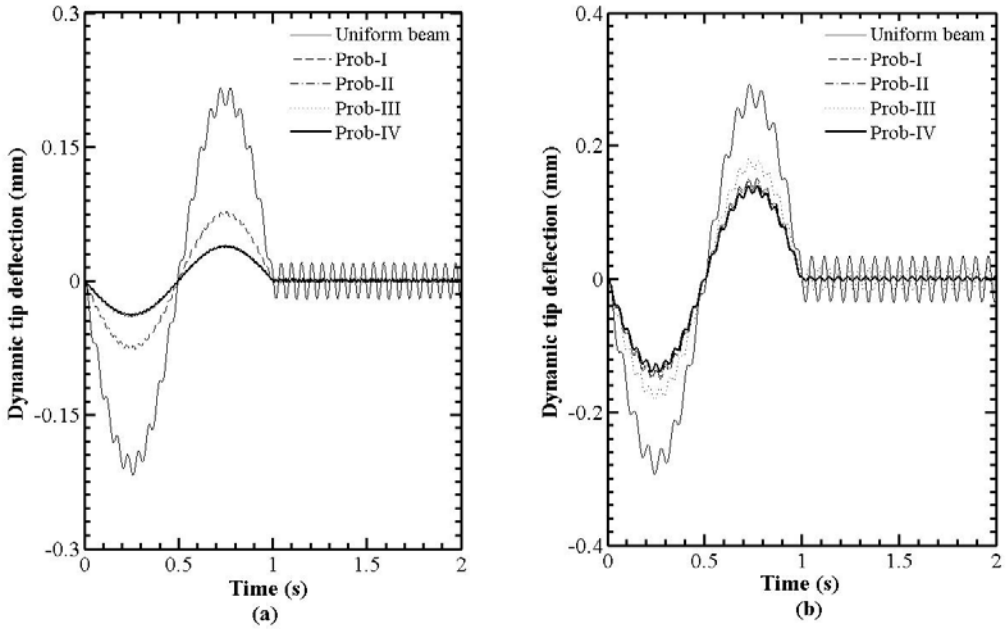

Figure 4.7 Comparison of dynamic tip deflection of beams optimized at (a) μ=0, (b) μ=0.2

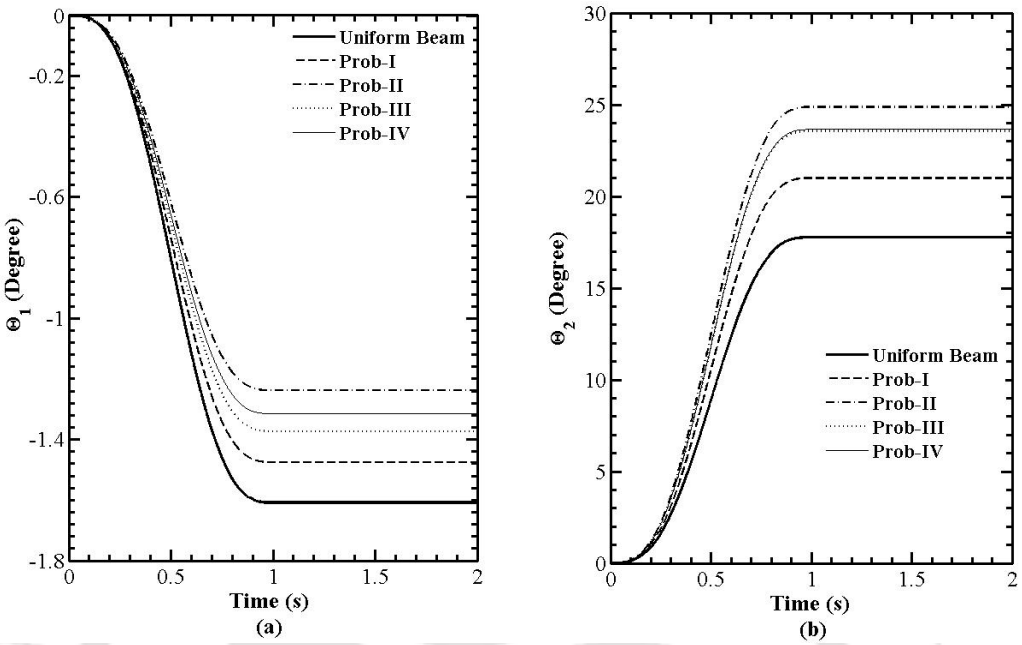

Figure 4.8 Comparisons of hub angles of flexible beam optimized at $\mu = 0$
(a) shoulder joint, (b) elbow joint

4.6.3 Beam and System Frequencies

Beam frequency is the frequency of the flexible link when it vibrates as a cantilever beam, whereas system frequency is the frequency when whole system (hubs+links) vibrates about the axis of rotation. Fundamental beam and system resonant frequencies of the optimized beams at $\mu = 0$ and $\mu = 0.2$ for that selective payloads are plotted in Figures 4.5 and 4.6. The fundamental beam frequencies of all the optimized beams increase with respect to uniform beam fundamental frequency. Prob-II and Prob-III attain the highest fundamental beam frequency and highest fundamental system frequency for without payload and payload cases respectively.

All the optimization problems increase the fundamental beam frequencies significantly but they result in less increment in case of higher payloads. It is also observed that difference of increment of fundamental beam/system frequencies for no payload cases are wider than that of payload cases.

4.6.4 Dynamic Response of the System

For sinusoidal torque (Eq. 4.33) at the joints, dynamic tip deflection of all the optimized beams are plotted in Figure 4.7. Excitation frequency (1 Hz) is kept away from the fundamental system frequencies for better comparison of dynamic responses of the optimized systems. All optimized beams at payload/no payload cases have vibration suppression with respect to the uniform beam rigid-flexible manipulator. However, advantage of vibration suppression through shape optimization reduces with the increase of payload mass. It is observed that Prob-IV suppress the dynamic tip deflection maximum as it is explicitly optimized under same condition.

Hub angles of all the optimized beams are shown in Figure 4.8 for payload $\mu=0$ and $\mu=0.2$. As inertia effects of optimized beams are reduced, optimized beams attain the higher hub rotation angle than the uniform beam manipulator. Prob-II and Prob-IV attain the highest hub angle for a given input torque for no payload cases. Similar trend is observed for higher payload cases also.

For overall improved dynamic response (vibration suppression/hub angle), Prob-IV is more effective. In actual practice, ranges of payloads are used during the robot operations. Single optimized shape may be designed to cater to a range of payloads to get overall improvement of dynamic response.

Table 4.3 Comparative Dynamic Response of Optimized Beams

Beam Shapes	Mass (M_2) (kg)	Fundamental frequency (Hz)				Static Tip Deflection (due to 1N force at tip of link2 optimized at)		Maximum Dynamic Tip Deflection (mm)		Elbow hub Angle (deg.)	
		Beam Frequency (Link 2)		System Frequency							
		μ=0	μ=0.2	μ=0	μ=0.2	μ=0	μ=0.2	μ=0	μ=0.2	μ=0	μ=0.2
Uni. Beam	0.1596	12.73	9.47	18.35	15.41	4.03	4.03	0.23	0.292	17.77	14.61
Prob-I	0.1596	24.99	14.51	32.05	21.09	2.63	2.63	0.077	0.150	21.0	16.38
Prob-II	0.1596	49.81	15.03	50.04	18.35	15.98	2.78	0.041	0.147	24.87	16.83
Prob-III	0.1596	41.26	13.10	54.52	21.12	9.22	2.84	0.042	0.175	23.56	15.99
Prob-IV	0.1596	41.20	11.12	48.23	21.03	6.20	2.68	0.039	0.147	23.65	16.65

Shape optimized beam for a particular payload ascertain the improvement of dynamic response for that selective payload. Importantly, it is observed that

optimized shapes at higher payloads always give improved dynamic response at lower payload but not vice-versa.

4.6.5 Active Constraint M^*

Dynamic responses of the optimized beams under different optimization problems are shown numerically in tabulated form (Table 4.3). It is observed that masses of the optimized flexible beams are equal to the mass of uniform beam (0.1596 kg). Thus, masses of the optimized beams are the active constraints in rigid-flexible robotic system.

4.7 Summary

In this work, the optimization of flexible link is carried out using four different optimization problems through linear modeling of revolute-jointed rigid-flexible manipulator. Finite element analysis has been performed and classical nonlinear optimization (SQP method) are used to solve the constrained optimization problems. A number of numerical experiments were conducted and the following important observation is noticed:

- For different payloads, there are different optimal shapes. These optimal shape extremize explicitly the particular objective function.
- Objective problem-IV is preferred for overall vibration suppression as well as maximum hub rotations.
- Objective functions related to rigid-flexible manipulator system conflict to each other. No single objective problem improves all the dynamic responses of the rigid-flexible robotic system.
- It is observed that masses of the optimized beams are the active constraints.

Chapter 5

Dynamic Modeling and Optimization of Double Link Flexible Manipulator

5.1 Introduction

Robotic manipulators are electro-mechanical devices used to move materials, parts, tools, or any object through variable programmed motions to perform varieties of tasks. Today's task demands high level of accuracy in end-effectors positioning. Versatility and applicability of the robotic manipulator vary depending upon the number of links. Single link planer manipulator can have different positions along the locus of circumference of a circle in a plane only. However, two-link planer manipulator can reach at almost all points on and inside the circle.

Since the links of the conventional robots are bulky due to high stiffness, much of the joint motor's power is utilized in overcoming the inertia of the system and holding them against the gravity. Moreover, the payload to robot weight ratio is low. Also, conventional robots are inefficient and slow. In order to solve these issues robotic systems are designed to be lightweight and thus they posses some level of flexibility. Lightweight and large dimension robotic multi-link manipulators are used in many engineering applications. These systems exhibit many advantages over their rigid counter-part. However, the greatest disadvantage of these manipulators is the vibration problem due to low stiffness. Due to flexible nature and distributed characteristics of the system, the dynamics are highly nonlinear and complex. Since the manipulator is distributed system, its control is a challenging task. A large number of flexible modes are required to accurately model its behavior. Therefore, to retain the advantages of the lightweight robotic system, accurate model, optimal design and efficient controllers have to be developed.

The dynamic characteristics of the flexible manipulators can be significantly improved by the proper design of its shape. For the same mass, shape of the flexible

manipulator can be designed for different objectives. Optimization problem to improve the dynamics of the robotic system is in fact multi-objective problem in nature. Therefore, it is beneficial to take some of the objectives as constraints.

5.2 Obtaining Elemental Equation of Manipulator

Rotating flexible beams behave as a nonlinear elastic beams and exhibit vibratory motions in both chord wise and flap wise directions. However, induced transverse force in the chord wise direction due to the applied excitation torque is much higher compared to the gravity force in flap wise direction and vibrations are predominantly in chord wise directions. In this work, model of Usoro *et al.* [1986] is adopted. Formulations are consistently linearized for small angular/transverse deflections under linear beam theory to reduce the complexity of the system modeling. Nevertheless, this simplified model may not be suitable to analyze the dynamic behaviors of flexible links manipulator with large deflections.

5.2.1 Modeling of First Link

Figure 5.1(a) shows single link flexible manipulator in which XOY and X_1OY_1 represents the stationary and moving co-ordinate frames, respectively. Motion of the link is represented by fixed XOY co-ordinate frame. The link is considered slender in this chapter. Hence, transverse shear and rotary inertia effects are neglected allowing it to be treated as an Euler-Bernoulli beam. Beam is assumed to vibrate predominantly in horizontal plane (XOY), neglecting gravity effects (which affects flap wise motion).

Consider a point P_1 in the i^{th} element on the manipulator at a distance x_1 from the hub. The point P_1 attains the position P_1' with respect to inertial frame of reference (XOY) after having rigid body motion $\theta_1(t)$ and flexural deflection $u(x_1,t)$. Flexural deflection $u(x_1,t)$ of point P_1 is approximated as

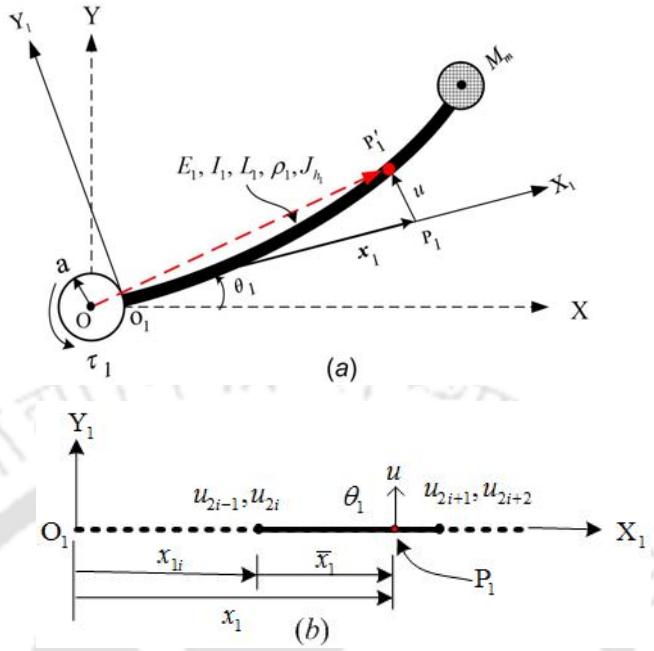

Figure 5.1 First link of manipulator: (a) configuration diagram and (b) typical i^{th} finite element having 5 dof.

$$u(x_1,t) = N_1u_{2i-1} + N_2u_{2i} + N_3u_{2i+1} + N_4u_{2i+2} = \lfloor N \rfloor \{U\}, \tag{5.1}$$

where $\lfloor N \rfloor = \lfloor N_1 \; N_2 \; N_3 \; N_4 \rfloor$, $\{U\}^T = \lfloor u_{2i-1} \quad u_{2i} \quad u_{2i+1} \quad u_{2i+2} \rfloor$ are the Hermitian shape functions and nodal vector respectively. In the FEM formulation of the manipulator, each element has 5 degrees of freedom. Detail of i^{th} element of the first link is shown in Figure 5.1(b). In the figure, θ_1 is the hub rotation and u_{2i-1}, u_{2i}, u_{2i+1} and u_{2i+2} are the transverse deflections and slopes at the first and second nodes of the element.

Dynamics of double link flexible manipulator is highly non-linear in nature. However, for very low torques excitation, system may behave very close to linear. The position vector of P_1' with respect to inertial system XOY for smaller angular displacement and small flexural deflection can be linearized as

$$\boldsymbol{r}_1 = \begin{Bmatrix} X_1 \\ Y_1 \end{Bmatrix} = \begin{bmatrix} a + x_1 \\ (a + x_1)\theta_1 + u \end{bmatrix}. \tag{5.2}$$

In finite element, variables are converted to nodal variables.

Let $Z_1 = \lfloor \theta_1 \quad u_{2i-1} \quad u_{2i} \quad u_{2i+1} \quad u_{2i+2} \rfloor$, then

$$\frac{\partial \mathbf{r}_1}{\partial t} = \left[\frac{\partial \mathbf{r}_1}{\partial z}\right]\dot{Z}_1^T \tag{5.3}$$

5.2.1.1 Kinetic Energy of the i^{th} Element of the 1^{st} Link

Kinetic energy of i^{th} element of the first link is given by

$$T_1^i = \frac{1}{2}\int_0^{h_1} m_1\left[\frac{\partial \mathbf{r}_1^T}{\partial t}\cdot\frac{\partial \mathbf{r}_1}{\partial t}\right]d\bar{x}_1. \tag{5.4}$$

By chain rule

$$\frac{\partial \mathbf{r}_1^T}{\partial t}\cdot\frac{\partial \mathbf{r}_1}{\partial t} = \dot{Z}_1^T\left[\frac{\partial \mathbf{r}_1}{\partial t}\right]^T\left[\frac{\partial \mathbf{r}_1}{\partial t}\right]\dot{Z}_1 \tag{5.5}$$

Substituting Eq. (5.5) in Eq. (5.4)

$$T_I^i = \frac{1}{2}\dot{Z}_1^T\left[\int_0^{h_1} m_1\left[\frac{\partial \mathbf{r}_1}{\partial t}\right]^T\left[\frac{\partial \mathbf{r}_1}{\partial t}\right]d\bar{x}_1\right]\dot{Z}_1 \tag{5.6}$$

Thus elemental mass matrix is given by

$$\left[M_1^{\,i}\right] = \int_0^{h_1} m_1\left[\frac{\partial \mathbf{r}_1}{\partial Z_1}\right]^T\cdot\left[\frac{\partial \mathbf{r}_1}{\partial Z_1}\right]d\bar{x}_1 = \begin{bmatrix} M_{11} & M_{12} & M_{13} & M_{14} & M_{15} \\ M_{21} & & & & \\ M_{31} & & & P_{1i} & \\ M_{41} & & & & \\ M_{51} & & & & \end{bmatrix}. \tag{5.7}$$

All the constants of the above matrix (Eq. 5.7) are expressed in Appendix-V.

5.2.1.2 Elastic Potential Energy of the i^{th} Element of 1^{st} Link

Potential energy of the i^{th} element of 1st link due to elastic deformation is given by

$$V_1^i = \frac{1}{2}\int_0^{h_1} E_1 I_1\left[\frac{\partial^2 u}{\partial x_1^2}\right]^2 d\bar{x}_1 = \{U\}^T\frac{1}{2}\int_0^{h_1} E_1 I_1\left[N''\right]^T\left[N''\right]d\bar{x}_1\{U\}. \tag{5.8}$$

Thus, elemental stiffness matrix is given by

$$\left[K_i^e\right] = \frac{1}{2}\int_0^{h_1} E_1 I_1\left[N''\right]^T\left[N''\right]d\bar{x}_1 = \frac{E_1 h_1}{3}\begin{bmatrix} 0 & 0 & 0 & 0 & 0 \\ 0 & 12 & h_1 & -12 & 6h_1 \\ 0 & h_1 & 4h_1^2 & -6h_1 & 2h_1^2 \\ 0 & -12 & -6h_1 & 12 & -6h_1 \\ 0 & 6h_1 & 2h_1^2 & -6h_1 & 4h_1^2 \end{bmatrix}. \tag{5.9}$$

5.2.2 Modeling of Second Link

Figure 5.2 (a) shows 2nd link flexible manipulator in which XOY represents the stationary and $X_1O_1Y_1, X_2O_2Y_2$ and $X_1'O_2Y_1'$ represent moving co-ordinate frames. Consider an infinitesimal link element P_2 on the manipulator at a distance x_2 from the link joint. Point P_2 attains the position P_2' after time 't' with respect to non-inertial frame of reference $(X_2O_2Y_2)$ after having rigid body motion $\theta_2(t)$ and transverse deflection $w(x_2,t)$.

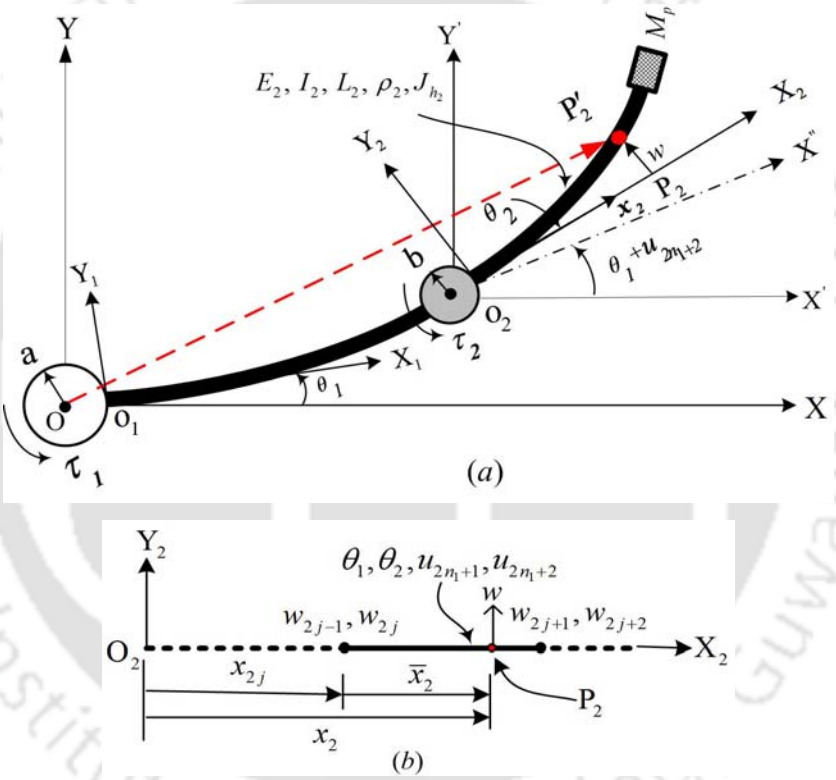

Figure 5.2 (a) Configuration diagram of 2nd link of manipulator, and (b) Typical j^{th} finite element of the 2nd link having 8 dof.

Flexural deflection $w(x_2,t)$ of point P_2 is approximated in finite element as

$$w(x_2,t) = S_1 w_{2j-1} + S_2 w_{2j} + S_3 w_{2j+1} + S_4 w_{2j+2} = \lfloor S \rfloor \{W\}, \tag{5.10}$$

where $\lfloor S \rfloor = \lfloor S_1 \; S_2 \; S_3 \; S_4 \rfloor$, $\{W\}^T = \lfloor w_{2j-1} \quad w_{2j} \quad w_{2j+1} \quad w_{2j+2} \rfloor$ are Hermitian shape functions and nodal vector respectively.

In the FEM formulation the manipulator is divided into 20 elements, each element having eight degrees of freedom. Detail of j^{th} element of the second link is shown in Figure 5.2(b), where θ_2 is the second link rotation and $w_{2j-1}, w_{2j}, w_{2j+1}$ and w_{2j+2} are the transverse deflections and slopes at the first and second nodes of the element along with the variables associated with the first link θ_1, u_{2n_1+1} and u_{2n_1+2}. The position vector of P_2' with respect to inertia system XOY is hereby also linearized as per the earlier discussion for smaller angular displacement and small flexural deflection to provide

$$\mathbf{r}_2 = \begin{bmatrix} X_2 \\ Y_2 \end{bmatrix} = \begin{bmatrix} (a + L_1 + b) + x_2 \\ \theta_1 (a + L_1 + b + x_2) + u_{2n_1+1} + (b + x_2)(\theta_2 + u_{2n_1+2}) + w \end{bmatrix}. \tag{5.11}$$

In finite element, variables are converted to nodal variables.

Let $Z_2 = \begin{bmatrix} \theta_1 & u_{2n_1+1} & u_{2n_1+2} & \theta_2 & w_{2j-1} & w_{2j} & w_{2j+1} & w_{2j+2} \end{bmatrix}$, then

$$\frac{\partial \mathbf{r}_2}{\partial t} = \left[\frac{\partial \mathbf{r}_2}{\partial z_2} \right] \dot{Z}_2^T \tag{5.12}$$

and

$$\frac{\partial \mathbf{r}_2^T}{\partial t} \cdot \frac{\partial \mathbf{r}_2}{\partial t} = \dot{Z}_2^T \left\{ \left(\frac{\partial \mathbf{r}_2}{\partial Z_2} \right)^T \right\} \left[\frac{\partial \mathbf{r}_2}{\partial Z_2} \right] \dot{Z}_2. \tag{5.13}$$

5.2.2.1 Kinetic Energy Computation of the j^{th} Element of the 2^{nd} Link

Kinetic energy of the second link of the j^{th} element is

$$T_2^j = \frac{1}{2} \dot{Z}_2^T \left[\int_0^{h_2} m_2 \left[\frac{\partial \mathbf{r}_2}{\partial t} \right]^T \cdot \left[\frac{\partial \mathbf{r}_2}{\partial t} \right] d\bar{x}_2 \right] \dot{Z}_2. \tag{5.14}$$

Thus, mass matrix of the element become

$$\left[M_2^j \right] = \int_0^{h_2} m_2 \left[\frac{\partial \mathbf{r}_2}{\partial t} \right]^T \cdot \left[\frac{\partial \mathbf{r}_2}{\partial t} \right] d\bar{x}_2. \tag{5.15}$$

Solving it we get

$$\left[M_2^j\right]=\begin{bmatrix} M_{11} & M_{12} & M_{13} & M_{14} & M_{15} & M_{16} & M_{17} & M_{18} \\ M_{21} & M_{22} & M_{23} & M_{24} & M_{25} & M_{26} & M_{27} & M_{28} \\ M_{31} & M_{32} & M_{33} & M_{34} & M_{35} & M_{36} & M_{37} & M_{38} \\ M_{41} & M_{42} & M_{43} & M_{44} & M_{45} & M_{46} & M_{47} & M_{48} \\ M_{51} & M_{52} & M_{53} & M_{54} & & & & \\ M_{61} & M_{62} & M_{63} & M_{64} & & P_{2j} & & \\ M_{71} & M_{72} & M_{73} & M_{74} & & & & \\ M_{18} & M_{82} & M_{83} & M_{84} & & & & \end{bmatrix}. \tag{5.16}$$

All the constants of the matrix given by Eq. (5.16) are provided in Appendix-VI.

5.2.2.2 Elastic Potential Energy of the j^{th} Element of 2^{nd} Link

The potential energy of the j^{th} element of the 2nd link due to elastic deformation is given as

$$V_2^{\,j}=\frac{1}{2}\int_0^{h_2} E_2I_2\left[\frac{\partial^2 w}{\partial x_2^2}\right]^2 \mathrm{d}\bar{x}_2=\lfloor W\rfloor^T\frac{1}{2}\int_0^{h_2} E_2I_2\lfloor S''\rfloor^T\lfloor S''\rfloor \mathrm{d}\bar{x}_2\lfloor W\rfloor. \tag{5.17}$$

Thus, the elemental stiffness matrix is given by

$$\left[K_2^{\,j}\right]=E_2I_2\int_0^{h_2}\lfloor S''\rfloor^T\lfloor S''\rfloor \mathrm{d}\bar{x}_2=\frac{E_2I_2}{h_2^3}\begin{bmatrix} 0 & 0 & 0 & 0 & 0 & 0 & 0 & 0 \\ 0 & 0 & 0 & 0 & 0 & 0 & 0 & 0 \\ 0 & 0 & 0 & 0 & 0 & 0 & 0 & 0 \\ 0 & 0 & 0 & 0 & 0 & 0 & 0 & 0 \\ 0 & 0 & 0 & 0 & 12 & 6h_2 & -12 & 6h_2 \\ 0 & 0 & 0 & 0 & 6h_2 & 4h_2^2 & -6h_2 & 2h_2^2 \\ 0 & 0 & 0 & 0 & -12 & -6h_2 & 12 & -6h_2 \\ 0 & 0 & 0 & 0 & 6h_2 & 2h_2^2 & -6h_2 & 4h_2^2 \end{bmatrix}. \tag{5.18}$$

5.3 Lagrange's Equation of Motion in Discretized Form

The kinetic energy and the potential energy of the system are obtained by computing the kinetic energy and potential energy of the each element of the system and summing over all the elements. Thus, global mass matrix and global stiffness can be obtained as

$$[M]=\sum_{i=1}^{n_1}\left[M_1^i\right]_g+\sum_{j=1}^{n_2}\left[M_2^j\right]_g \tag{5.19}$$

and

$$[K]=\sum_{i=1}^{n_1}\left[K_1^i\right]_g+\sum_{j=1}^{n_2}\left[K_2^j\right]_g, \tag{5.20}$$

where $\left[M_1^i\right]_g$, $\left[M_2^j\right]_g$ denote the mass matrices of i^{th} element of first link and j^{th} element of second link respectively expressed in global form and $\left[K_1^i\right]_g$, $\left[K_2^j\right]_g$ denotes the stiffness matrices of i^{th} element of first link and j^{th} element of second link respectively expressed in global form.

Total kinetic energy and potential energy can be expressed as

$$T=\frac{1}{2}[\dot{q}]^T[M][\dot{q}] \text{ and } V=\frac{1}{2}[q]^T[K][q] \tag{5.21}$$

respectively, where $[M]$ and $[K]$ are the global matrices and $[q]$ is the global nodal vector defined as $\left[\theta_1 \quad u_1 \quad . \quad . \quad u_{2n_1+2} \quad \theta_2 \quad w_1 \quad . \quad . \quad w_{2n_2+2}\right]$. Lagrangian of the system is given by $L=T-V$. Then, Lagrange's equations of motion of this dynamic system is written as

$$\frac{\partial}{\partial t}\left[\frac{\partial L}{\partial \dot{\boldsymbol{q}}}\right]-\frac{\partial L}{\partial \boldsymbol{q}}=\boldsymbol{F_q}, \tag{5.22}$$

where $\boldsymbol{F}_q$ are the generalized forces. Being linear system, global mass and stiffness matrix is constant and equation of motion comes as

$$[M]\{\ddot{\boldsymbol{q}}\}+[K]\{\boldsymbol{q}\}=\{\boldsymbol{F_q}\}. \tag{5.23}$$

Order of global mass matrix [M] and global stiffness matrix is $(2n_1+2n_2+6)\times(2n_1+2n_2+6)$ and global load vector is $(2n_1+2n_2+6)\times 1$.

5.4 Boundary Conditions

5.4.1 Natural Boundary Conditions

Natural boundary condition are applied at the second joint of the manipulator system i.e., component of the shear force at the end point of the first link $(\tilde{F}_{1,2n_1-1})$ is to be balanced by the shear force at the same node to the second link $(\tilde{F}_{2,1})$ of the manipulator given by

$$\tilde{F}_{1,2n_1-1} + \tilde{F}_{2,1}\cos(\theta_2 + u_{2n_1+1}) = 0. \tag{5.24}$$

Other forced boundary conditions are

(i) bending moment at the end of links

$$E_1 I_1 \left.\frac{\partial^2 u}{\partial x_1^2}\right|_{(L_1,t)} = -\tau_2, \tag{5.25}$$

$$E_2 I_2 \left.\frac{\partial^2 w}{\partial x_2^2}\right|_{(L_2,t)} = 0, \tag{5.26}$$

and

(ii) shear force at the end of second link

$$\frac{d}{dx_2}\left(E_2 I_2 \frac{\partial^2 w}{\partial x_2^2}\right)\Bigg|_{(L_2,t)} = 0. \tag{5.27}$$

5.4.2 Essential Boundary Conditions

Link 1 and link 2 are considered as a rotating cantilever beams. Hence, slope and deflection at the first node of the links should be zero with respect to time *'t'*, *i.e.,*

$$u_1(0,t) = 0, \tag{5.28}$$

$$\left.\frac{\partial u_1}{\partial x_1}\right|_{(0,t)} = 0, \tag{5.29}$$

and

$$w_1(0,t) = 0, \tag{5.30}$$

$$\left.\frac{\partial w_1}{\partial x_2}\right|_{(0,t)} = 0. \tag{5.31}$$

Neglecting load vector, Eq. (5.23) becomes standard eignvalue problem, which is solved to obtain natural beam and system frequencies. Numerical integration of Eq. (5.23) is carried out by using Newmark's integration scheme to obtain transverse deflection u and w, rigid body motion θ_1 and θ_2 and its derivatives.

5.5 Effect of Hub Inertias and Tip Loads

Effects of hub inertia, motor mass and payload mass may be incorporated in the global mass matrix and stiffness matrix using Dirac delta function as described by Dixit *et al.* [2006] and shown in Table 5.1. In this work, the inertia of the motor mass and payload are neglected.

Table 5.1 Additional terms in the mass matrix elements

Matrix Element	Additional term in the mass matrix element
$M(1,1)$	$J_{h_1} + M_m L_1^2 + M_p (L_1 + L_2)^2$
$M(1, 2n_1+2)$, $M(2n_1+2,1)$	$M_m L_1 + M_p (L_1 + L_2)$
$M(2n_1+2, 2n_1+2)$	M_m
$M(2n_1+4, 2n_1+4)$	$J_{h_2} + M_p L_2^2$
$M(2n_1+2n_2+5, 1)$ $M(1, 2n_1+2n_2+5)$	$M_p L_2$
$M(2n_1+2n_2+5, 2n_1+2n_2+5)$	M_p

5.6 Model Validation

The structural dimension of Tokhi *et al.* [2001] is considered for the first link and very small length (10 mm) is considered for the second link for the program instruction code validation. Here the same bang-bang excitation torque about the shoulder axis of rotation is considered. Simulation results for dynamic tip deflections and hub angles for without payload are plotted in Figure 5.3 and it is observed that tip responses and hub angles are very close to that of Tokhi *et al.* [2001]. (The results of Tokhi *et al.* are almost similar; hence they are not plotted here.) Dynamic response is also plotted as per structural dimension considered for double link flexible manipulator by Ge *et al.* [1996] in Figure 5.4. Excited control torques are as per position and derivative (PD) control and energy-based robust (EBR) control strategy as per Eqs. (3.30) and (3.33), respectively. Simulated results are well agreed with the result of Ge *et al.* [1996]. (The results of Ge et al. are not plotted here, as they are almost same as the present results.) Hence, the developed

model may be considered for shape optimization of rotating link for three different optimization problems.

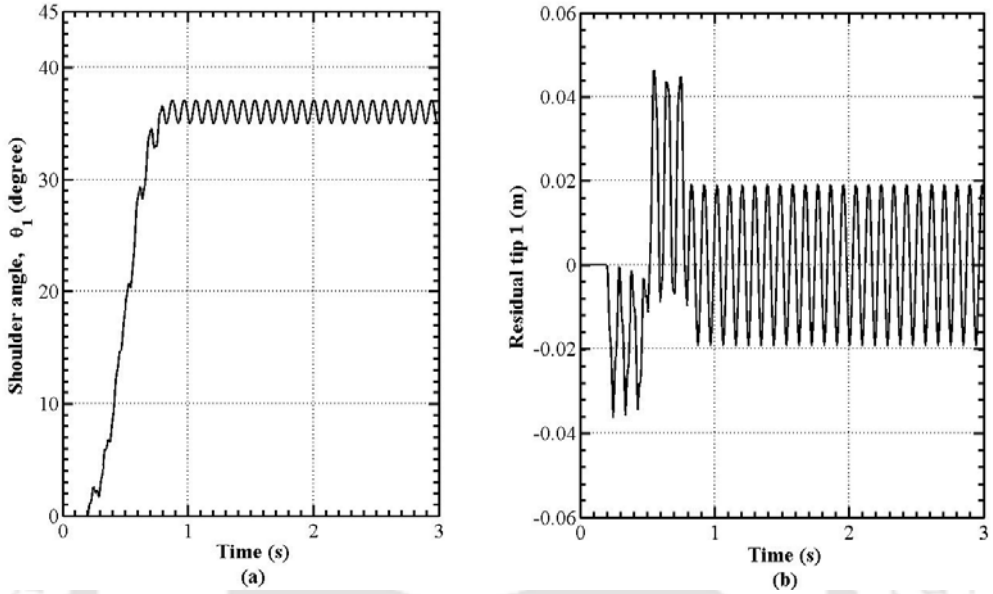

Fig. 5.3 Typical results: (a) hub Angle (shoulder) and (b) residual vibration of tip

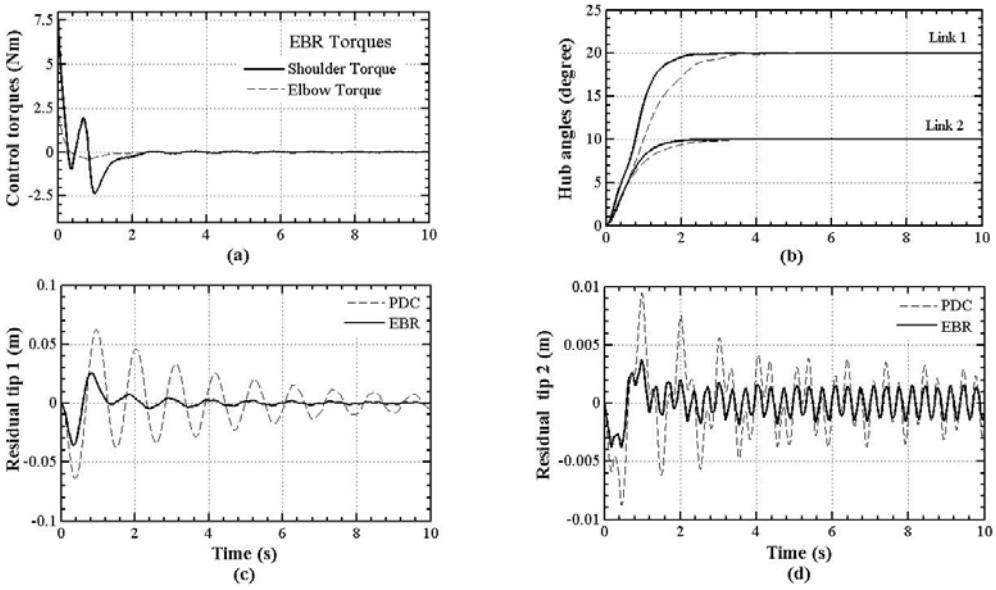

Fig. 5.4 Effect of control torques: (a) control torques (EBR), (b) hub angle, (c) residual vibration (tip1), (d) residual vibration (tip2)

For the final angular position of the links ($\theta_{f_1} = 20^0$ and $\theta_{f_2} = 10^0$), profiles of the required control torques are plotted as per position and derivative (PD)

control and energy-based robust (EBR) control law. It is observed that they agree well with the result of Ge *et al*. [1996]. Hence, the developed model is considered for shape optimization of rotating links for optimization problems.

5.7 Results and Discussion

Before shape optimization of the double link flexible manipulator, it is very essential to observe its dynamic behavior due to the effect of the system parameters and different torque profile excitation and its amplitude.

5.7.1 Parametric Study

In this section, a comparative analysis has been carried out for uniform as well as shape optimized double link flexible revolute manipulator. For the numerical study, a manipulator having uniform diameter 0.01 m, length 1.0 m, mass per unit length 217.3 gm/m, Young's modulus of elasticity 69 GPa is considered for both the links. Damping of the system is neglected. Most of the numerical simulations are carried out subjected to a sinusoidal torque given in Eq. 5.32 about the axis of rotation,

$$\left.\begin{array}{ll} \tau_k = \tau_{m_k} \sin \pi t, & 0 \le t \le 2 \\ = 0, & 2 < t \le 4 \end{array}\right] k = 1, 2 \qquad (5.32)$$

where, τ_k, τ_{m_k} and t represent applied torque, torque amplitude and time duration respectively. Torques τ_1 and τ_2 are applied to the hub axis and joint axis, respectively.

The dynamic behaviors depend upon many parameters of double links flexible manipulator and also dynamic response consists of several desired objectives *viz*. higher hub angle, less static deflection, less residual vibration, less response and settling time, *etc*. Improved dynamic response is a multi objective problem. Here, some parametric study is carried out to analyze the dynamic behaviour of double link flexible manipulator.

5.7.1.1 Dynamic Response due to Different Payloads

Dynamic behaviour of the double link flexible manipulator changes with respect to the change of payloads at the tip of second link as shown in Figure 5.5. It is

observed that with the increase of payloads, the magnitudes of hub angle and joint angle reduce. Residual vibration is considerably more at tip of 1st link or 2nd link depending upon the input torque at hub joint or link joint respectively.

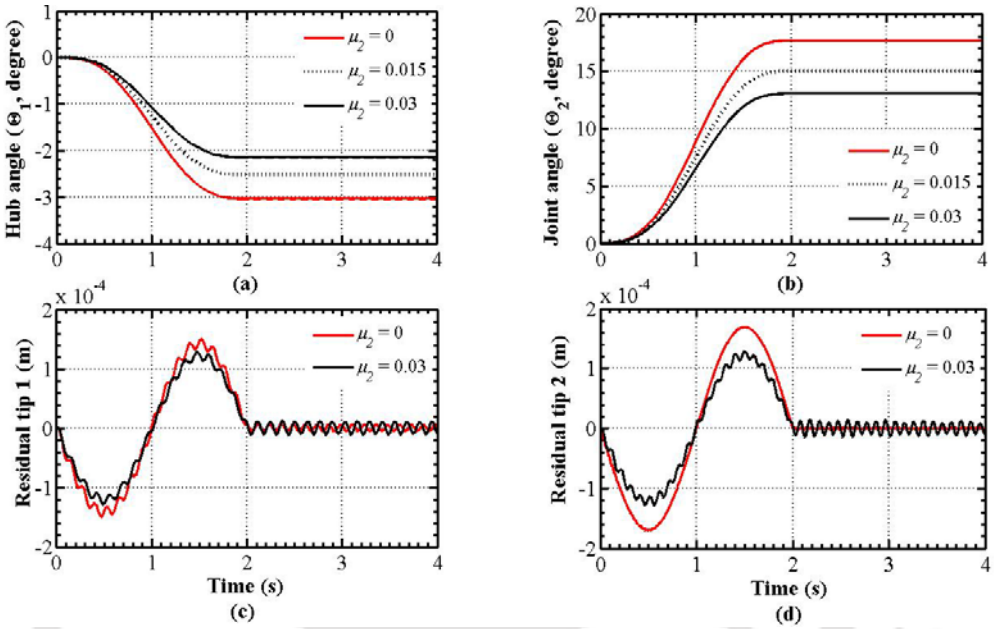

Fig. 5.5 Dynamic response due to payloads at the tip (a) Hub angle, (b) Joint angle, (c) Residual Tip 1, (d) Residual Tip 2 with $\mu_1 = 1,\ \beta = 5, \tau_{m_1} = 0$ and $\tau_{m_2} = 0.02$ N.m

It is also observed that there is very small effect in dynamic response with the increase of hub inertia. Similar trend is observed in dynamic response due to the variation of motor mass (tip load at link1) and hub mass.

5.7.1.2 Effect of Link Lengths on Dynamic Response

Dynamic response of the double link flexible manipulators also depends upon the links length ratios. Payload ratios (μ_1, μ_2) are defined as the ratio of payload to beam mass and link length ratio (α) is length of second link to first link. For the payloads ratios $\mu_1 = 0.01,\ \mu_2 = 0.02,\ \beta = 5$ and input torques $\tau_{m_1} = 0.2$ Nm and $\tau_{m_2} = 0.04$ Nm, effects of different links length ratios (α) is plotted in Figure 5.6, keeping length of the first link constant ($L_1 = 1.0$ m). The lesser the length of link 2 with respect to Link 1, the better the dynamic response i.e. more hub/joint angle and lesser residual

vibration for the given set of torque. Therefore, designer should not prefer the longer second link with respect to the first link.

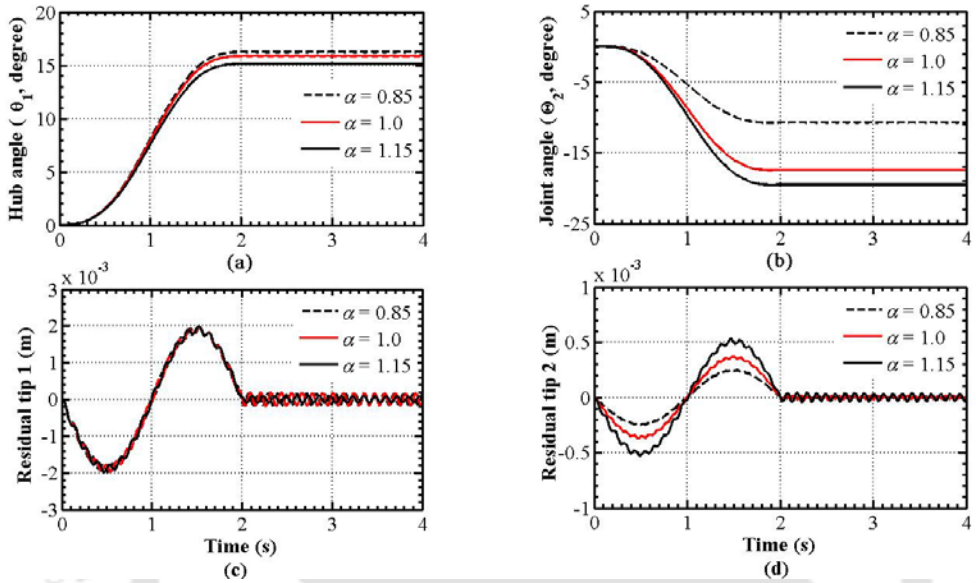

Fig. 5.6 Dynamic response due to variation of link lengths (a) Hub angle, (b) Joint angle, (c) Residual Tip 1, (d) Residual Tip 2 with $\mu_1 = 0.01, \mu_2 = 0.02,$ $\beta = 5, \tau_{m_1} = 0.2\,\text{Nm}$ and $\tau_{m_2} = 0.04\,\text{Nm}$

5.7.1.3 Dynamic Response due to Different Input Torques

In double link flexible manipulator dynamic response depends upon the magnitude of input torques at the hub and joint between link 1 and 2. For the payloads ratios $\mu_1 = 0.4,\ \mu_2 = 0.02,\ \beta = 5$ and the input torque $\tau_{m_1} = 0.4\,\text{Nm}$, dynamic response due to the variation of torque τ_2 is plotted in Figure 5.7. It is observed that there is a decrease of the hub angle and increase of joint angle with the increase of torque amplitude. As the magnitude of applied torque τ_2 increases, there is considerable increment in the residual vibration of the tip of second link. Similar trend is also observed due to the variation of input torque τ_1 at the hub joint (result not shown here). Thus, tip vibration increases for a particular link with the increase of torque amplitude acting in that particular link. Overall angular displacement depends upon the set of input torques at the joints.

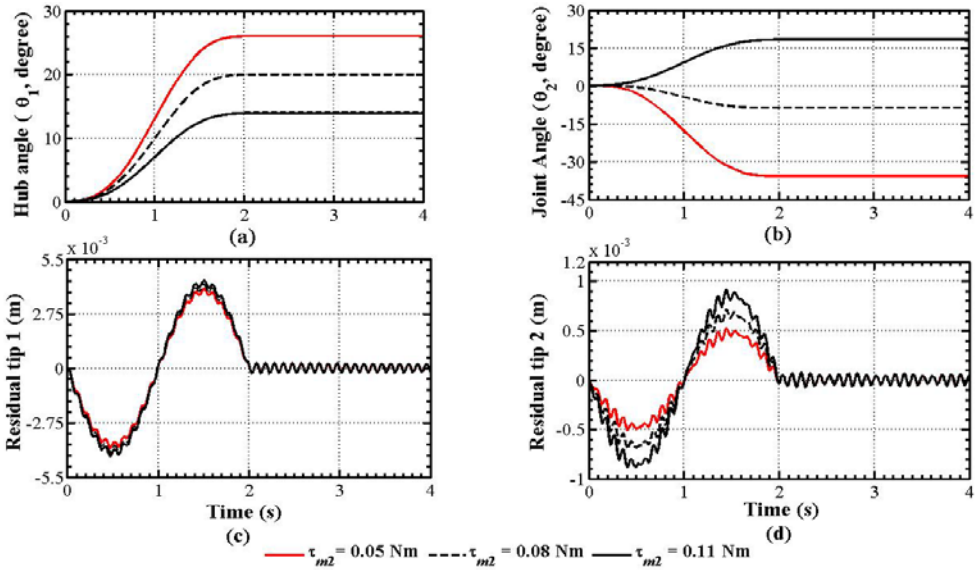

Fig. 5.7 Dynamic response due to variation of applied torque (a) Hub angle, (b) Joint angle, (c) Residual Tip 1, (d) Residual Tip 2 with $\mu_1 = 0.4, \mu_2 = 0.02,$ $\beta = 5$ and $\tau_{m_1} = 0.4$ Nm

5.7.1.4 Comparative Dynamic Response due to Different Torque Profile

Different torque profiles shown in Figure 5.8 are considered for the comparison of dynamic response of double link flexible manipulator. All the torque profiles have same amplitude *i.e.* 0.5 Nm and same duration of excitation *i.e.* 4 sec. Dynamic response due to different torque profiles are shown in Figure 5.8.

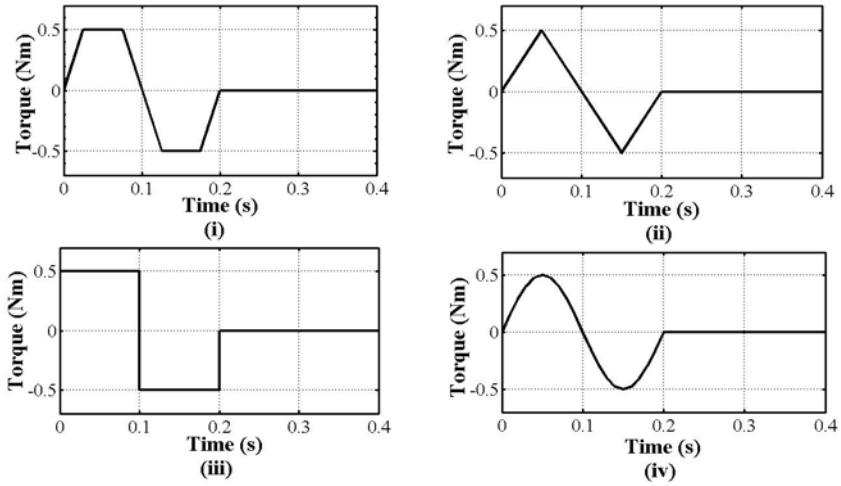

Fig. 5.8 Different torque profiles (a) Trapezoidal, (b) Triangular, (c) Bang-bang, (d) Sinusoidal

Triangular torque profile gives the lesser hub angles to the links. Bang-bang torque gives high input energy to the system giving high hub angle as well joint angle. However, due to sudden change, bang-bang torque produces high residual vibration to the system. Sinusoidal torque may be preferred for smooth operations of the system.

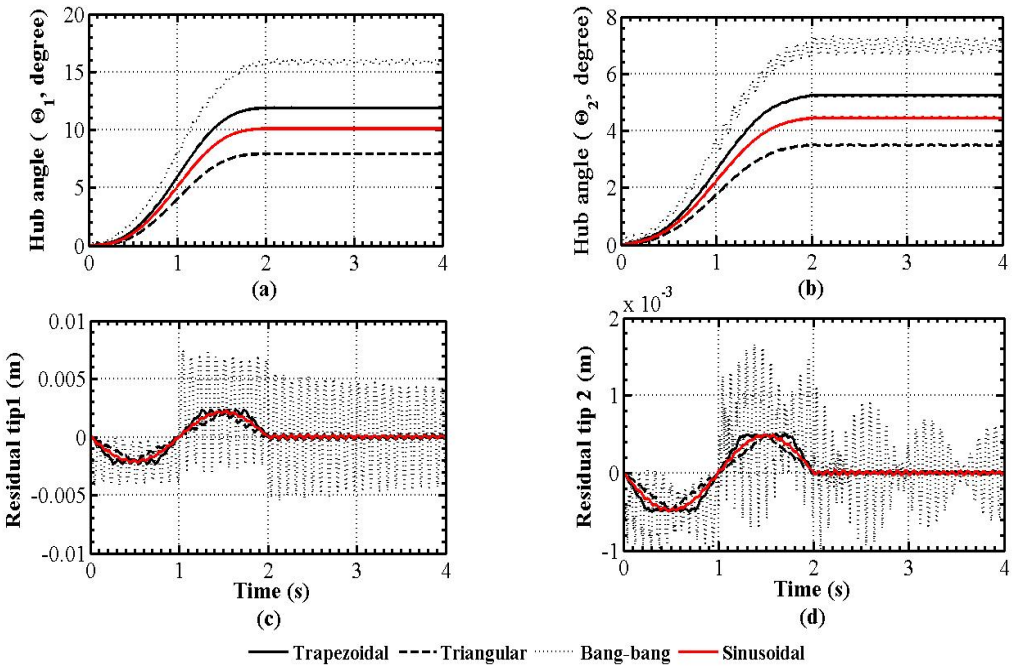

Fig. 5.9 Dynamic response due to different torque profiles (a) Hub angle, (b) Joint angle, (c) Residual Tip 1, (d) Residual Tip 2 with $\mu_1 = 0.02, \mu_2 = 0.02$, $\beta = 5, \tau_{m_1} = 0.2$ Nm and $\tau_{m_2} = 0.06$ Nm

5.7.2 Shape Optimization

In this section, a comparative analysis has been carried out for uniform as well as shape optimized double link flexible revolute manipulator. For the numerical study, the manipulator having uniform diameter 0.01 m, mass density 2710 kg/m^3, Young's modulus of elasticity 71.1 GPa are considered for both the links. Lengths of the links 1.0 m and 0.8 m, hub radii 15 mm and 10 mm, hub inertia 1.0 kg.m^2 and 0.02 kg.m^2 are considered for first and second link respectively. Motor mass and payload mass are considered 0.1 kg and 0.04 kg respectively. Damping of the system is neglected. The system parameters are shown in Table 5.3.

Table 5.2 System parameters

Parameters	Link 1	Link 2
Length	L_1=1.0 m	L_2=0.8 m
Young' modulus	E_1=71.1×10^9 N/m^2	E_2=71.1×10^9 N/m^2
Diameter	d_1=0.01 m	d_2=0.01 m
Mass density	ρ_1=2710 kg/m^3	ρ_2=2710 kg/m^3
Hub inertia	J_{h_1}=1.0 kg.m^2	J_{h_2}=0.02 kg.m^2
Hub radius	a=0.015 m	b=0.01 m
Payload	M_m=0.1 kg	M_p=0.04 kg

Unless otherwise stated, numerical simulations are carried out subjected to the bang-bang torques τ_1 and τ_2 applied to the shoulder joint axis and elbow joint axis respectively. Torque amplitudes of 1.0 Nm and 0.1 Nm are considered for τ_{m_1} and τ_{m_2} respectively for numerical experiments. The torque profiles are shown in Figure 5.10.

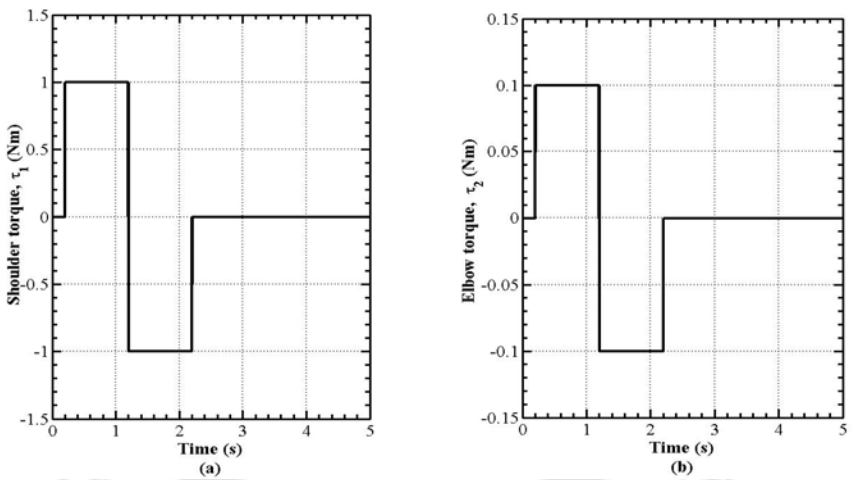

Figure 5.10 Bang-bang torque (a) at shoulder joint, (b) at elbow joint

5.7.2.1 Dynamic Response due to Payload

The dynamic behavior of double links flexible manipulator depends upon many system parameters *viz*., link lengths, link masses, tip loads, hub inertias and excitation amplitude and frequency. As we are more concerned about the effect of payload in the flexible robotic system, its dynamic behavior is plotted in Figure 5.11. It is observed that with the increase of payload, the magnitude of hub (shoulder) angle and joint (elbow) angle reduce. Residual vibration considerably

increases at the tips of both the links. These dynamic responses are compared with the results of optimized links under similar environment for vibration confinement (suppression).

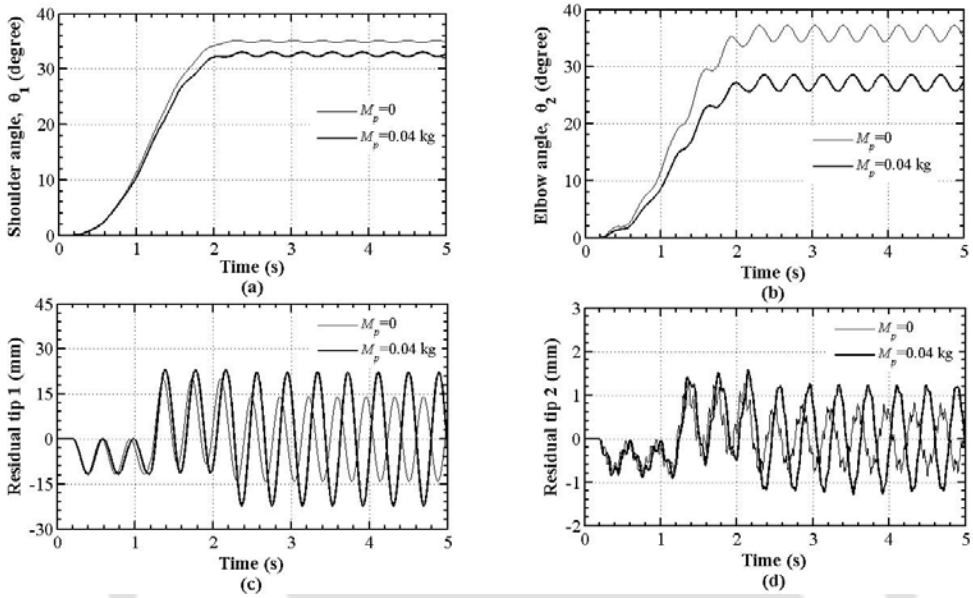

Figure 5.11 Dynamic response due to payloads at the tip 2, (a) shoulder hub angle, (b) Elbow hub angle, (c) Residual vibration of Tip 1, (d) Residual vibration of Tip 2

5.7.2.2 Optimization Procedure

Lengths of the manipulator are decided at the design stage of robotic system. Cross-section variation is the option for optimization to improve mechanically the dynamic behaviour. In this chapter, circular cross-section is considered because of the ease of the manufacturing. Three different optimization problems as shown in Table 5.2 are considered for shape optimization.

Table 5.3 Different optimization problems

Optimization Problem	Objective	Constraint
I (Prob-I)	Minimization of static tip deflection of links	$M_i^* - M_i \le 0$
II (Prob-II)	Maximization of fundamental beam frequency of links	$M_i^* - M_i \le 0$
III (Prob-III)	Maximization of fundamental beam frequency of links	$M_i^* - M_i \le 0$ $\delta_i^* - \delta_i \le 0$
Permissible Bound : $X_i^{LB} < X_i < X_i^{UB}$ (i =1 for link 1 and 2 for link 2)		

In the optimization problems, $X = [\, d_1 \;\; d_2 \;\; . \;\; . \;\; . \;\; d_{n-1} \;\; d_n \,]^T$ is a design vector with d_j indicating diameter of the j^{th} element of a link. For first link n is equal to n_1 and for the second link it is equal to n_2. X_i^{LB} and X_i^{UB} are the vectors of lower and upper bounds of design variables respectively.

In this work, MATLAB function "*fmincon*", which uses SQP technique for constrained optimization of nonlinear function is employed. Optimized links obtained through optimization problem-I, II, and III are expressed as Prob-I, Prob-II, and Prob-III respectively. Optimized shapes of the manipulator for the optimization problem defined in Table 5.2 are plotted in Figures 5.12–5.14. Optimized shapes under Prob-I are obtained to minimize the static tip deflection due to 1 N force at the tips of the links.

However, in other optimization problems, shoulder link is optimized for motor mass as a tip load and elbow link is optimized for no payload and payload of 0.04 kg cases. Mass of the optimized links are less than or equal to the mass of the individual links. There are different optimal shapes for different payloads on the elbow link. Optimised shape for 0.04 kg payload is analysed further for comparative study. Plotted optimised shapes extremize that particular objective function under that given constraints. Numerical results shown in Table 5.4 of the optimized beams are as per the defined objective functions and constraints.

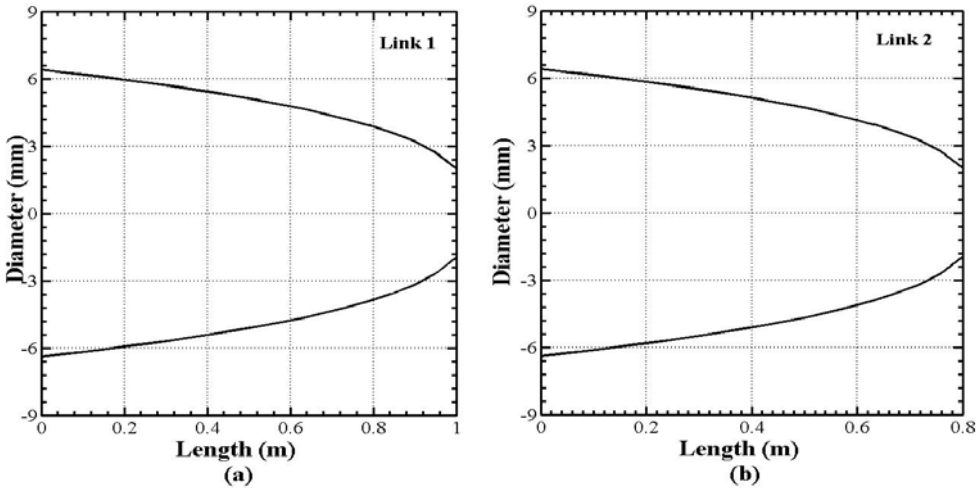

Figure 5.12 Optimized shape of Prob-I (a) First link (b) Second link,

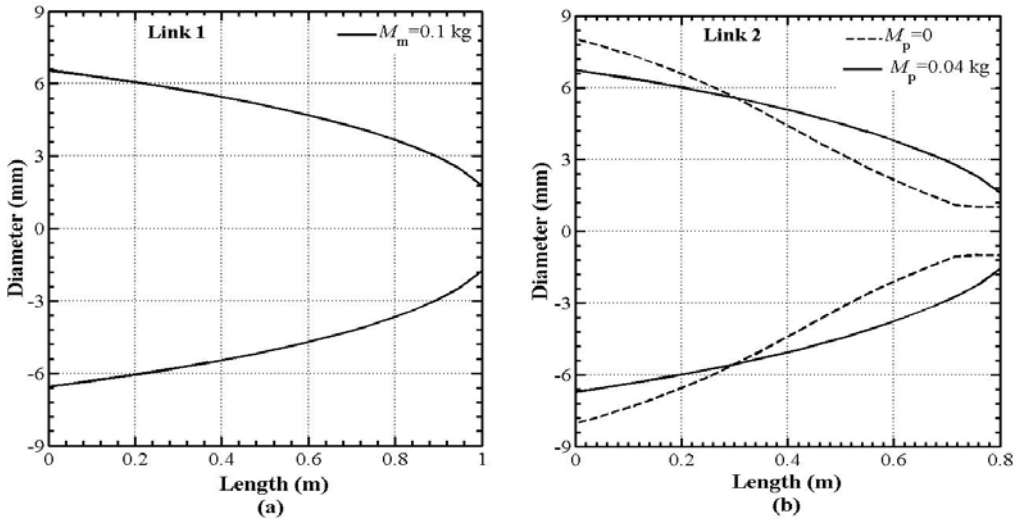

Figure 5.13 Optimized shape of Prob-II (a) First link (b) Second link

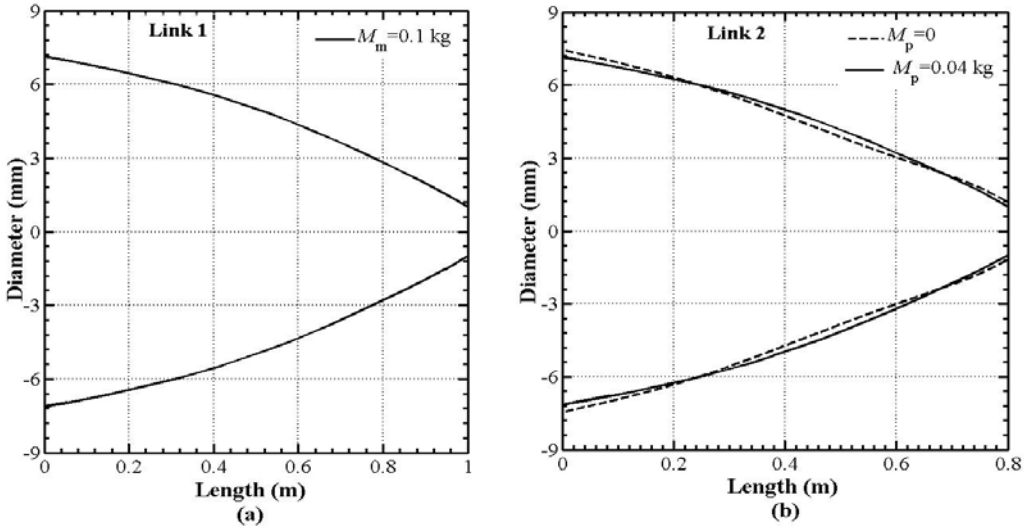

Figure 5.14 Optimized shape of Prob-III (a) First link (b) Second link

Table 5.4 Comparative optimized parameters

Parameter/ Type of links	Mass (kg)		Fundamental frequency (Hz)			Static tip deflection due to 1 N at tip (mm)	
	Link 1	Link 2	Link 1	Link 2	Whole system	Link 1	Link 2
Uniform links	0.2128	0.1703	4.195	7.887	2.041	9.551	4.89
Prob-I	0.2128	0.1703	5.872	11.783	2.583	6.229	3.186
Prob-II	0.2128	0.1703	5.926	12.087	2.411	6.291	3.339
Prob-III	0.2128	0.1703	5.064	10.656	5.682	9.551	4.891

5.7.2.3 Optimised Dynamic Response

Comparative dynamic response (hub angles) of shape optimised links for 0.1 kg motor mass and 0.04 kg payload are plotted in Figure 5.15. It is observed that Prob-III attained the higher overall hub angles rotations with respect to uniform links as well as Prob-I and Prob-II under the same set of input torques. Hub angle rotation has significant importance as for as the system input energy to the system is concerned.

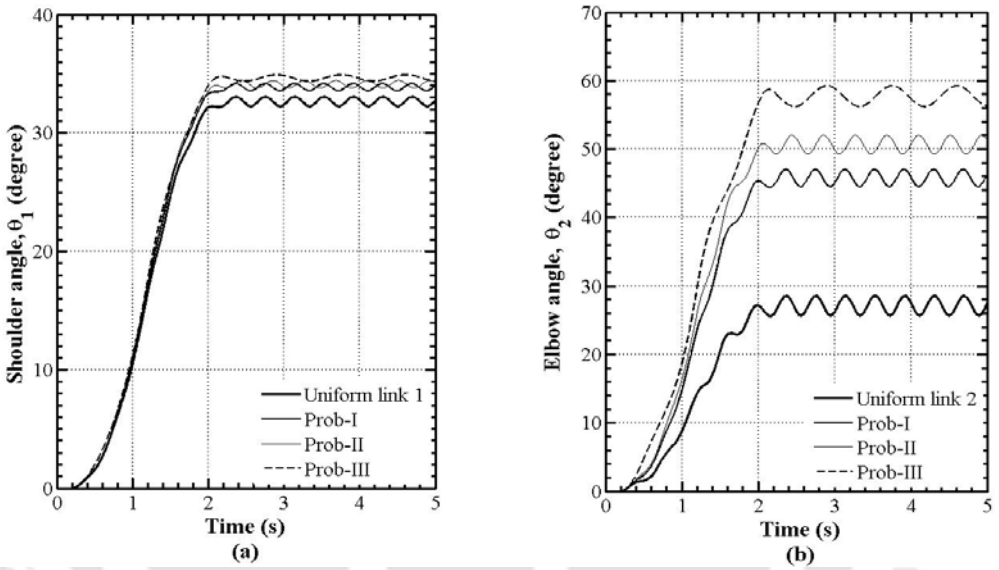

Figure 5.15 Comparative hub angle due to bang-bang torques at joints (a) shoulder joint, (b) elbow joint

Residual vibration of tip 1 and tip 2 are plotted in Figures 5.16–5.18 for different optimization problems. Prob-II has the lowest residual vibration. Residual tip vibration delays the subsequent operation of robotic system. It is observed that optimised links reduce the system residual vibrations. For overall improved dynamic response (hub angles and residuals), designer may opt Prob-II among the three optimized cases. For faster manufacturing process operations, residual vibration of the robotic links should be suppressed.

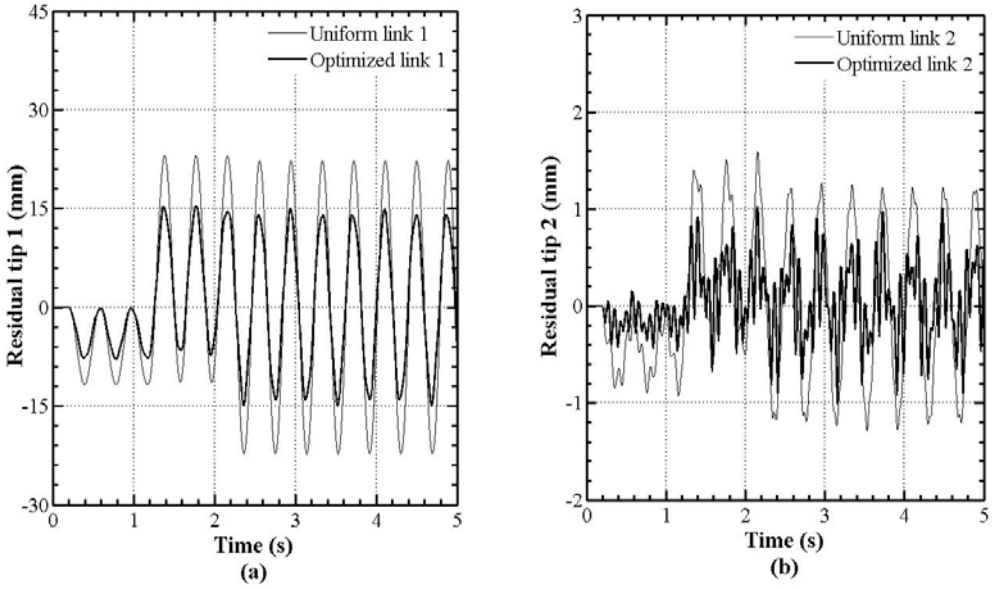

Figure 5.16 Comparative residuals of Prob-I due to bang-bang torques at joints, (a) link 1, (b) link 2

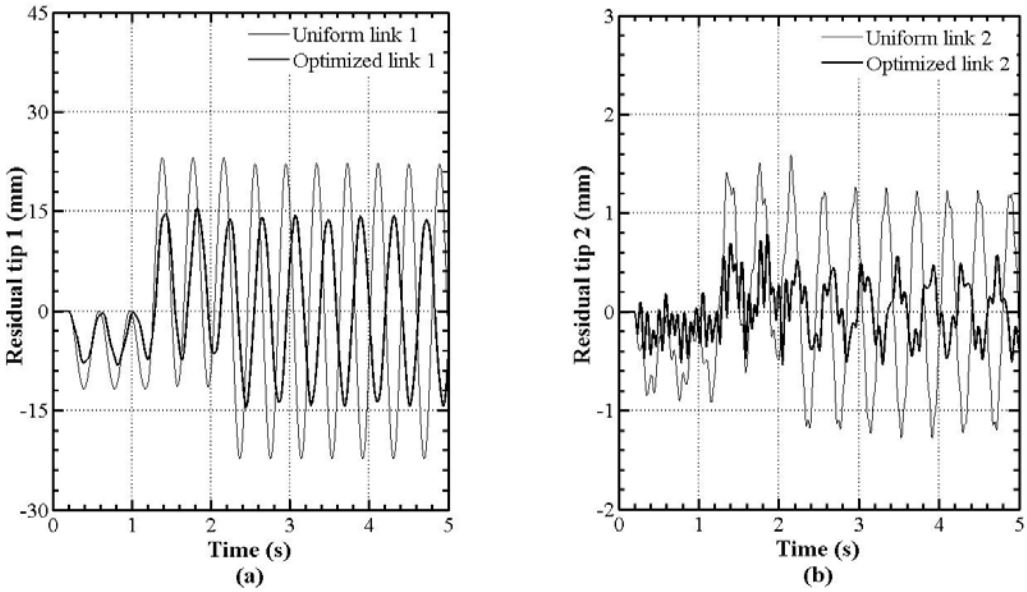

Figure 5.17 Comparative residuals of Prob-II due to bang-bang torques at joints, (a) link 1, (b) link 2

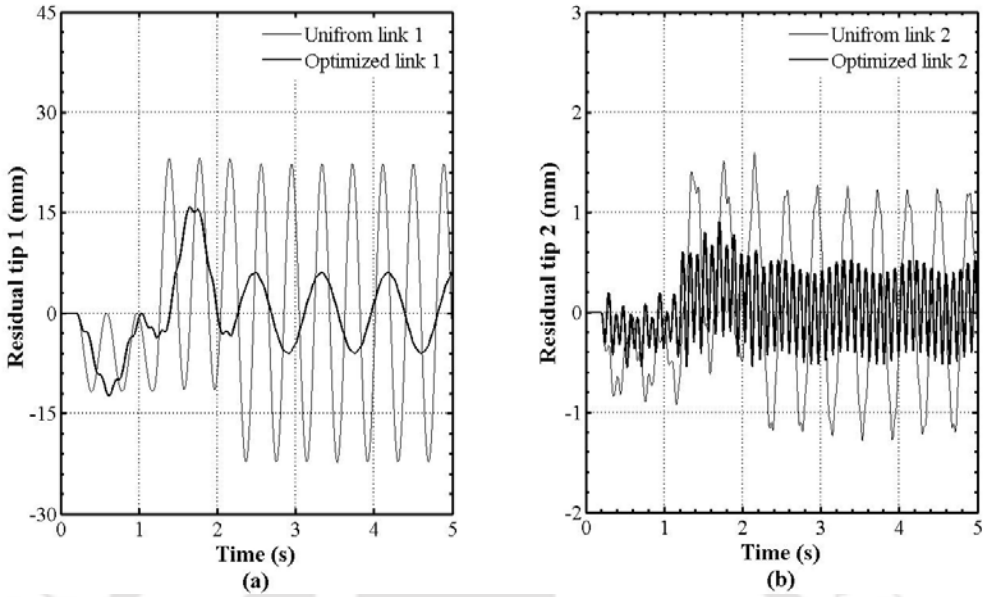

Figure 5.18 Comparative residuals of Prob-III due to bang-bang torques at joints, (a) link 1, (b) link 2

5.7.2.4 Optimised Links under Controlled Torques Excitations

Developing control strategy is another way to improve the dynamic response of a plant. However, addition of sub-system to the plant moves towards the instability which require further thorough analysis. Ge *et al.* [1996] presented the energy based robust (EBR) control strategy for double link flexible manipulator given by Eq. (5.35). For the input bang-bang torques at the joints (Figure 5.4), final angular positions are attained as $\theta_{f_1} = 34.1^0$ and $\theta_{f_2} = 49.6^0$. For the same final angular positions, EBR control torques are excited and compared results are plotted in Figures 5.19–5.20.

Control torques for the given final angular positions are shown in Figure 5.13(a). Obviously, there will be different control torques profiles for different final position of the links. It is observed that settling time is more in case of control torques (Figure 5.13b).

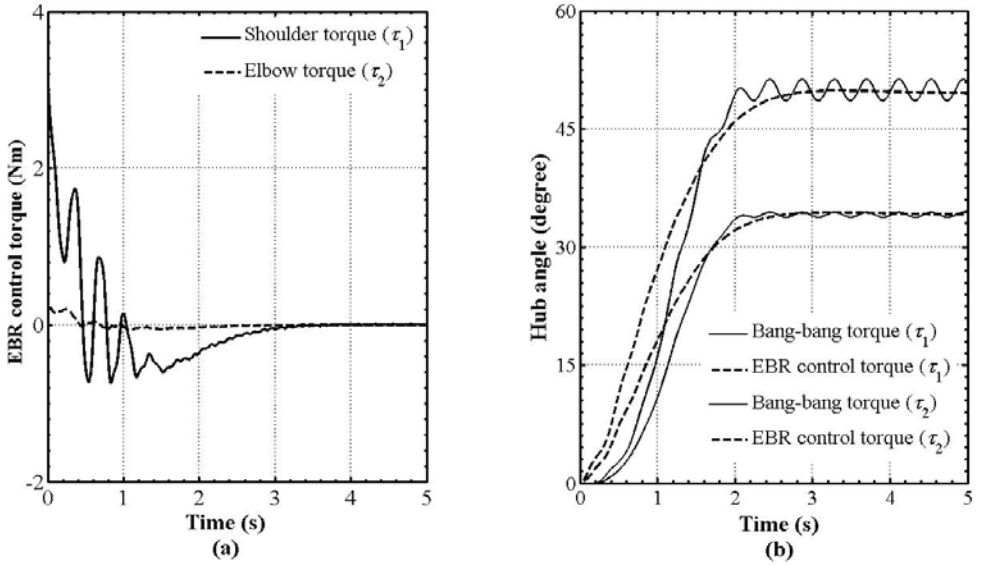

Figure 5.19 (a) Control effort (EBR) of Prob-II, (b) Hub Angles

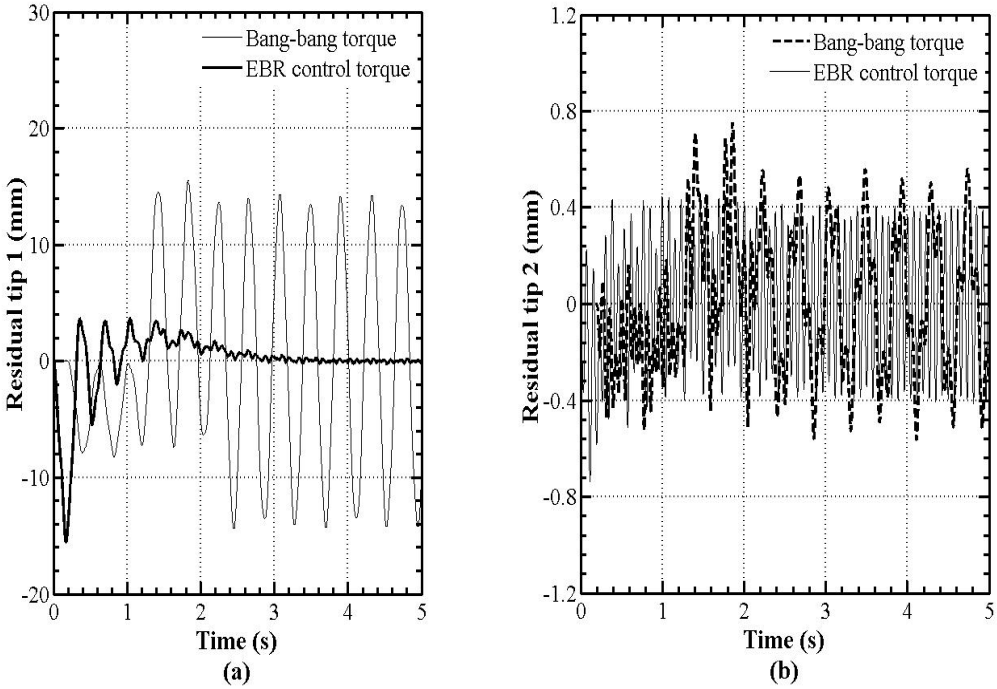

Figure 5.20 Comparative tip residuals of Prob-II (a) link 1, (b) link 2

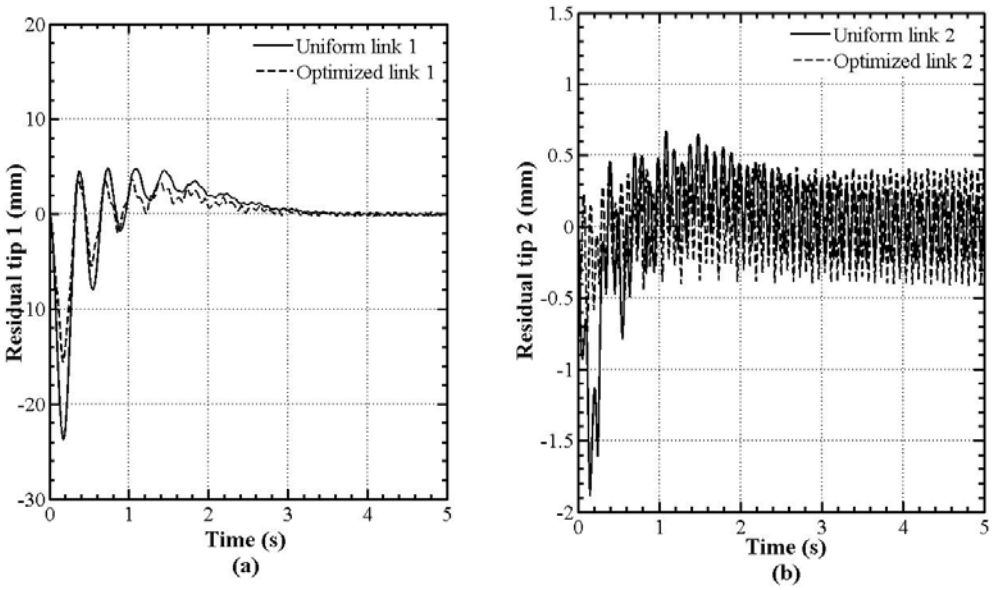

Figure 5.21 Comparative tip residual of Prob-II due to control torque (a) link 1, (b) link 2

From Figure 5.20, it is observed that residual vibrations of the optimized links are further suppressed in case of control torques excitations with respect to bang-bang torques. It is also observed (Figure 5.21) that residual vibrations of optimized links with control torques excitations are improved with respect to the uniform links under same excitation. Therefore, optimal control strategy for an optimized system may be the prime goal for a system designer.

5.7.2.5 Effect of Active Constraint M^*

Dynamic responses of the optimized beams under different optimization problems are shown in Table 5.3. It is observed that mass of the optimized beams is equal to the mass of uniform links (0.2128 kg and 0.1703 kg, respectively) and hence it is an active constraint. To observe the sensitivity of the effect of optimized mass, mass of the optimized beam is increased by 10% (*i.e.* $M^*=1.1M$). Optimized shapes look similar, albeit scaled (Figure 5.5).

Increasing mass of optimized links (Prob-II) suppress further the residuals but due to increase of inertia, hub rotation angles are reduced. Improved dynamic response due to increase of mass is plotted in Figures 5.23–5.24 and numerical

results are shown in Table 5.5 for comparative study. It is observed that dynamic response of the system is very sensitive towards the mass of the optimized links.

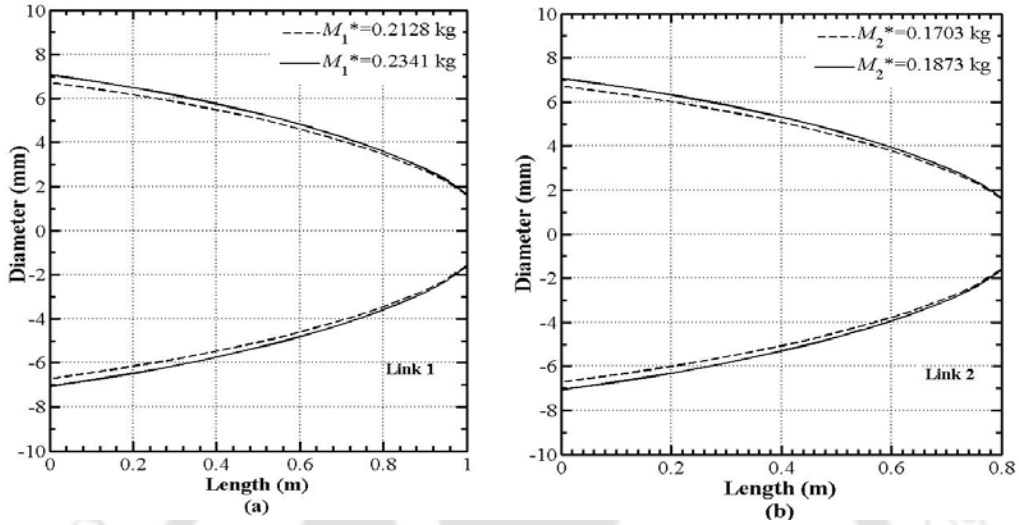

Figure 5.22 Optimal Shapes (Prob-II) of (a) Link 1, (b) Link 2

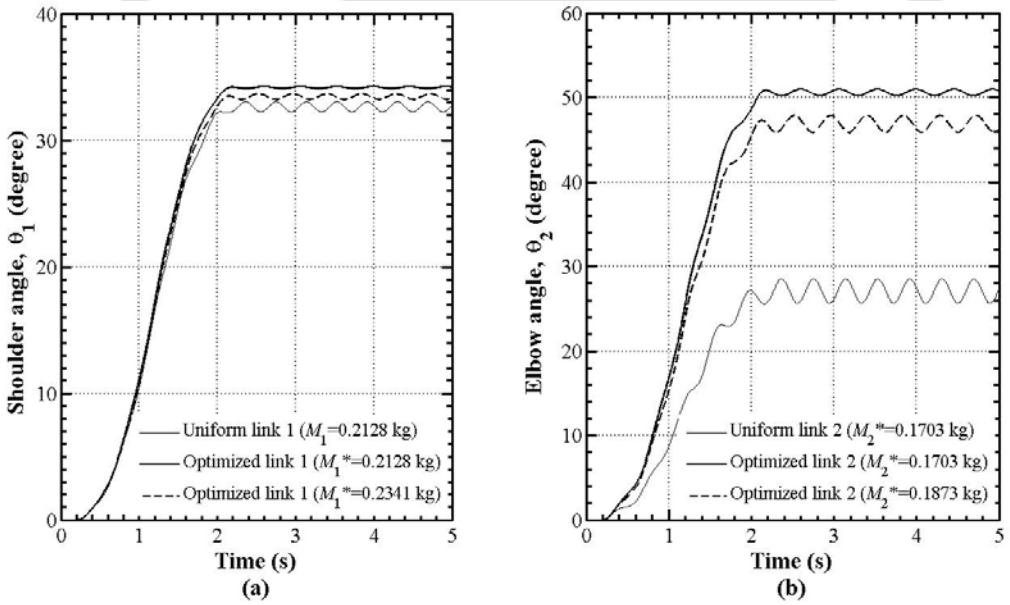

Figure 5.23 Joint angles (Prob-II) due to bang-bang torque (a) link 1, (b) link 2

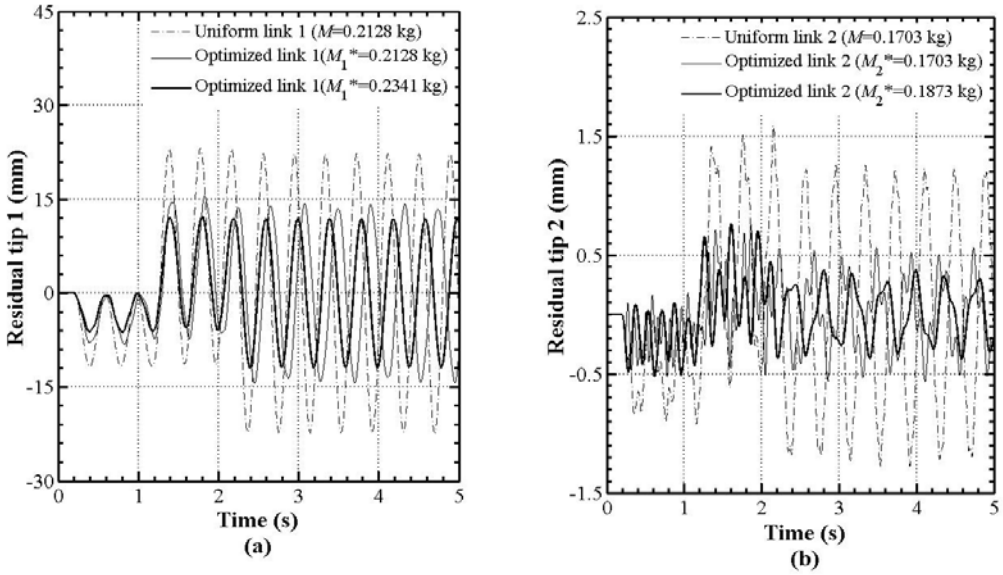

Figure 5.24 Tip residual (Prob-II) due to bang-bang torque (a) link 1, (b) link 2

Table 5.5 Comparative parameters due to increased rigidity

Parameter/ Type of links	Fundamental frequency (Hz)			Static tip deflection due to 1 N load at tip (mm)		Maximum dynamic tip deflection (mm)	
	First link	Second link	Whole System	First link	Second link	First link	Second link
Uniform links	4.195	7.887	2.041	9.551	4.890	17.146	1.226
Prob-II ($M^*=M$)	5.926	12.083	2.403	6.292	3.340	15.046	0.629
Prob-II ($M^*=1.1M$)	6.451	13.171	2.785	5.244	2.777	14.135	0.614
Sensitivity	Hz/kg			mm/kg		mm/kg	
	24.63	51.09	9.97	-49.18	-33.11	-42.77	-0.88

However, as we increase the mass of the links, system become more rigid and bulky which require more energy to overcome the inertia during motion. Therefore, designer must take the best compromise to retain the advantages of flexible links system.

5.8 Summary

Dynamics of double link flexible manipulator is highly complex and nonlinear in nature. Model is linearized to reduce the complexity of the model and tried to predict the behaviour of the system under low amplitude of vibration excitation. Based on numerical analysis, following observation are noted –

- Dynamics of double link flexible manipulator highly depends upon system parameters *viz.* payloads at tip and link joint, link lengths, input torque magnitude and profile and hub inertia.
- Optimization problem-II (maximization of fundamental frequencies of links under its mass constraints) gives the overall improved dynamics of the system.
- Vibration suppression of optimized links further improved through proper control strategy.
- Mass of the optimized links are active constraints. Therefore, improved dynamics of the optimized links are sensitive towards the increase of link masses.

Chapter 6

Conclusions and Scope of Future Works

6.1 Conclusions

In this thesis, shape optimization of revolute-jointed flexible robotic manipulators is carried out theoretically on single flexible link, rigid-flexible links, and double flexible inks manipulator. Theoretical models are developed for all the cases with the help of basic mechanics and finite element method. Consistent mass and stiffness matrices are obtained and thus the distributed system is converted to discrete system. Finally, Lagrangian method is used to obtain the equation of motion of the whole system in generalized form for further dynamic analysis. Various optimization problems are designed from the derived finite element equations for shape optimization of the links.

Optimum system design has always a great importance in engineering analysis. There are several proposed optimization problems for revolute-jointed flexible manipulator. Optimal design and proper control strategy are the high end technical aspects in the real applications of the dynamical system. In true sense, optimal control of the optimized mechanical systems may be the prime goal of the engineer.

Dynamics of flexible robotics systems are highly complex and non-linear in nature. However, linearized models are used for the shape optimization. In this work, due to high number of design variables in finite element form, a classical technique sequential quadratic programming (SQP) is used for shape optimization.

The important contributions as well as observations of this thesis can be summarized as follows:

- Various optimization problems are designed and analyzed for single/multi link flexible manipulators. There are different shapes for different

optimization problems. Optimized shapes extremize exclusively that particular objective problem. There are further variations of the optimized shapes for different payload in almost all the optimization problems.

- In all the optimization problems, masses of the links are redistributed towards the root of the individual links. This tends to enhance its rigidity.
- Improvement of the system parameters (frequency *etc*.) through shape optimization is more significant for no-payload case. Fundamental frequency of optimized single link manipulator (Prob-I) is increased by 391% for no payload case and 140% for payload of 50% of the beam mass. The improvement decrease with the increase of payload. For no payload case, system frequency is increased by 195.8% (Prob-IV); static tip deflection is reduced by 34.83% Prob-II) and dynamic tip deflection is reduced by 66.16% (Prob-III).
- Links optimized at higher payload always behave with overall improved dynamics even for lower payloads but not the vice-versa.
- In practice, different optimized links cannot be used for corresponding payloads, as it will delay the manufacturing process. Hence, single optimized shape may be designed to cater to a range of payloads (μ=0–0.7).
- All the optimization problems suppress the vibrations (residuals) considerably. However, there is a specific shape, which suppresses it the most (75% for $\mu = 0$ and 42% for $\mu = 0.2$).
- Almost, similar shapes are obtained in the case of rigid-flexible links and double flexible links manipulators with respect to single link flexible manipulator. Here, individual link masses are considered as constraints.
- In case of bang-bang, trapezoidal, triangular and sinusoidal torque profiles having same amplitude and time period, sinusoidal torque produces less vibration and bang-bang torque gives the higher hub angle (3.8^0) with respect to the other torque profiles.
- Sometimes, there are no feasible solutions for shape optimization of links in higher mode of vibrations.

- Some objectives conflict with each others. Shape optimization of flexible robotic system is a pareto-optimal problem. Shape optimized links for one objective may have even poorer performance in other objective than in the case of the uniform links.
- Dynamics of multi-link flexible robotic systems are very sensitive towards its system parameters and a set of excitation torques.
- In all the optimization problems, it is observed that the mass of the optimized links are the active constraints. By increasing the mass of the optimized links (10%), it is observed that robotic system moves towards the rigid system. To retain the advantages of the flexible system, best compromise should be made.
- Controlled torque(s) obviously suppress the vibration of non-optimized flexible robotic system. However, it suppresses the vibrations more in the case of optimized one (more than 50%).

6.2 Scope of future works

- Some other optimization problems may be designed treating it as a multiobjective problem for overall static and dynamic response improvement of the flexible robotic system.
- Shape optimization may be carried out through non-linear modeling considering large deflection during the motion of the flexible robotic system.
- Shape optimization of links of double link manipulator may be done considering combined masses of the links as constraint.
- Parametric study and dynamics of optimized robotic system may be verified experimentally.
- Controlled torques may be applied to optimized and non-optimized robotic system experimentally for comparative study.
- Electro-mechanical modeling of the flexible manipulators is an important research area. Torque characteristics curve of motors can be analyzed properly for developing a proper control strategy. The effect of mass,

weight and inertia of the motor armature can be effectively incorporated for accurate dynamic modeling of flexible robotic manipulator. The optimization of motor can be integrated with the shape optimization of the manipulators.

- Due to the development of new manufacturing technology, non-circular sections may be considered for shape optimization of the flexible links. Standard cross-sections like square, rectangular, triangular, *etc.* can be analyzed for flexural vibration in the direction of its principal axes; however, in other direction there may be unsymmetrical bending vibration. It may be necessary to carryout two-dimensional or three-dimensional analysis. Gunjal and Dixit [2007] have carried out shape optimization of rotating cantilever beam having rectangular cross-section. They considered flap wise as well as chord wise vibrations. Their approach can also be used for the shape optimization of robotic manipulators of rectangular cross-section.

References

Alberts, T.E., Xia, H., and Chen, Y., (1992), Dynamic analysis to evaluate viscoelastic passive damping augmentation for the space shuttle remote manipulator system, ASME Journal Dynamic System, Measurement and Control, **114**, pp. 468–474.

Arteaga, M., (1998), On the properties of a dynamic model of flexible robot manipulators, ASME Journal Dynamic System, Measurement and Control, **120(1)**, pp. 8–14.

Asada, H., Ma, Z.D., and Tokumaru, H., (1990), Inverse dynamics of flexible robot arm: modeling and computation for trajectory control, ASME Journal Dynamic System, Measurement and Control, **112**, pp. 177–185.

Balas, M.J., (1978), Feedback control of flexible systems, IEEE Transaction on Automatic Control, **23(4),** pp. 673-679.

Balchut, J., (1982), A note on optimal design of a beam with a mass at its end, **88(2)**, pp. 203-208.

Baruh, H., and Tadikonda, S.S.K., (1989), Issues in the dynamics and control of flexible robot manipulators, AIAA Journal of Guidance, Control and Dynamics, **12(5)**, pp. 659–671.

Bathe, K.J., (1996), Finite element procedure, Prentice Hall, New Jersey.

Bayo, E. (1989), Timoshenko versus Bernoulli-Euler beam theories for inverse dynamics of flexible robots, International Journal of Robotics and Automation, **4(1)**, pp. 53–56.

Benati, M., and Morro, A., (1988), Dynamics of chain of flexible links, ASME J. of Dyn. Sys., Meas., and Control, **110**, pp. 410–415.

Bellezza, F., Lanari, L., and Ulivi, G., (1990), Exact modeling of the flexible slewing link, Proceedings of the IEEE Intl. Conf. on Robotics and Automation, pp. 734–739.

Berger, M. and Porat, I., (1989), On non-smooth beam shapes for maximum transverse natural frequencies, Journal of Sound and Vibration, **132(3)**, pp. 423-432.

Book, W.J., (1984), Recursive Lagrangian dynamics of flexible manipulator arms, The Intl. J. of Robotics Research, **3(3)**, pp. 87–101.

Boyer, F., and Coiffet, P., (1996), Generalisation of Newton–Euler model for flexible manipulators, International Journal of Robotic systems, **13(1)**, pp. 282–293.

Bricout, J.N., Debus, J.C., and Micheau, P., (1990), A finite element model for the dynamics of flexible manipulator, Mechanism and Machine Theory, **25(1)**, pp. 119–128.

Brach, R.M, (1968), On the external fundamental frequencies of vibrating beams, International Journal of Solid Structure, **4**, pp. 667-674.

Cai, G.P., Hong, J.Z., and Young, S.X., (2005), Dynamic analysis of a flexible hub–system with tip mass, Mechanics Research Communication, **32**, pp. 173–190.

Cannon, R.H., and Schmitz, E., (1984), Initial experiments on end-point control of a flexible one-link robot, The International Journal of Robotics Research, **3(3)**, pp. 62–75.

Chang, L.W., and Cannon, K.P., (1990), A dynamic model on a single link flexible manipulator, ASME Journal of Vibration and Acoustics, **112**, pp. 138–143.

Chen, W., (2001), Dynamic modeling of multi-link flexible robotic manipulators, Computers and Structures, **79(2)**, pp. 183–195.

Choi, B.O., and Krishnamurthy, K., (1994), Unconstrained and constrained motion control of a planar two-link structurally-flexible robotic manipulator, J. of Robotic Systems, **11**, pp. 557–571.

Chung, J., and Yoo, H.H., (2002), Dynamic analysis of a rotating cantilever beam by using the finite element method, Journal of Sound and Vibration, **249(1)**, pp. 147–164.

Courant, R. (1943), Variational methods for the solution of problems of equilibrium and vibrations, Bulletin of the American Mathematical Society, **49**, pp. 1-23.

Dado, M.H.F., and Soni, A.H., (1987), Dynamic response analysis of 2-R robot with flexible joints, Proceedings of the IEEE International Confrence on Robotics and Automation, **4**, pp. 479–483.

DeLuca, A., and Siciliano, B., (1991), Closed form dynamic model of planar multilink lightweight robots, IEEE Transactions on Systems, Man and Cybernetics SMC-21, **4**, pp. 826–839.

DeLuca, A., and Siciliano, B., (1990), Explicit dynamic modeling of a planar two-link flexible manipulator, Proceedings of the IEEE Confrence on Decision and Control, **2**, pp. 528–530.

Dixit, U.S., Kumar, R., and Dwivedy, S.K., (2006), Shape optimization of flexible robotic manipulators, Journal of Mechanical Design, **128**, pp. 559-565.

Dogan, A., and Iftar, A., (1998), Modeling and control of a two-link flexible robot manipulator, Proceedings of the 1998 IEEE International Confrence on Control Applications, **2**, pp. 761–765.

Elwary, M.H.S. and Barr, A.D.S., (1983), Optimal design of beams under flexural vibration, Journal of Sound and Vibration, **88(2)**, pp. 175-195.

Everett, L.J., Jennchen, T., and Compere, M., (1999), Designing flexible manipulators with the lowest natural frequency nearly independent of position, IEEE Trans. on Robotics and Automation, **15(4)**, pp. 605–611.

Farid, M., and Lukaiewicz, S.A., (2000), Dynamic modeling of spatial manipulators with flexible links and joints, Computers and Structures, **75**, pp. 419–437.

Fukuda, T. (1985), Flexibility control of elastic robot arms, Journal of Robotic Systems, **2(1)**, pp. 73–88.

Fukuda, T., and Arakawa, A. (1987), Modeling and control characteristics for a two-degrees-of-freedom coupling system of flexible robotic arms, JSME, Series C, **30**, pp. 1458–1464.

Fukuda, T., Arai, F., Hosogai, H., and Yajima, N., (1988), Flexibility control of flexible structures (Modeling and control method of bending-torsion coupled vibration), JSME, Series C, **31(3)**, pp. 575–581.

Fu, K.S., Gonzalez, R.C., and Lee, C.S.G., (1987), Robotics: Control, Sensing, Vision, and Intelligence, McGraw Hill Book Company, New York City, USA.

Ge, S.S., Lee, T.H., Zhu, G., (1996), Energy-based robust controller design for multi-link flexible robots, Mechatronics, **6(7)**, pp. 779–798.

Ge, S.S., Lee, T.H., and Zhu, G., (1998), Asymptotically stable end-point regulation of a flexible SCARA/Cartesian robot, IEEE/ASME Transactions Mechatronics, **3(2)**, pp.138–144.

Ge, S.S., Lee, T.H., and Zhu, G., (1997), A nonlinear feedback controller for a single-link flexible manipulator based on finite element model, Journal of Robotic Systems, **14(3)**, pp. 165–178.

Green, A., and Sasiadek, J.Z., (2004), Dynamics and trajectory tracking control of a two-link robot manipulator, Journal of Vibration and Control, **10(10)**, pp. 1415–1440.

Gunjal, S.K. and Dixit, U.S., (2007), Vibration analysis of shape-optimized rotating cantilever beams, Engineering Optimization, **39(1)**, pp. 105-123.

Hakki, A.I., Bingul, Z., and Kizir, S., (2012), Cascade fuzzy logic control of a single-link flexible-joint manipulator, Turk Journal of Electrical Engineering & Computer Science, **20(5)**, pp. 713-726.

Hegde, G.S., Vinod, M.S., and Shankar, A., (2009), Optimum dynamic design of flexible robotic manipulator, International Journal of Mechanical Material Design, **5**, pp. 315-325.

Jonker, B., (1989), A finite element dynamic analysis of flexible spatial mechanisms with flexible links, Computer Methods in Applied Mechanics and Engineering, **76(1),** pp. 17–40.

Jonker, B., (1990), A finite element dynamic analysis of flexible manipulators, The International Journal of Robotics Research, **9(4)**, pp. 59–74.

Kalra, P. and Sharan, A.M., (1990), On the automated generation of dynamic equations for flexible robotic manipulators, International Journal of Robotics and Automation, **5(2)**, pp. 92–97.

Kalra, P. and Sharan, A.M., (1991), Accurate modelling of flexible manipulators using finite element analysis, Mechanism and Machine Theory, **26(3)**, pp. 299–313.

Karihaloo, B.L. and Nicordson, F.I., (1973), Optimal design of vibrating cantilevers, Journal of Optimization Theory and Application, **11(6)**, pp. 638-654.

Khorrami, F., (1989), Analysis of multi-link flexible manipulators via asymptotic expansions, Proceedings of the IEEE Confrence on Decision and Control, **3**, pp. 2089–2094

Khorrami, F., and Jain, S., (1992), Experimental results on an inner/outer loop controller for a two-link flexible manipulator, Proceedings of the IEEE International Confrence on Robotics and Automation, **1**, pp. 742–747.

Kovecses, J., (1998), A distributed parameter model for the dynamics of flexible-link robot, Journal of Robotic Systems, **115(5)**, pp. 281–298.

Kress, R., Love, L., and Dubey, R., (1997), Waste tank cleanup manipulator modeling and control, Proceedings of the IEEE International Confrence on Robotics and Automation, **1**, pp. 662–668.

Krishnamurthy, K., (1989), Dynamic modelling of a flexible cylindrical manipulator, Journal of Sound and Vibration, **132**, pp. 143–154.

Lee, J.D., and Wang, B.L., (1988), Dynamic equations for a two-link flexible robot arm, Computers and Structures, **29(3)**, pp. 469–477.

Lee, J.D., and Wang, B.L., (1988), Optimal control of a flexible robot arm, Computers and Structures, **29(3)**, pp. 459–467.

Lee, H.H., (2005), New dynamic modeling of flexible-link robots, ASME Journal Dynamic System, Measurement and Control, **127**, pp. 307–309.

Li, Y.F., and Wang, G.L., (2000), On the internal dynamics of flexible manipulators based on symmetric dichotomy, IEEE Proceedings of Control Theory Applications, **147(1)**, pp. 59–70.

Liao, Y.S., (1993), A generalized method for the optimal design of beams under flexural vibration, Journal of Sound and Vibration, **167(2)**, pp. 193-202.

Lou, Y. Gong, W., Li, Z., Zhang, J., and Yang, G., (2009), Proceeding of IEEE International Confrence on Robotics and Automation, Japan, pp. 1768-1773.

Low, K.H., and Vidyasagar, M. (1988), A Lagrangian formulation of the dynamic model for flexible manipulator systems, ASME Journal Dynamic System, Measurement and Control, **110**, pp. 175–181.

Magee, D.P., and Book, W.J., (1993), Eliminating multiple modes of vibration in a flexible manipulator, Proceedings of the IEEE International Confrence on Robotics and Automation, **2**, pp. 274–279.

Milford, R.I., and Asokanthan, S.F., (1999), Configuration dependent eigen frequencies for a two-link flexible manipulator: experimental verification, Journal of Sound and Vibration, **222(2)**, pp. 191–207.

Mohamed, Z., and Tokhi, M.O., (2004), Command shaping techniques for vibration control of a flexible robot manipulator, Mechatronics, **14**, pp. 69–90.

Morris, A.S., and Madani, A., (1995), Static and dynamic modeling of a two-flexible-link robot manipulator, Robotica, **14(3)**, pp. 289–300.

Moulin, H., and Bayo, E., (1991), On the accuracy of end-point trajectory tracking for flexible arms by noncausal inverse dynamic solutions, ASME Journal Dynamic System, Measurement and Control, **113**, pp. 320–324.

Nagaraj, B.P., Nataraju, B.S., and Ghosal, A., (1997), Dynamics of a two-link flexible system undergoing locking: mathematical modelling and comparison with experiments, Journal of Sound and Vibration, **207(4)**, pp. 567–589.

Nagarajan, S. and Turcic, D.A., (1990), Lagrangian formulation of the equations of motion for the elastic mechanisms with mutual dependence between rigid body and elastic motions, Part 1: Element level equations equations, ASME Journal Dynamic System, Measurement and Control, **112(2),** pp. 203–214.

Nagarajan, S. and Turcic, D.A., (1990), Lagrangian formulation of the equations of motion for the elastic mechanisms with mutual dependence between rigid body and elastic motions, Part II: System equations, ASME Journal Dynamic System, Measurement and Control, **112(2),** pp. 215–224.

Naganathan, G., and Soni, A.H., (1987), Coupling effects of kinematics and flexibility in manipulators, The International Journal of Robotics Research, **6(1)**, pp. 75–84.

Naganathan, G., and Soni, A.H., (1988) Nonlinear modeling of kinematic and flexibility effects in manipulator design, ASME Journal of Mechanisms, Transmissions and Automation in Design, **110**, pp. 243–254.

Naganathan, G., and Soni, A.H. (1987), Coupling effects of kinematics and flexibility in manipulators, The International. Journal of Robotics Research, **6(1)**, pp. 75–84.

Nicordson, F.I., (1965), On the optimal design of a vibrating beam, Quaterly of Applied Mathematics, **23(1)**, pp. 47-53.

Oakley, C.M., and Cannon, R.H., (1990), Anatomy of an experimental two-link flexible manipulator under end-point control, Proceedings of the IEEE Confrence on Decision and Control, **2**, pp. 507–513.

Oldhoff, N. and Parbery, R., (1982), Designing vibrating beams and rotating shafts for maximum difference between adjacent natural frequencies, International Journal of Solids and Structure, **30(1)**, pp. 63-75.

Ower,, J.C., and Vegte, J.V., (1987), Classical control design for a flexible manipulator: modeling and control system design, IEEE Journal of Robotics and Automation, RA, 3(5), pp. .

Prager, W. and Taylor, J.E., (1968), Problems of optimal structure design, ASME Transactions Journal of Applied Mechanics, March'68, pp. 102-106.

Queiroz, M.S., Donepudi, S., Burg, T., and Dawson, D.M., (1998), Model-based control of rigid-link flexible joint robots: an experimental evaluation, Robotica, **16**, pp. 11–21.

Rakhsha, F., and Goldenberg, A.A., (1985), Dynamic modeling of a single link flexible robot, Proceedings of the IEEE International Confrence on Robotics and Automation, pp. 984–989.

Rao, S.S., (2013), Engineering Optimization: Theory and Practice, New Age International Publishers, New Delhi, India.

Rosado, V.O.G., and Yuhara, E.A.O., (1999), Dynamic modeling and simulation of a flexible robotic manipulator, Robotica, **17**, pp. 523–528.

Rovner, D.M., and Cannon, R.H., (1987), Experiments toward on-line identification and control of a very flexible one-link manipulator, The Intl. J. of Robotics Research, **6(4)**, pp. 3–19.

Sheu, C.Y., (1968), Elastic minimum weight design for specified fundamental frequency, International Journal of Solid Structure, **4**, pp. 953-958

Singh, T., (1991), Dynamics and Control of Flexible Arm Robots, Ph.D. Thesis, Mechanical Engineering, Waterloo University, Canada.

Sunada, W. H., and Dubowsky, S. (1981), The application of finite element methods to the dynamic analysis of spatial and coplanar linkages, ASME Journal of Mechanical Design, **103**, pp. 643–651.

Sunada, W., and Dubowsky, S., (1983), On the dynamic analysis and behaviour of industrial robotic manipulators with elastic members, ASME Journal of Mechanism, Transmissions and Automation in Design, **105(1)**, pp. 42–51.

Taha, H.A., (2000), Operations Research An Introduction, Prentice-Hall of India Pvt. Ltd., New Delhi, India.

Theodore, R.J., and Ghosal, A., (1995), Comparison of the assumed modes and finite element models for flexible multi-link manipulators, The International Journal of Robotics Research, **14(2)**, pp. 91–111.

Teng, Y., and Cai, G.P., (2007), Frequency characteristics of a flexible hub–beam system with arbitrary settling position of attached mass, Journal of Vibration and Control, **13(6)**, pp. 769–794.

Tokhi, M.O., Mohamed, Z., and Shaheed, M.H., (2001), Dynamic characterisation of a flexible manipulator system, Robotica, **19**, pp. 571–580.

Tokhi, M.O., Mohamed, Z., Amin, S.H.M., and Mamat, R., (2000), Dynamic characterization of a flexible manipulator system: theory and experiments, Proceedings of TENCON, **3**, pp. 167–172.

Tomei, P., and Tornambe, A., (1988), Approximate modeling of robots having elastic links, IEEE Transactions on Systems, Man and Cybernetics, **18(5)**, pp. 831–840.

Tomei, P., and Tornambe, A., (1988), Approximate modeling of robots having elastic links, IEEE Transactions on Systems, Man and Cybernetics, **18(5)**, pp. 831–840.

Usoro, P.B., Nadira, R., and Mahil, S.S., (1986), A finite element/Lagrangian approach to modeling light weight flexible manipulators, ASME Journal of Dynamic System, Measurement and Control, **108**, pp. 198–205.

Wang, P.K.C., and Wei, J.D., (1987), Vibration in a moving flexible robot arm, Journal of Sound and Vibration, **116(1)**, pp. 149–160.

Wang, D., and Vidyasagar, M., (1991), Transfer function for a single flexible link, The International Journal of Robotics Research, **10(5)**, pp. 540–549.

Wang, F.Y., (1995), Optimum design of vibrating cantilevers: A classical problems revisited, Journal of Optimization Theory and applications, **84(3)**, pp. 635-652.

Wang, F.Y. and Guan, G., (1992), Influence of rotatory inertia, shear and bending on vibrations of flexible manipulators, Journal of Sound and Vibration, **171(4)**, pp. 433-452.

Wang, F.Y. and Russell, J.L., (1992), Optimum shape construction of flexible manipulators with tip loads, Proceeding of 31st IEEE Confrence on Decision and Control, Arizona, pp. 311-316.

Wang, F.Y. and Russell, J.L., (1995), Optimum shape construction of flexible manipulator with total weight constraints, IEEE Transactions on System Man and Cyber., **25(4)**, pp. 605-614.

Xu, D. and Ananthasuresh, G.K., (2003), Freeform skeletal shape optimization of compliant mechanism, Journal of Mechanical Design, **125**, pp. 253-261.

Yigit, A.S., (1994), On the stability of PD control for a two-link rigid-flexible manipulator. ASME, Journal of Dynamic System, Measurement and Control, **116**, pp. 208-215.

Yang, Z., and Sadler, J.P., (1990), Large-displacement finite element analysis of flexible linkage, ASME Journal of Mechanical Design, **112**, pp. 175–182.

Yang, H., Hong, J., and Yu, Z., (2003), Dynamic modeling of a flexible hub-beam system with tip mass, Journal of Sound and Vibration, **266**, pp. 759-774.

Yang, Z., (1997), Prediction of the dynamic response of flexible manipulators from a modal database, Mechanism and Machine Theory, **32(6)**, pp. 679–689.

Yang, T.W., Xu, W.L., and Tso, S.K., (2001), Dynamic modeling based on real-time deflection measurement and compensation control for flexible multi-link manipulators, Dynamics and Control, **11(1)**, pp. 5–24.

Yoo, H.H., Cho, J.E., and Chung, J., (2006), Modal analysis and shape optimi-zation of rotating cantilever beams, Journal of Sound and Vibration, **290**, pp. 223-241.

Yoshikawa, T., Hosoda, K., Doi, T., and Murakami, H., (1994), Dynamic trajectory tracking control of flexible manipulator by macro-micro manipulator system, Proceedings of the IEEE International Confrence on Robotics and Automation, pp. 1804–1809.

You, C., Hong, J., and Cai, G.P., (2006), Modelling study of flexible hub–beam system with large motion and with considering the effect of shear deformation, Journal of Sound and Vibration, **295**, pp. 282–293.

Yuan, B.S., Book, W.J. and Huggins, J.D., (1993), Dynamics of flexible manipulator arms: alternative derivation, verification, and characteristics for control, ASME Journal of Dynamic, Measurement and Control, **115**, pp. 394-404.

Zhang, C.X., and Yu, Y.Q., (2004), Dynamic analysis of planar cooperative manipulators with link flexibility, ASME Journal of Dynamic System, Measurement and Control, **126** pp. 442–448.

Zhang, X., Xu, W., Nair, S.S., and Chellabonia, V.S., (2005), PDE modeling and control of a flexible two-link manipulator, IEEE Transactions on Control Systems Technology, **13(2)**, pp. 301–312.

Appendices

Appendix-I

Constant of Eq. (3.12)

$$\mathrm{P}_i = \frac{m_1 h_1}{420}\begin{bmatrix} 156 & 22h_1 & 54 & -13h_1 \\ 22h_1 & 4h_1^2 & 13h_1 & -3h_1^2 \\ 54 & 13h_1 & 156 & -22h_1 \\ -13h_1 & -3h_1^2 & 22h_1 & 4h_1^2 \end{bmatrix},$$

$$M_{nl} = \{u_i\}' P_i \{u_i\},$$

$$M_{11} = mah(a+h) + 2mah^2(i-1) + \frac{mh^3}{3}\left(3i^2 - 3i + 1\right),$$

$$M_{12} = M_{21} = \frac{mh}{20}\{10a + h(10i-7)\},$$

$$M_{13} = M_{31} = \frac{mh^2}{60}\{5a + h(5i-3)\},$$

$$M_{14} = M_{41} = \frac{mh}{20}\{10a + h(10i-3)\},$$

$$M_{15} = M_{51} = -\frac{mh^2}{60}\left(5a + h(5i-2)\right).$$

Appendix-II

Constant of Eq. (4.14)

$$P_i = \frac{m_2 h}{420}\begin{bmatrix} 156 & 22h & 54 & -13h \\ 22h & 4h^2 & 13h & -3h^2 \\ 54 & 13h & 156 & -22h \\ -13\text{h} & -3h^2 & -22h & 4h^2 \end{bmatrix},$$

$$M_{11} = m_2 h\left\{\left(\text{a}+\text{b}+L_1\right)^2 + \text{h}\left(a+b+L_1\right)\left(2i-1\right)\right\} + \frac{m_2 h^3}{3}\left(3i^2-3i+1\right),$$

$$M_{12} = M_{21} = \frac{m_2 h}{2}\left(a+b+L_1\right)\left\{\left(2i-1\right)h+2b\right\} + \frac{m_2 h^2 b}{2}\left(2i-1\right) + \frac{m_2 h^3}{3}\left(3i^2-3i+1\right)$$

$$M_{13} = M_{31} = \frac{m_2 h}{2}\left(a+b+L_1\right) + \frac{\text{m}_2 h^2}{20}\left(10i-7\right),$$

$$M_{14} = M_{41} = \frac{m_2 h^2}{12}\left(a+b+L_1\right) + \frac{m_2 h^3}{60}\left(5i-3\right),$$

$$M_{15} = M_{51} = \frac{m_2 h}{2}\left(a+b+L_1\right) + \frac{m_2 h^2}{20}\left(10i-3\right),$$

$$M_{16} = M_{61} = -\frac{m_2 h^2}{12}\left(a+b+L_1\right) - \frac{m_2 h^3}{60}\left(5i-2\right),$$

$$M_{22} = m_2 b h^2\left(2i-1\right) + m_2 b^2 h + \frac{m_2 h^3}{3}\left(3i^2-3i+1\right),$$

$$M_{23} = M_{32} = \frac{m_2 b h}{2} + \frac{m_2 h^2}{20}\left(10i-7\right),$$

$$M_{24} = M_{42} = \frac{m_2 b h^2}{12} + \frac{m_2 h^3}{60}\left(5i-3\right),$$

$$M_{25} = M_{52} = \frac{m_2 bh}{2} + \frac{m_2 h^2}{20}(10i - 3),$$

$$M_{26} = M_{62} = -\frac{m_2 bh^2}{12} - \frac{m_2 h^3}{60}(5i - 2).$$

Appendix-III

Constant of Eq. (4.24)

$$M'(1,1) = J_1 + \frac{M_1}{3}\left\{3a(a+L_1) + L_1^2\right\} + J_2 + M_m(a+L_1)^2 + M_p(a+L_1+b+L_2)^2,$$

$$M'(1,2) = M'(2,1) = J_2 + M_p(a+L_1+b+L_2)(b+L_2),$$

$$M'(2,2) = J_2 + M_p(b+L_2)^2,$$

$$M'(1,2n+2) = M'(2n+2,1) = M_p(a+L_1+b+L_2),$$

$$M'(2,2n+2) = M'(2n+2,2) = M_p(b+L_2),$$

$$M'(2n+2,2n+2) = M_p.$$

Appendix-IV

Constant of Eq. (4.26)

$$D_{11} = J_1 + \frac{1}{3}m_1 L_1^3 + m_2 L_1^2 L_2 + \frac{1}{3}m_2 L_2^3 + M_m L_1^2 + M_P\left(L_1^2 + L_2^2\right)$$

$$+ m_2 L_1 L_2^2 C_2 + 2m_p L_1 L_2 C_2 + J_2, \quad \left(S_2 = \sin\theta_2,\ C_2 = \cos\theta_2\right)$$

$$D_{12} = D_{21} = J_2 + \frac{1}{3}m_2 L_2^3 + \frac{1}{2}m_2 L_1 L_2^2 C_2 + M_p L_2^2 + M_p L_1 L_2 C_2,$$

$$D_{22} = J_2 + \frac{1}{3}m_2 L_2^3 + M_p L_2^2,$$

$$\phi_1 = -\frac{1}{2}m_2 L_1 L_2^2 S_2 \dot{\theta}_2^2 - m_2 L_1 L_2^2 \dot{\theta}_1 \dot{\theta}_2 S_2 - M_p L_1 L_2 S_2 \dot{\theta}_2^2 - 2M_p L_1 L_2 S_2 \dot{\theta}_1 \dot{\theta}_2,$$

$$\phi_2 = \frac{1}{2} m_2 L_1 L_2^2 S_2 \dot{\theta}_1^2 + -M_p L_1 L_2 S_2 \dot{\theta}_1^2$$

Appendix-V

Constant of Eq. (5.7)

$$\mathrm{P}_{1i} = \frac{m_1 h_1}{420} \begin{bmatrix} 156 & 22h_1 & 54 & -13h_1 \\ 22h_1 & 4h_1^2 & 13h_1 & -3h_1^2 \\ 54 & 13h_1 & 156 & -22h_1 \\ -13h_1 & -3h_1^2 & 22h_1 & 4h_1^2 \end{bmatrix},$$

$$M_{11} = m_1 a h_1 (a + h_1) + 2 m_1 a h_1^{\,2} (i-1) + \frac{m_1 h_1^3}{3} \left(3i^2 - 3i + 1\right),$$

$$M_{12} = M_{21} = \frac{m_1 h_1}{20} \{10a + h(10i - 7)\},$$

$$M_{13} = M_{31} = \frac{m_1 h_1^2}{60} \{5a + h(5i - 3)\},$$

$$M_{14} = M_{41} = \frac{m_1 h_1}{20} \{10a + h(10i - 3)\}$$

$$M_{15} = M_{51} = -\frac{m_1 h_1^2}{60} \{5a + h(5i - 2)\}$$

Appendix-VI

Constant of Eq. (5.16)

$$\mathrm{P}_{2j} = \frac{m_2 h_2}{420} \begin{bmatrix} 156 & 22h_2 & 54 & -13h_2 \\ 22h_2 & 4h_2^2 & 13h_2 & -3h_2^2 \\ 54 & 13h_2 & 156 & -22h_2 \\ -13h_2 & -3h_2^2 & 22h_2 & 4h_2^2 \end{bmatrix},$$

$$M_{11} = m_2 h_2 \left(L_1 + a + b\right)^2 + m_2 h_2^2 \left(L_1 + a + b\right)(2j - 1) + \frac{m_2 h_2^3}{3} \left(3j^2 - 3j + 1\right),$$

$$M_{12} = M_{21} = \frac{m_2 h_2}{2} \left(2(L_1 + a + b) + h_2 (2j - 1)\right),$$

$$M_{13} = M_{31} = m_2 \frac{h_2^3}{3} \left(3j^2 - 3j + 1\right) + \frac{m_2 h_2^2}{2} \left(L_1 + a + b\right)(2j - 1),$$

$$M_{13} = M_{31} = M_{41} = M_{14},$$

$$M_{15} = M_{51} = \frac{m_2 h_2}{20}\left(10(L_1 + a + b) + h_2(10j - 7)\right),$$

$$M_{16} = M_{61} = \frac{m_2 h_2^2}{60} h_2^2\left(5(L_1 + a + b) + h_2(5j - 3)\right),$$

$$M_{17} = M_{71} = \frac{m_2 h_2}{20}\left(10(L_1 + a + b) + h_2(10j - 3)\right),$$

$$M_{18} = M_{81} = \frac{-m_2 h_2^2}{60}\left(54h_2^2 + 5h_2^3 j - 2h_2^3\right),$$

$$M_{22} = m_2 h_2,$$

$$M_{23} = \frac{m_2 h_2^2}{2}\left(2j - 1\right),$$

$$M_{24} = M_{42} = M_{23} = M_{32},$$

$$M_{25} = M_{52} = \frac{m_2 h_2}{2},$$

$$M_{26} = M_{62} = \frac{m_2 h_2^2}{12},$$

$$M_{27} = M_{72} = \frac{m_2 h_2}{2},$$

$$M_{28} = M_{82} = \frac{-m_2 h_2^2}{12},$$

$$M_{33} = M_{34} = M_{43} = \frac{m_2 h_2^3}{3}\left(3j^2 - 3j + 1\right),$$

$$M_{35} = \frac{m_2 h_2^2}{20}\left(10j - 7\right),$$

$$M_{36} = M_{63} = \frac{m_2 h_2^3}{60}\left(5j - 3\right),$$

$$M_{37} = M_{73} = \frac{m_2 h_2^2}{20}\left(10j - 3\right),$$

$$M_{38} = M_{83} = \frac{-m_2 h_2^3}{60}\left(5j - 2\right).$$

Appendix-VII

Sequential Quadratic Programming (SQP) Method

Sequential Quadratic Programming (SQP) method is one of the most successful and newest methods for solving nonlinear constrained optimization problems. SQP methods may be interpreted as Newton's method applied to the solution of the Karush–Kuhn–Tucker (KKT) conditions. SQP solves a sequence of quadratic programming (QP) problems till the convergence is obtained. The solution of a QP problem requires solving a set of linear conditions along with the additional conditions that either a constraint is active or the corresponding Lagrange multiplier is zero. A method similar to Simplex method of linear programming can be employed [Taha, 2000]. Thus, the procedure is very fast and provides unique answer for a QP. Of course, the procedure has to be repeated several times, each time with a current point.

There are several variants of SQP methods. All of them have the following advantages:

(1) The starting guess point can be infeasible.

(2) It requires the gradients of only active constraints.

(3) It can handle equality as well as inequality constraints.

(4) There is a convergence proof for a class of problems.

A brief description of SQP method is as follows [Rao, 2013]. Consider the following optimization problem with l equality and m inequality constraints:

Minimize $f(\mathbf{x})$,

subject to

$$h_i(\mathbf{x}) = 0, \quad i = 1 \text{ to } l \tag{A.1}$$

and

$$g_j(\mathbf{x}) \le 0, \quad j = 1 \text{ to } m$$

where $\mathbf{x} = (x_1, x_2, ..., x_n)^T$ is a column vector of n real-valued design variables. In Eq. (A.1), f is a linear or nonlinear objective functions, h_i is a linear or nonlinear

equality constraint and g_j is a linear or nonlinear inequality constraint. The Lagrange function, $L(\mathbf{x},\lambda)$, corresponds to the problem of Eq. (A.1) is given by

$$L(\mathbf{x},\lambda) = f(\mathbf{x}) + \sum_{j=1}^{m} \lambda_j g_j(\mathbf{x}) + \sum_{i=1}^{l} \lambda_{m+i} h_i(\mathbf{x}), \tag{A.2}$$

where λ_j and λ_{m+i} are the Lagrange multipliers for the j^{th} inequality constraint and i^{th} equality constraints respectively. The KKT necessary conditions can be stated as

$$\nabla L = 0, \tag{A.3}$$

or

$$\nabla f + \sum_{j=1}^{m} \lambda_j \nabla g_j + \sum_{i=1}^{l} \lambda_{m+i} \nabla h_i = 0, \tag{A.4}$$

or,

$$\nabla f + [A]\lambda = 0, \tag{A.5}$$

along with the constraint equations:

$$g_j(\mathbf{x}) = 0, \;\; j = 1 \text{ to } m, \tag{A.6}$$

and

$$h_i(\mathbf{x}) = 0, \;\; i = 1 \text{ to } l, \tag{A.7}$$

where ∇ is the gradient operator and $[A]$ is an $n\times(m+l)$ matrix whose j^{th} and $(m+i)^{th}$ columns denote the gradient of the function of g_j and h_i respectively. Equations (A.5), (A.6) and (A.7) represent a set of $(n+m+l)$ nonlinear equations in $(n+l+m)$ unknowns (x_i, i = 1,2,…,n; λ_s, s = 1, 2,…, m, m+1, …m+l). These nonlinear equations can be solved using Newton's method. At the k^{th} approximate point:

$$\begin{bmatrix} [\nabla^2 L] & [A] \\ [A]^T & [0] \end{bmatrix}_k \begin{Bmatrix} \Delta\mathbf{x} \\ \Delta\lambda \end{Bmatrix}_k = -\begin{Bmatrix} \nabla L \\ \mathbf{d} \end{Bmatrix}_k, \tag{A.8}$$

where

$$\Delta\mathbf{x}_k = \mathbf{x}_{k+1} - \mathbf{x}_k, \tag{A.9}$$

$$\Delta\lambda_k = \lambda_{k+1} - \lambda_k \tag{A.10}$$

and

$$\mathbf{d} = \left(g_1, g_2, ...g_m, h_{m+1}, h_{m+2}, ..., h_{m+l}\right)^T. \tag{A.11}$$

The expression of the matrix $\left[\nabla^2 L\right]_{n\times n}$ denotes the Hessian matrix of the Lagrange function. Using Eq. (A.10) for $\Delta\lambda_k$ and Eq. (A.5) for ΔL_k; the first partitioned row of Eq. (A.8) becomes:

$$\left[\nabla^2 L\right]_k \Delta\mathbf{x}_k + \left[A\right]_k \lambda_{k+1} = -\nabla f_k \quad . \tag{A.12}$$

The second partitioned row of Eqs. (A.8) and (A.12) can now be combined as

$$\begin{bmatrix} \left[\nabla^2 L\right] & \left[A\right] \\ \left[A\right]^T & \left[0\right] \end{bmatrix}_k \begin{Bmatrix} \Delta\mathbf{x}_k \\ \lambda_{k+1} \end{Bmatrix} = -\begin{Bmatrix} \nabla f_k \\ \mathbf{d}_k \end{Bmatrix}. \tag{A.13}$$

Eq. (A.13) can be solved to find the change in the design vector $\Delta\mathbf{x}_k$ and the new value of the Lagrange multipliers, λ_{k+1}.The iterative process indicated by Eq. (A.13) can be continued until convergence is achieved.

Now consider the minimization of the following quadratic objective function:

$$Q = \nabla f_k\left(\mathbf{x}\right)^T \Delta\mathbf{x} + \frac{1}{2}\Delta\mathbf{x}^T \left[\nabla^2 L\right]_k \Delta\mathbf{x},$$

subject to

$$\begin{aligned} g_j\left(\mathbf{x}\right) + \nabla g_j^T \Delta\mathbf{x} \le 0, \quad & j = 1, 2, \ldots, m, \\ h_i\left(\mathbf{x}\right) + \nabla h_i^T \Delta\mathbf{x} = 0, \quad & i = 1, 2, \ldots, l. \end{aligned} \tag{A.14}$$

The gradients of the constraint functions are evaluated at point $\mathbf{x}_k$. It can be easily verified that the same KKT necessary conditions are obtained of this quadratic from objective function with linear constraints as in Eq. (A.13). The expression $\nabla f\left(\mathbf{x}\right)^T$ is $\left\{\frac{\partial f}{\partial x_1} \quad \frac{\partial f}{\partial x_2} \quad \cdots \quad \frac{\partial f}{\partial x_n}\right\}$ and Hessian matrix $[\nabla^2 L]$ of the Lagrangian is defined as

$$\left[\nabla^2 L\right] = \begin{bmatrix} \frac{\partial^2 L}{\partial x_1^2} & \frac{\partial^2 L}{\partial x_1 \partial x_2} & \cdots & \frac{\partial^2 L}{\partial x_1 \partial x_n} \\ \frac{\partial^2 L}{\partial x_2 \partial x_1} & \frac{\partial^2 L}{\partial x_2^2} & \cdots & \frac{\partial^2 L}{\partial x_2 \partial x_n} \\ \cdots & \cdots & \cdots & \cdots \\ \cdots & \cdots & \cdots & \cdots \\ \cdots & \cdots & \cdots & \cdots \\ \frac{\partial^2 L}{\partial x_n \partial x_1} & \frac{\partial^2 L}{\partial x_n \partial x_2} & \cdots & \frac{\partial^2 L}{\partial x_n^2} \end{bmatrix}. \tag{A.15}$$

The gradients and the Hessian matrix are evaluated at the guess point.

The above analysis indicates that moving in the direction of $\Delta\mathbf{x}$, one will get the minimum. One can assume that the minimum point $\mathbf{x}_p$ is obtained by the expression:

$$\mathbf{x}_p = \mathbf{x} + \alpha\Delta\mathbf{x}, \tag{A.16}$$

where α is a step length chosen to reduce the value of a suitable merit function along the direction $\Delta\mathbf{x}$. Once the value of $\mathbf{x}_p$ is substituted in the merit function, the merit function becomes the function of scalar α. The optimum value of α can be found by a one-dimensional search technique *e.g.*, golden section search algorithm [Rao, 2013]. The merit function can be the penalty function of the following form:

$$M = f(\mathbf{x}) + \sum_{j=1}^{m} \beta_j \left(\max\left[0, g_j(\mathbf{x})\right]\right) + \sum_{i=1}^{l} \beta_{m+i} \left|h_i(\mathbf{x})\right|, \tag{A.17}$$

where β_j is a suitable penalty parameter.

At the obtained optimum point $\mathbf{x}_p$, the objective function is again converted to the form of Eq. (A.14), *i.e.*, a quadratic approximation for the function and a linear approximation for the constraints is used. After this, the procedure is repeated starting from solving a QP problem. Thus, the optimization process is iterative and the iterations are continued till the convergence is obtained. In the present work, inbuilt function FMINCON of MATLAB® is used to implement SQP algorithm**.**

Publications from this research work

Journals

1. Mahto, S. and Dixit, U.S. (**2012**), Comparative dynamic response of a optimized single link flexible manipulator, Applied Mechanics and Materials, 110-116, pp. 4748–4756.
2. Mahto, S. (**2014**), Shape optimization of revolute-jointed single link flexible manipulator for vibration suppression, Mechanism and Machine Theory (Elsevier), 75, pp. 150–160.
3. Mahto, S. and Dixit, U.S. (**2014**), Shape optimization of revolute-jointed rigid-flexible manipulator, J. Inst. Eng. India Ser. C (Springer, India), 95(4), pp. 335–346.
4. Mahto, S. and Dixit, U.S. (**2014**), Parametric study of double link flexible manipulator, Universal J. of Mechanical Engineering (HR Pub., USA), 2(7), pp. 211–219.
5. Mahto, S., Gogoi, A.K., and Dixit, U.S., Vibration confinement of double link flexible manipulator through shape optimization (to be communicated).

Conferences

1. Mahto, S. and Dixit, U.S. (**2010**), Optimal shapes of single link flexible manipulator for maximizing higher natural frequencies, International Conf. on Theoretical, Applied, Computational and Experimental Mechanics (ICTACEM 2010), December 27-29, 2010, IIT Kharagpur, India. (ISBN: 978-93-80813-03-5).
2. Mahto. S. (**2011**),Shape optimization of revolute joint single link flexible robotic manipulator for vibration suppression, Proceeding of 15th National Conf. on Machine and Mechanism (NaCoMM2011),30th Nov-2nd Dec, 2011, IIT Madras, Chennai. (Its advance version is published as International Journal paper #2)
3. Mahto, S. and Dixit, U.S. (**2011**), Optimized design of single link flexible manipulator, Proceeding of ASME International Conf. (IMECHE 2011), Vol. 7, Part-A, pp. 183–90, Denver, USA.
4. S. Mahto, A.K. Gogoi and U.S. Dixit, A Comparative Study of Improved Dynamics of Single Link Flexible Revolute-Jointed Robotic Manipulator, December 14-17, 2015, Indian Institute of Technology Guwahati, India, paper id 00177 (10 pages)